SANDIA NATIONAL LABORATORIES
WASTE ISOLATION PILOT PLANT

SUMMARY REPORT FOR THE 2023 REPLACEMENT PANELS PLANNED CHANGE REQUEST PERFORMANCE ASSESSMENT

REVISION 1

Author:	Sarah Brunell	Signature on File	2/15/2024
Author:	James Bethune	Signature on File	2/15/2024
Author:	Paul Docherty	Paul Docherty	2/15/2024
Author:	Dwayne Kicker	Signature on File	2/15/2024
Author:	Sungtae Kim	Sungtae Kim	2/15/2024
Author:	Seth King	[signature]	2/15/2024
Author:	Jennifer Long	Signature on File	2/15/2024
Author:	Todd Zeitler	Signature on File	2/15/2024
	Print	Signature	Date
Technical Reviewer:	Clifford Hansen	Signature on File	2/15/2024
	Print	Signature	Date
QA Reviewer:	Shelly R. Nielsen	Shelly R. Nielsen	2-15-2024
	Print	Signature	Date
Management Reviewer:	Steve Wagner	[signature]	2/15/2024
	Print	Signature	Date

ERMS #581044

FEBRUARY 2024

WIPP:4.4.1.2.1:PA:QA-L:578831

Information Only

This page intentionally left blank.

Information Only

EXECUTIVE SUMMARY

As currently certified, the Waste Isolation Pilot Plant (WIPP) includes ten panels for the emplacement of waste. Due to lost capacity, not all of the volume of the ten panels will be used for waste disposal. The DOE plans to submit a Planned Change Request (PCR) for use of two new panels, termed replacement panels, to provide an equivalent disposal capability. The DOE may consider excavating up to seven panels beyond the two replacement panels, defined here as additional panels, to meet the Land Withdrawal Act (LWA) waste volume. The Replacement Panels Planned Change Request Performance Assessment (RPPCR PA) has been executed by Sandia National Laboratories (SNL) to quantify the long-term performance of the repository with both replacement and additional panels.

This report summarizes the RPPCR PA. The RPPCR PA results are primarily compared to the results of the 2019 Compliance Recertification Application (CRA-2019) Performance Assessment. Select RPPCR PA results are also compared to the 2021 Additional Panels Performance Assessment (APPA) to isolate and quantify the impact of the increased repository volume. Compared to the CRA-2019 analysis, mean total normalized releases for the RPPCR analysis are increased at all probabilities. Cuttings and cavings releases continue to dominate total releases at the highest probabilities. Direct brine releases and spallings releases are the main contributors to total releases at lower probabilities. The changes in releases mainly result from the changes to the model for salt creep closure onto the waste, the inventory, and an increase in the drilling frequency. Radionuclide activity entering the Culebra has been significantly reduced by the updated long-term borehole permeability distribution. As a result, releases from the Culebra are significantly reduced.

Comparison of the RPPCR PA results to the CRA-2019 and APPA indicate that the replacement and additional panels have little impact on cuttings, cavings, spallings and direct brine releases. Releases through the Culebra for the four western-most additional panels are higher than releases for the existing panels. Releases through the Culebra from the replacement panels show similar behavior to those from the existing panels.

Mean total releases from the RPPCR PA are also compared to total releases from the EPA's CRA19_COMB analysis. The RPPCR PA sees higher releases at the upper compliance point probability and lower releases at the lower compliance point probability compared to the CRA19_COMB results.

Total normalized releases in the RPPCR PA are below regulatory limits. As a result, the RPPCR PA demonstrates that the WIPP repository, with replacement panels, would continue to comply with the containment requirements of 40 CFR Part 191.

Information Only

Revision History

This report was revised based on comments from DOE. Changes were made throughout the document to improve clarity and readability. Technical details from the supporting analysis reports were added to provide a more complete overview of the RPPCR PA analysis.

Information Only

TABLE OF CONTENTS

1.0 INTRODUCTION 1

2.0 CHANGES SINCE THE CRA-2019 PA 3

2.1 Updates to the Inventory 4
2.2 Updates to Radionuclide Mobilization 5
2.3 Additional Waste and Operations Areas 6
2.4 Changes to Repository Parameters 7
2.5 Changes to Iron Surface Area Calculation 8
2.6 Changes to Repository Pressure at Closure 9
2.7 Update to the Porosity Surface 9
2.8 Updates Related to the Castile Brine Reservoir 11
2.8.1 Salado Flow Model 11
2.8.2 Probability of Intrusion 11
2.9 Permeability of a Borehole after Plug Failure and Degradation 12
2.10 Update to the Culebra Transport Procedure 12
2.11 Recalibration of T-fields 14
2.12 Updates to the Borehole Drilling Frequency and Plugging Pattern Probabilities. 14
2.13 Sampling of Uncertain Parameters 15
2.14 Hardware and Computational Code Updates 16

3.0 METHODOLOGY FOR THE RPPCR 17

3.1 Review of FEPs and Conceptual Models 17
3.2 Salado Flow 18
3.2.1 Repository Representation in BRAGFLO 18
3.2.2 Panel Groups 19
3.2.3 Modeling Scenarios 20
3.3 Cuttings, Cavings, and Spallings 21
3.4 Radionuclide Activities for Solid Releases 22
3.5 Direct Brine Release Volumes 22
3.5.1 Model Representation in BRAGFLO_DBR 22
3.5.2 Initial Conditions 24
3.5.3 Modeling Scenarios 25

Information Only

3.6 Mobilized Radionuclide Concentrations 26
3.7 Salado Transport 27
3.8 Flow and Transport in the Culebra 28
3.9 Calculation of CCDFs for Releases 29
3.9.1 Panel Neighboring Assignments 29
3.9.2 Method for Determining Confidence Intervals 31
3.10 Run Control 31

4.0 RESULTS 35

4.1 Inventory 35
4.1.1 Total Waste Volume 35
4.1.2 Inventory by EPA Units 36
4.1.3 Waste Stream Activity Concentration 38
4.1.4 Total Radionuclide Activity 42
4.2 Salado Flow 48
4.3 Cuttings, Cavings, and Spallings 51
4.3.1 Cuttings and Cavings 52
4.3.2 Spallings 53
4.4 Direct Brine Release Volumes 57
4.5 Mobilized Radionuclide Concentrations 61
4.6 Salado Transport 62
4.7 Culebra Flow and Transport 64
4.8 Releases by Release Mechanism 70
4.8.1 Cuttings and Cavings Releases 70
4.8.2 Spallings Releases 73
4.8.3 Direct Brine Releases 76
4.8.4 Culebra Releases 79
4.8.5 Total Releases 84
4.8.6 Sensitivity Analysis for Total Releases 87
4.9 Comparison to EPA analysis 90

5.0 ADDITIONAL ANALYSES 95

5.1 Homogeneous Waste Loading 95
5.2 Replacement Panel Performance 95

Information Only

6.0 SUMMARY 97

7.0 REFERENCES..... 99

Information Only

LIST OF TABLES

Table 2-1. Iron, Lead, and CPR Inventories (PAIR-2018 and PAIR-2022) 5
Table 2-2. Repository Model Parameters updated in the RPPCR 8
Table 2-3. Culebra Release Point Coordinates (Bethune 2023) 14
Table 2-4. Updated Drilling Parameters for the RPPCR (Brunell 2023) 15
Table 3-1. Panel Groups in the RPPCR BRAGFLO Grid (Hansen et al. 2023a) 20
Table 3-2. BRAGFLO Modeling Scenarios for the RPPCR (King 2023) 21
Table 3-3. DBR Scenarios (Docherty and King 2023) 26
Table 3-4. Lumped and Represented Radionuclides (Kim 2023) 27
Table 3-5. Panel Neighbor Relationships for RPPCR (Hansen et al. 2023a) 30
Table 3-6. Panel Neighbor Relationships for CRA-2019 31
Table 3-7. WIPP PA Codes Used for the RPPCR (Long 2023) 33
Table 4-1. Half-lives of important WIPP Radionuclides 35
Table 4-2. WIPP CH- and RH-TRU Waste Streams by Total Scaled Volume from RPPCR Inventory (Kicker 2023b) 36
Table 4-3. WIPP CH- and RH-TRU Waste Streams by Total EPA Units (calendar year 2083) from RPPCR Inventory (Kicker 2023b) 37
Table 4-4. WIPP CH- and RH-TRU Waste Streams by Total EPA Units (calendar year 12083) from RPPCR Inventory (Kicker 2023b) 38
Table 4-5. WIPP CH- and RH-TRU Waste Streams Ordered by Concentration at Closure (Calendar Year 2083) from RPPCR Inventory (Kicker 2023b) 40
Table 4-6. WIPP CH- and RH-TRU Waste Streams Ordered by Concentration at 10,000 Years after Closure (Calendar Year 12083) from RPPCR Inventory (Kicker 2023b) 42
Table 4-7. Highest Activity Isotopes in WIPP CH- and RH-TRU Waste at Closure and After 10,000 Years (Kicker 2023b) 45
Table 4-8. Fraction of Realizations with more than 10% of Initial Iron Remaining Uncorroded After 10,000 Years (King 2023) 51
Table 4-9. Cavings Area Statistics for the RPPCR and CRA-2019 (Kicker 2023a) 53
Table 4-10. Intrusion Scenarios used in Calculating Direct Brine and Spallings Releases (Kicker 2023a) 54
Table 4-11. Summary Spallings Results by Intrusion Scenario (Kicker 2023a) 54
Table 4-12. Summary Spallings Results by Intrusion Location (Kicker 2023a) 55
Table 4-13. DBR Volume Summary (Docherty and King 2023) 58
Table 4-14. Number of the Screened-in Vectors (Kim 2023) 63

Information Only

Table 4-15. Mean Cumulative Lumped Radionuclides Discharges (in EPA Units) Through a Borehole to the Culebra at 10,000 Years (Kim 2023) 64

Table 4-16. Statistics on the Three-Replicate Mean for Total Releases 87

Table 4-17. Stepwise Ranked Regression Analysis for Mean Total Releases for Replicate 1 of the CRA-2019 and RPPCR Analyses 89

Table 4-18. Stepwise Ranked Regression Analysis for Mean Total Releases for Replicate 2 of the CRA-2019 and RPPCR Analyses 89

Table 4-19. Stepwise Ranked Regression Analysis for Mean Total Releases for Replicate 3 of the CRA-2019 and RPPCR Analyses 90

Table 4-20. Borehole Plugging Pattern Parameters 91

Table 4-21. Colloid Enhancement Parameters 92

Table 4-22. Baseline Solubility Parameters 93

Table 4-23. Statistics on the Overall Mean for Total Releases 94

Information Only

LIST OF FIGURES

Figure 2-1. Current Repository Footprint and Proposed Replacement and Additional Waste Panels 7

Figure 2-2. Legacy Porosity Response Surface from Figure 3-9 of Vignes et al. (2023) 10

Figure 2-3. RPPCR Porosity Response Surface from Figure 3-8 of Vignes et al. (2023).....11

Figure 2-4. Culebra Release Point Locations 13

Figure 3-1. BRAGFLO Grid for the RPPCR with Modeled Area Descriptions (King 2023).....19

Figure 3-2. CRA-2019 DBR Grid with Simulated Intrusion Locations (Docherty and King 2023) 23

Figure 3-3. RPPCR DBR Grid with Simulated Intrusion Locations (Docherty and King 2023)..24

Figure 3-4. Transfer of Initial Pressure and Saturation from the BRAGFLO Salado Flow Grid to the DBR Grid (Docherty and King 2023).....25

Figure 4-1. CCDFs for Waste Stream Concentration in an Intersected Waste Stream, EPA Units per m^3 at Closure (Calendar Year 2083) from Figure 1 of Kicker (2023b).....39

Figure 4-2. CCDFs for Waste Stream Concentration in an Intersected Waste Stream at 10,000 Years after Closure (Calendar Year 12083) (Kicker 2023b) 41

Figure 4-3.Total Activity in EPA Units (top) and Curies (bottom) for WIPP CH- and RH-TRU Waste from Closure to 10,000 Years After Closure (Kicker 2023b) 43

Figure 4-4. Overall Activity Concentrations in WIPP CH- and RH-TRU Waste from Closure to 10,000 Years After Closure (Kicker 2023b).....44

Figure 4-5. Total Activity in EPA Units (top) and Curies (bottom) for Dominant Isotopes in WIPP CH and RH-TRU Waste from Closure to 10,000 Years (Kicker 2023b) 47

Figure 4-6. Mean Brine Saturation in the Waste Panel (King 2023).....49

Figure 4-7. Mean Brine Pressure in the Waste Panel (King 2023).....49

Figure 4-8. Mean Cumulative Total Gas Generation (King 2023).....50

Figure 4-9. Mean Cumulative Brine Flow up the Borehole (King 2023).....50

Figure 4-10. Mean Waste Panel Porosity (King 2023).....51

Figure 4-11. Cuttings and Cavings Area as a Function of Waste Shear Strength for RPPCR (Kicker 2023a) 52

Figure 4-12. Cumulative Frequency of Spallings Volume in the RPPCR and the CRA-2019 (Kicker 2023a) 56

Figure 4-13. Spallings Concentration from Closure to 10,000 Years (Kicker 2023a) 56

Figure 4-14. Release Volume Frequency, All Non-zero Releases (Docherty and King 2023).....59

Figure 4-15. Release Volume Frequency, L, M, and U Non-zero Releases Only (Docherty and King 2023) 59

Information Only

Figure 4-16. Release Volumes, All Non-zero Releases (Docherty and King 2023) 60
Figure 4-17: Release Volumes by Scenario, All Non-zero Releases (Docherty and King 2023) .60
Figure 4-18. Log10 of the Solubility for the Lumped Radionuclides in Castile Brine (Kim 2023) 61
Figure 4-19. Means Radionuclide Concentrations of Lumped and Total Actinides in 33,804 m^3 Castile Brine over Time (Kim 2023) 62
Figure 4-20. Total Activity Concentration in Castile Brine vs Time for 3 Replicates (Kim 2023) 62
Figure 4-21. Particle Travel Paths and Travel Time to the LWB Exceedance Probabilities, Full Mining Scenario (Bethune 2023).....65
Figure 4-22. Particle Travel Paths and Resultant Travel Time to the LWB Exceedance Probabilities, Partial Mining Scenario (Bethune 2023) 66
Figure 4-23. Exceedance Probabilities of Cumulative Mass Discharge to the LWB by 10,000 Years by Release Point (rows) and Radionuclide (columns), Full Mining Scenario (Bethune 2023) 68
Figure 4-24. Exceedance Probabilities of Cumulative Mass Discharge to the LWB by 10,000 Years by Release Point (rows) and Radionuclide (columns), Partial Mining Scenario (Bethune 2023) 69
Figure 4-25. Cuttings and Cavings Releases for Replicate 1 of the RPPCR.....71
Figure 4-26. 3-Replicate Mean CCDFs for Cuttings and Cavings Release Volumes 72
Figure 4-27. Three-Replicate Mean CCDFs for Waste Volume in Cuttings and Cavings Release Volumes 72
Figure 4-28. Three-Replicate Means for Cuttings and Cavings Releases with Confidence Limits 73
Figure 4-29. Three-Replicate Mean CCDFs for Spallings Volumes.....74
Figure 4-30. Three-Replicate Mean CCDFs for Waste Volume in Spallings Volumes.....74
Figure 4-31. Spallings Releases for Replicate 1 of the RPPCR 75
Figure 4-32. Three-Replicate Means for Spallings Releases with Confidence Limits.....76
Figure 4-33. Three-Replicate Mean CCDFs for Direct Brine Volumes.....77
Figure 4-34. Three-Replicate Means for Direct Brine Releases with Confidence Limits.....78
Figure 4-35. Direct Brine Releases for Replicate 1 of the RPPCR 78
Figure 4-36. Radionuclide Transport to the Culebra for Replicate 1 of the RPPCR.....80
Figure 4-37. Three-Replicate Means for Radionuclide Transport to the Culebra with Confidence Limits 80
Figure 4-38. Releases from the Culebra for Replicate 1 of the RPPCR.....81

Information Only

Figure 4-39. Total Releases to and from the Culebra by Radionuclide for the CRA-2019 (Three-Replicate Means) 81
Figure 4-40. Releases to and from the Culebra by Radionuclide for the RPPCR (Three-Replicate Means)....82
Figure 4-41. Radionuclide Releases from the Culebra by Release Point for the RPPCR (Three-Replicate Means) 83
Figure 4-42. Three-Replicate Means for Transport Releases from the Culebra with Confidence Limits 84
Figure 4-43. Total Releases for Replicate 1 of the RPPCR....85
Figure 4-44. 3-Replicate Means for Release Components for the CRA-2019 85
Figure 4-45. Three-Replicate Means for Release Components for the RPPCR....86
Figure 4-46. Confidence Limits on the Three-Replicate Mean for Total Releases 86
Figure 4-47. Total Mean Releases from the RPPCR and CRA19_COMB 94

Information Only

1.0 INTRODUCTION

The Waste Isolation Pilot Plant (WIPP), located in southeastern New Mexico, has been developed by the U.S. Department of Energy (DOE) for the geologic (deep underground) disposal of transuranic (TRU) waste. Containment of TRU waste at the WIPP is regulated by the U.S. Environmental Protection Agency (EPA) according to the regulations set forth in Title 40 of the Code of Federal Regulations (CFR), Part 191 (U.S. EPA 1993).

The DOE demonstrates compliance with the containment requirements according to the Certification Criteria in 40 CFR Part 194 (U.S. EPA 1996) by means of performance assessment (PA) calculations. The WIPP PA calculations estimate the probability and consequence of potential radionuclide releases from the repository to the accessible environment for a regulatory period of 10,000 years after facility closure. PA models and input parameters are modified and refined with improved information regarding important WIPP features, events, and processes. Planned changes to the repository and/or the components therein also result in updates to WIPP PA models.

As currently certified, the WIPP includes ten panels for waste emplacement. Due to a loss of capacity, not all of the volume of the ten panels will be used for waste disposal. The DOE plans to submit a Planned Change Request (PCR) to excavate two panels, termed replacement panels, to provide an equivalent disposal capability, and may consider excavating up to seven panels beyond the two replacement panels, defined here as additional panels, to provide the additional disposal capacity needed to reach the legislated WIPP waste volume limit (Hansen 2020). The Replacement Panels Planned Change Request (RPPCR) PA was executed to quantify the long-term performance of the repository with the replacement and additional panels in support of the PCR submittal. The RPPCR PA is detailed in the analysis plan AP-204 (Hansen et al. 2023a). Within this report RPPCR refers to the PA, not to the complete Planned Change Request.

This report summarizes the methods and results of the RPPCR. Results of the RPPCR are primarily compared to the results of the 2019 Compliance Recertification Application PA (CRA-2019) to assess repository performance in terms of the most recent regulatory submittal. Changes from the CRA-2019 PA that are incorporated into the RPPCR PA including inventory updates, updates related to the replacement and additional panels, updates due to new information and model revisions since the CRA-2019 PA, and updates to the PA codes and computing platform are detailed in Section 2.0. Select RPPCR results are also compared to the 2021 Additional Panels Performance Assessment (APPA) (Hansen 2020; Brunell et al. 2021) to isolate the impact of the increased repository volume. Mean CCDFs of total releases from the RPPCR are also compared to total releases from the EPA's CRA19_COMB analysis (U.S. EPA 2022a).

Information Only

This page intentionally left blank.

Information Only

2.0 CHANGES SINCE THE CRA-2019 PA

This section describes the differences between the CRA-2019 PA and the RPPCR PA.

The RPPCR includes the following updates to models and parameters based on new or revised information:

- The repository inventory is based on the 2022 Performance Assessment Inventory Report.
- Actinide mobilization and colloidal calculations are updated with the new thermodynamic database and inventory parameters.
- The actinide oxidation state model is extended to accommodate actinide-specific oxidation state distributions.
- Iron surface area is calculated with the iron inventory rather than projected inventory based on optimal loading.
- The BRAGFLO porosity surface is updated with a new model of creep closure.
- Castile brine reservoir porosity and pore volume are updated based on a reassessment of WIPP-12 data.
- The upper bound of the borehole permeability parameter distribution is updated.
- Culebra T-fields are recalibrated with additional observation data and an updated calibration method.
- Drilling frequency and borehole plugging patterns are updated with new data.

Additional changes are made to accommodate the new waste panels, including:

- Updates to repository area and volume parameters.
- An update to waste area pressure at time of closure with the new waste storage volume.
- Additions to the computational grid of the BRAGFLO repository flow model for the new waste panel regions.
- A new waste region added to the BRAGFLO direct brine release model.
- Additional mass release points added to the SECOTP2D Culebra transport models to simulate mass discharge from the additional panels.
- New panel neighboring relationships added to the CCDFGF software. New panel groups are defined to associate releases to the Culebra with the new Culebra mass release points.

Finally, the PA software is updated to accommodate the migration to a new computing platform.

The APPA analysis included those changes related to the new waste panels in the BRAGFLO models and the updated repository parameters. The APPA did not include updates to the Culebra flow or transport models.

Many updates in this section involve WIPP PA parameters. WIPP PA parameters are defined by a unique material and property pair. By convention, these parameters are written in all upper case with the material and property separated by a colon (i.e. MATERIAL:PROPERTY). Parameter definitions, values, distributions, and units can be found in Kim and Feng (2023).

Information Only

2.1 Updates to the Inventory

The Land Withdrawal Act (LWA) legislated waste capacity of WIPP is 175,564 m^3 (U.S. Congress 1992, U.S. Congress 1996). The CRA-2019 inventory was scaled up to the full legislated volume of WIPP (Van Soest 2018). The APPA analysis used the same inventory as the CRA-2019.

The RPPCR waste inventory is based on the 2022 Annual Transuranic Waste Inventory Report (U.S. DOE 2022a) and is detailed in the Performance Assessment Inventory Report (PAIR) - 2022 (Van Soest 2022). For the RPPCR PA analysis, radionuclides in each waste stream have been subjected to radioactive decay and ingrowth through the closure date of 2083. The inventory data has been scaled up to a full repository assuming that a full repository would contain a volume of waste equal to the LWA volume limit, consistent with previous performance assessments. The increased waste storage volume from the new panels, discussed in Section 2.3, increases the physical volume where waste can be emplaced but does not increase the volume of the waste emplaced in the repository.

For the CRA-2019, waste container volumes are based on the outermost container. In contrast, the innermost waste container is used for the RPPCR container volume (Kicker 2023c, Table 1; NMED 2023). Also, the amount of surplus plutonium approved for disposal at WIPP has increased (Van Soest 2022). Finally, the assumed closure date of the repository moved from 2033 to 2083. With these changes, the activity of the inventory at closure increases to 6.51×10^6 Ci in RPPCR from 6.14×10^6 Ci in the CRA-2019.

The mass of most waste and packaging materials has also increased. The mass of iron-based metals in the inventory has increased from 6.31×10^7 kg in the CRA-2019 to 7.47×10^7 kg in the RPPCR (Table 2-1). Iron-based metals provide the reactants that reduce radionuclides to lower oxidation states. During the CCA, the anticipated quantity of iron was 2.0×10^7 kg. With the RPPCR iron inventory at 7.47×10^7 kg, the existing panels in the south half of the repository and the replacement and additional panels in the west half of the repository are expected to separately meet the minimum 2.0×10^7 kg of iron anticipated to be emplaced in the CCA. In Appendix WCL and Appendix WCA of the 1996 Compliance Certification Application (CCA), it was noted that the anticipated quantity of these metals to be emplaced in the WIPP is two to three orders of magnitude in excess of the quantity required to assure reducing conditions. Hence, the iron mass in the inventory for the RPPCR PA is also sufficient to maintain reducing conditions in the RPPCR.

Appendix WCL of the CCA also sets a maximum emplacement mass of cellulose, plastic, and rubber (CPR) at 2.0×10^7 kg. This maximum limit is based on the expected MgO emplacement at the time of the CCA and ensures a sufficient quantity of MgO to react with the CO_2 produced from the degradation of CPR material. Since the CCA, an MgO excess factor (sometimes referred to as an MgO safety factor) has been defined to scale the MgO emplaced with the CPR material emplaced (Marcinowski 2004; U.S. EPA 2004). The MgO excess factor has made the CCA Appendix WCL limit on CPR obsolete. For the RPPCR, the total mass of CPR material in the inventory is 2.14×10^7 kg (Table 2-1). With the MgO excess factor, the MgO emplaced will be sufficient to react all CO_2 produced from the CPR mass in the RPPCR.

Information Only

Table 2-1. Iron, Lead, and CPR Inventories (PAIR-2018 and PAIR-2022)

Material	PAIR-2018 (CRA-2019) (kg)	PAIR-2022 (RPPCR) (kg)
Iron	6.31E+07	7.47E+07
Lead	1.38E+07	1.04E+07
Cellulose	5.96E+06	7.17E+06
Plastics	1.06E+07	1.29E+07
Rubber	1.22E+06	1.32E+06
Total CPR	1.78E+07	2.14E+07

Since the CRA-2019, four new shielded container variants were added to the payload containers for WIPP waste (U.S. DOE 2023). The 2022 ATWIR (U.S. DOE 2022a) includes the use of these containers. In response to the Planned Change Notice on the additional shielded container variants, the EPA raised concerns about an increase in both steel and lead from the container use and expressed an expectation that the effects on surface area calculations for both steel and lead would be evaluated (U.S. EPA 2023).

The updated iron surface area calculation described in Section 2.5 accounts for iron corrosion of the new shielded containers without additional changes to the iron corrosion model. Compared to the CRA-2019 inventory, the mass of lead has decreased from 1.38×10^7 kg to 1.04×10^7 kg (Table 2-1). In the CRA-2019 completeness comment CC5-SCR-9 response, it was shown that gas generation from lead corrosion can be screened out of the WIPP PA calculation based on low consequence (U.S. DOE 2021). The CC5-SCR-9 response calculation assumed that all lead in the repository was in the original SC-30G1 containers and, much like the updated iron surface area calculation, converted the mass of lead into a surface area using the container dimensions. Given that the new shielded containers will increase the dimensions of the lead shielding compared to the SC-30G1, resulting in a decrease in the surface area per kilogram of lead, and given the decrease in lead mass in the inventory, the lead surface area in the RPPCR would be less than calculated for the CC5-SCR-9 response calculation. Therefore, the CC5-SCR-9 response calculation can still be considered bounding for gas generation from lead corrosion, which continues to be screened out of the PA based on low consequence.

2.2 Updates to Radionuclide Mobilization

Updates to the RPPCR affect the dissolved and colloidal source terms for the Salado flow, actinide mobilization, and Salado transport models. Baseline solubility parameters and An(III,IV) solubility uncertainty distributions (SOLMOD3:SOLVAR and SOLMOD4:SOLVAR) were updated due to changes in the inventory, thermodynamic model, and literature screening criteria (Domski 2023a, Domski 2023b).

Information Only

In the RPPCR, the oxidation state model is extended to include the behavior of the different multi-valence actinides across a range of oxidation-reduction (redox) potentials. The PA parameter database uses materials NP, PU, and U to define properties for radionuclides Np, Pu, and U respectively. New parameters (property OXCUTOFF for materials NP, PU, and U) are implemented in the RPPCR based on the recommended values from Lucchini and Swanson (2023). Plutonium is the only multi-valent actinide where the OXCUTOFF value introduces a change in the realized oxidation state. The new PU:OXCUTOFF parameter is set to 0.25, meaning 25% of realizations assume the +III state-controlled Pu solubility and 75% of realizations assume the +IV state-controlled Pu solubility. Microbial and intrinsic colloidal enhancement parameters are also updated for the RPPCR based on Lucchini and Swanson (2023).

2.3 Additional Waste and Operations Areas

The DOE plans to excavate additional volume for waste disposal, comprising two replacement waste panels (numbered 11 and 12) and potentially seven additional panels (numbered 13 to 19) to the west of the current repository footprint (Figure 2-1, adapted from Sjomeling 2019). In the design used for this analysis, Panels 11 through 19 are similar to Panels 1 through 8, except that the abutment pillars (between the waste rooms and the access drifts) are increased from 61.0 m (200 ft) to 122.0 m (400 ft) and the isolation pillars (separating two panels) are increased from 61.0 m (200 ft) to 91.5 m (300 ft).

Five access drifts running east-west connect the new panels with the rest of the repository. Unlike the access drifts in the south that comprise Panel 10, there is no plan to place waste in the west access drifts. There are no plans for panel closures between the new western drifts and the existing operations and experimental areas (Sjomeling 2019).

The computational grids for flow in the Salado (Section 3.2.1) and for direct brine release (DBR) (Section 3.5.1) are updated to account for the new panels. The logic for assigning panel neighboring is also extended to account for the new panels (Section 3.9.1).

Information Only

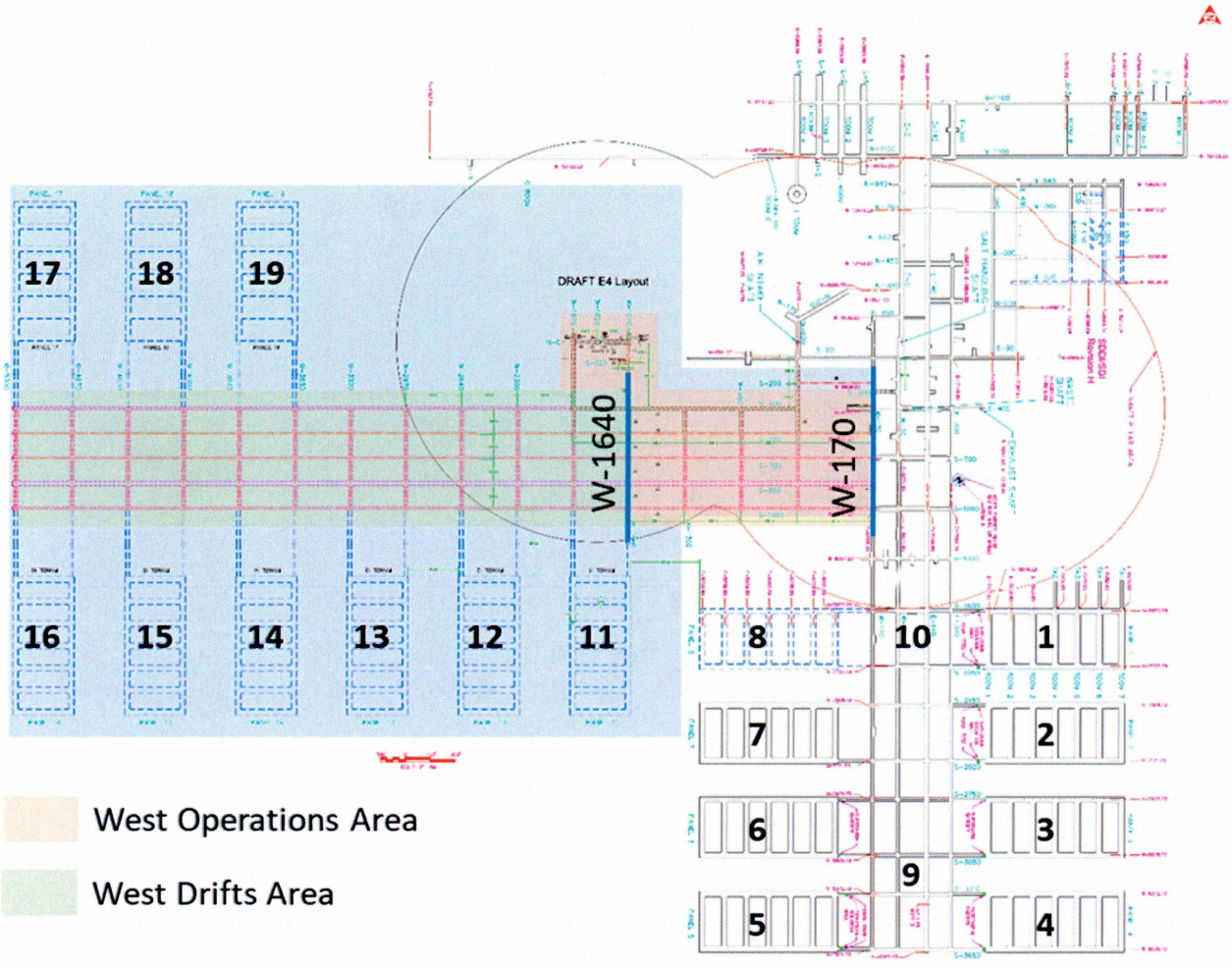

Figure 2-1. Current Repository Footprint and Proposed Replacement and Additional Waste Panels

2.4 Changes to Repository Parameters

The repository model parameters for waste storage volume (REFCON:VREPOS), the area of the berm placed over the waste panels (REFCON:ABERM), the area of contact-handled (CH) waste disposal (REFCON:AREA_CH), and the fraction of the repository volume occupied by CH waste (REFCON:FVW) have been updated (Table 2-2).

Information Only

Table 2-2. Repository Model Parameters updated in the RPPCR

Material	Property	Description	CRA-2019 Value	RPPCR Value	Units
REFCON	VREPOS	Excavated storage volume of the repository	438,406.08	853,284.89	m^3
REFCON	ABERM	Area of the berm placed over waste panels	628,500	1,268,303	m^2
REFCON	AREA_CH	Area for contact-handled (CH) waste disposal	111,500	216,952	m^2
REFCON	FVW	Fraction of the repository volume occupied by waste	0.385	0.197	-

2.5 Changes to Iron Surface Area Calculation

One factor in the rate of gas generation from iron corrosion is the initial surface area of iron in the repository. In past PAs, including in the CRA-2019 PA and APPA, the surface area concentration was defined as:

$$D_s = \frac{A_d n_d}{V_r} \quad (1)$$

Where:

- D_s is the surface area concentration in m^2 (iron)/m^3 (repository volume),
- A_d is the surface area of iron associated with a waste disposal drum (parameter REFCON:ASDRUM, m^2/drum),
- n_d is the optimal number of waste drums that can be loaded into a single room (parameter REFCON:DRROOM), and
- V_R is the initial volume of a single room in the repository (parameter REFCON:VROOM, m^3).

Based on previous estimates (Brush 1991; Day 2015), the specified parameters result in an iron surface area concentration D_s = 11.2 m^2 (iron)/m^3 (repository volume). Given the waste storage volume (REFCON:VREPOS) for CRA-2019 of 438,406.08 m^3, a total iron surface area of 4.91 × 10^6 m^2 was used in the CRA-2019 PA.

For the RPPCR, a new approach for the iron surface area calculation is used. This approach ties the iron surface area to the iron mass in the inventory rather than to the optimal loading and volume of the repository. An estimate of the iron surface area per kilogram of iron was made based on an estimate of the iron surface area for already emplaced waste. A new parameter defining the surface area (in m^2) per kilogram of iron (REFCON:FESAPKG) is defined with a value of 0.105 m^2/kg (King 2021d). For the RPPCR, this gives a total iron surface area of 7.84 × 10^6 m^2. If this approach for the iron surface area calculation had been used in CRA-2019 PA, the total iron surface area would have been 6.62 × 10^6 m^2.

Information Only

As discussed in Section 2.1, four new shielded container variants were added for WIPP waste. The RPPCR uses a single iron surface area to account for iron corrosion of all containers and waste materials. The updated iron surface area calculation uses the mass of iron in the inventory and an average mass to square meter conversion factor. Steel thickness in the new shielded containers ranges from a nominal 0.625 in to 4.5 in (0.01588 m to 0.1143 m), much larger than the average steel thickness of 0.05 inches (0.00122 m) used in the surface area calculation. Consequently, the surface area per kilogram of the new shielded containers would be much less than the 0.105 m^2/kg value currently defined (REFCON:FESAPKG). A higher value of surface area per kilogram would give a higher surface area and a conservatively higher iron corrosion rate. The new shielded containers are a small fraction of all waste containers, thus, using the current value of 0.105 m^2/kg for the surface area calculation results in a slightly conservative simplification for the iron corrosion model.

2.6 Changes to Repository Pressure at Closure

Microbial biodegradation of CPR materials occurs at a high initial rate with a lower long-term rate (Nemer et al. 2005). The long-term rate is modeled in the PA calculation. The initial high rate of degradation is accounted for by setting the initial pressure at repository closure above atmospheric pressure.

The increase in initial pressure is calculated with the ideal gas law and dependent on the waste storage volume. Therefore the new waste storage volume requires an update to this pressure. A methodology for calculating initial pressure is set forth in Nemer et al. (2005). Since the CPR inventory changes frequently, a dynamic calculation for the increase in pressure above atmospheric is added to the ALGEBRACDB1 step of the Salado flow calculation. To do this the CAVITY_1 and CAVITY_2 PRESSURE values are redefined as atmospheric pressure (101,325 Pa), and a new parameter named WAS_AREA:EGRATMIC is defined for the moles of gas generated per kilogram of CPR from early-time biodegradation (King 2021c). With these new parameters, and the updated CPR inventory, the initial waste area pressure for the RPPCR is 1.16×10^5 Pa. The initial pressure in the CRA-2019 was 1.28×10^5 Pa.

2.7 Update to the Porosity Surface

The creep closure of the salt onto the waste is simulated in detail with a geomechanical model. This detailed model is executed with each of a range of gas generation functions (called f-curves) to produce a set of output pressures and porosities in the repository. This set of outputs is made into a response surface for porosity as a function of time and pressure. This response surface function is used in the Salado flow calculation to model the effects of creep closure in the waste area on fluid flow in and around the repository. The response surface used in the Salado flow model is updated based on the new disposal room porosity model by Vignes et al. (2023).

The legacy porosity response surface used in the CRA-2019 is shown in Figure 2-2. The updated response surface used in the RPPCR is shown in Figure 2-3. Of note for the Salado flow solution, at low pressures the porosity is lower for the RPPCR as compared to the CRA-2019. The two porosity surfaces have different shapes that will lead to different behaviors in the Salado flow simulations. Qualitatively, adding gas (going to higher f-curves) tends to have a response in both

Information Only

pressure and porosity in the legacy surface. In the new surface, the primary response of adding gas below the range of lithostatic pressure of about 15 MPa is to raise the pressure. Once the pressure is close to lithostatic, adding gas will primarily result in an increase to porosity. See Vignes et al. (2023) for a discussion on the development of the new porosity response surface and see Section 4.2 and King (2023) for a discussion of the effect on the Salado flow results.

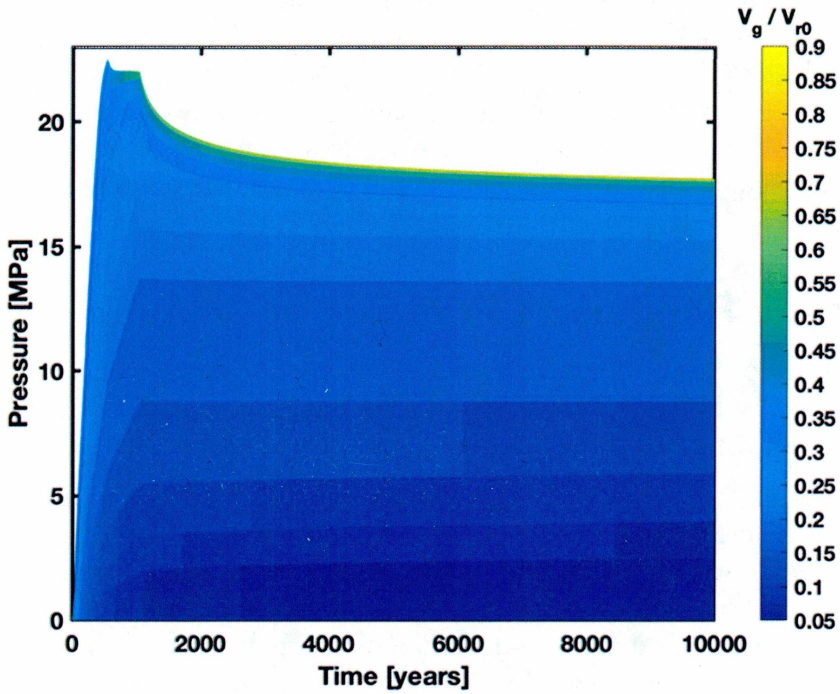

Figure 2-2. Legacy Porosity Response Surface from Figure 3-9 of Vignes et al. (2023)

Information Only

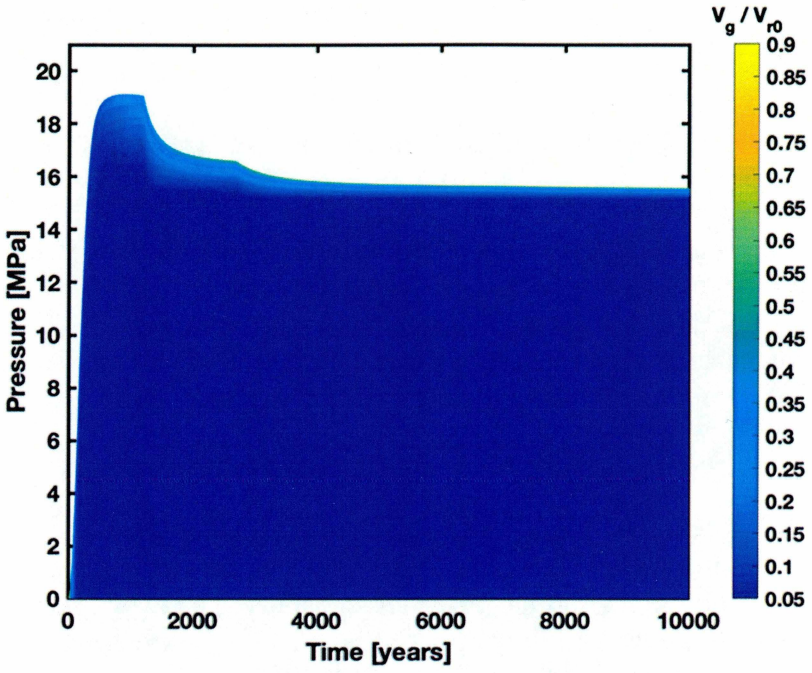

Figure 2-3. RPPCR Porosity Response Surface from Figure 3-8 of Vignes et al. (2023)

2.8 Updates Related to the Castile Brine Reservoir

2.8.1 Salado Flow Model

Gross and Gjerapic (2022) observed that brine flow and well pressures from two wells (WIPP-12 and ERDA-6) that produced brine from the Castile were better described by a two-domain hydrogeologic model. Their fitted model predicts a somewhat smaller upper bound for the Castile reservoir pore volume than was used in the CRA-2019. Docherty (2023a) further investigated the Castile reservoir model representation in BRAGFLO, recommending an extended representation of the reservoir in the BRAGFLO grid as shown in Figure 3-1 (Section 3.2.1). The modeled porosity of the Castile (based on the sampled rock compressibility CASTILER:COMP_ROCK) is updated for this updated grid volume and the maximum pore volume from Gross and Gjerapic (2022).

2.8.2 Probability of Intrusion

Time Domain Electromagnetic (TDEM) sounding data is used to derive a probability of encountering pressurized brine in the Castile Formation under the WIPP repository (WIPP PA parameter GLOBAL:PBRINE). Zeitler (2023b) examined the existing TDEM data and found that it adequately covers the replacement panels, numbers 11 and 12, for which the DOE is seeking approval, and thus the existing GLOBAL:PBRINE distribution is adequate for the replacement panels. The existing GLOBAL:PBRINE distribution is also used for the additional panels 13 to

Information Only

19. As noted in Section 2.13, a small change to the GLOBAL:PBRINE distribution is made to ensure a full range of probabilities is defined.

2.9 Permeability of a Borehole after Plug Failure and Degradation

In the CRA-2019, the base 10 log of the permeability of a borehole after plug failure and degradation of borehole materials (material BH_SAND, properties PRMX_LOG, PRMY_LOG, PRMZ_LOG) was specified as a uniform distribution between −16.3 and −11 log(m^2). Gjerapic et al. (2023) recommended a new upper bound for this distribution of −14 log(m^2). The RPPCR uses this recommendation, sampling the log of the borehole permeability uniformly between −16.3 and −14 log(m^2).

2.10 Update to the Culebra Transport Procedure

The CRA-2019 Culebra transport model considered only a single radionuclide mass release point above the center of the currently permitted 10-panel repository. The two replacement waste panels (numbered 11 and 12) and seven additional panels (numbered 13 through 19) extend to the west of the current repository footprint away from the CRA-2019 release point (Figure 2-4, modified from Bethune and Brunell 2022). The RPPCR includes the CRA-2019 Culebra release point (CRP1), plus three additional Culebra release points (CRP2 through CRP4) to characterize transport through the Culebra over the additional panel region (Bethune and Brunell 2022). The UTM NAD27 Zone 13N coordinates of the release points are listed in Table 2-3.

Information Only

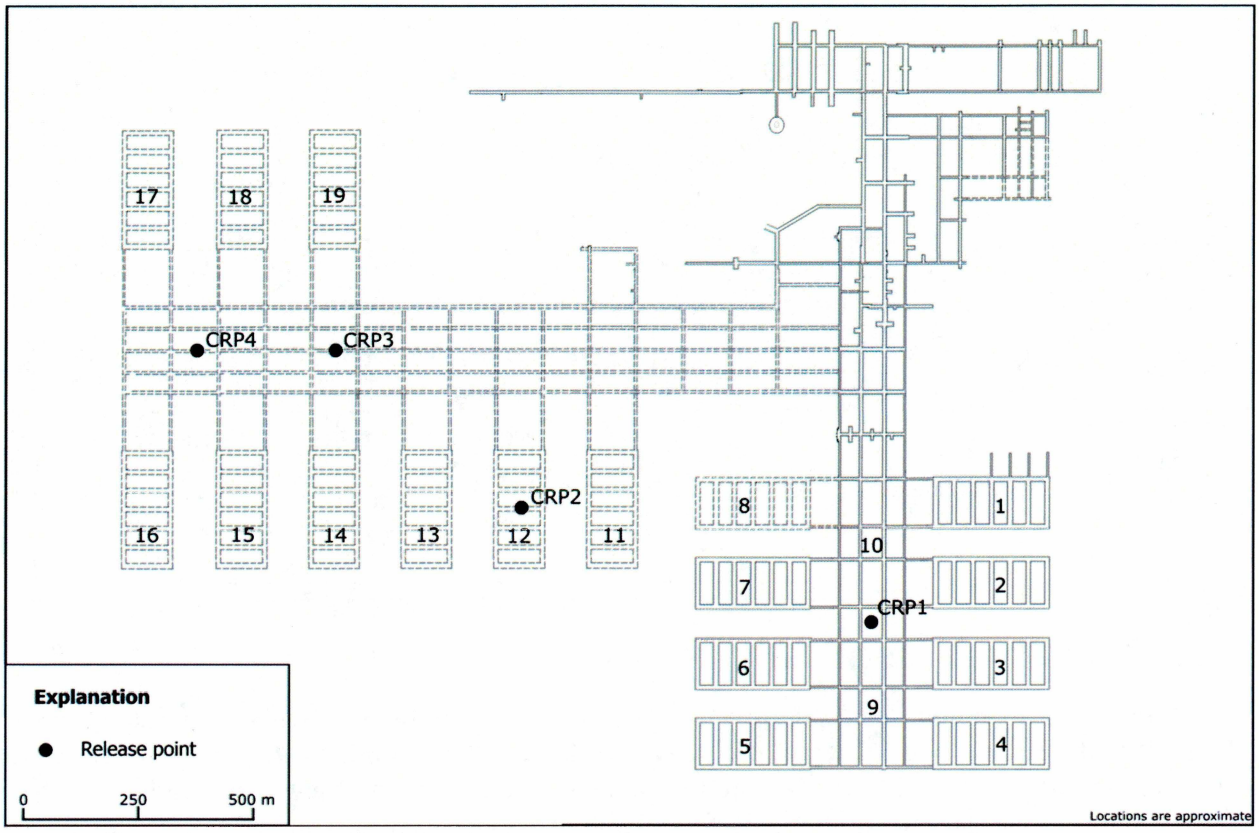

Figure 2-4. Culebra Release Point Locations

Information Only

Table 2-3. Culebra Release Point Coordinates (Bethune 2023)

Culebra Release Point	X-Coordinate (m)	Y-Coordinate (m)	Description
CRP1	613597.5	3581385.2	CRA-2019 release point, centroid of Panels 1 through 10.
CRP2	612828.3	3581621.4	New release point, centroid of Panels 11 through 13.
CRP3	612424.1	3581961.0	New release point, centroid of Panels 14 and 19.
CRP4	612120.2	3581957.6	New release point, centroid of Panels 15 through 18.

2.11 Recalibration of T-fields

The Culebra flow model incorporates spatially variable, calibrated fields of transmissivity, storativity, anisotropy, and recharge (collectively referred to as T-fields). A geostatistical model produces an ensemble of 1,000 uncalibrated parameter fields from quantitative and qualitative observations of hypothesized hydrogeologic controls (Hart et al. 2008). The T-fields used in CRA-2019 were calibrated with the Parameter ESTimation (PEST) software and MODFLOW-2000 groundwater flow simulator (Hart et al. 2009). For the RPPCR, 1,000 base T-fields are calibrated with updated steady-state and transient targets and model boundary conditions using the PEST++ Iterative Ensemble Solver (PEST++ IES) and the MODFLOW6 groundwater flow simulator (Bowman et al. 2023). The calibrations were evaluated on their ability to recreate observed head data, and the best 100 calibrations were selected for use in the RPPCR (Bowman et al. 2023).

2.12 Updates to the Borehole Drilling Frequency and Plugging Pattern Probabilities.

WIPP regulations require that current drilling practices are assumed for future inadvertent intrusions. The DOE continues to survey drilling activity in the Delaware Basin in accordance with the criteria established in 40 CFR Part 194.33. Local well operators are surveyed annually to provide the WIPP project with information on drilling practices, Castile brine encounters, etc. Survey results through August 2022 are documented in the 2022 Delaware Basin Monitoring Annual Report (U.S. DOE 2022b). The drilling frequency parameter (GLOBAL:LAMBDAD) is updated in Brunell (2023) based on U.S. DOE (2022b).

For CRA-2019, only wells within the Designated Potash Area (DPA) were used for determining the plugging pattern of wells modeled in the performance assessment (Day 2023). The EPA disagreed with this approach in their review of the CRA-2019 (U.S. EPA 2022c). An alternative approach using a nine-township area surrounding the WIPP site was proposed (Day 2023) and found acceptable by the EPA (Santillan 2023). The probabilities of wells having one-, two-, and

Information Only

three-plugs have been updated for the RPPCR with the data from Day (2023). Brunell (2023) translated the information from Day (2023) into PA parameters. Table 2-4 summarizes the updated drilling frequency (described as drilling rate) and plugging pattern probabilities used in the RPPCR.

Table 2-4. Updated Drilling Parameters for the RPPCR (Brunell 2023)

Material	Property	Description	Units	CRA-2019 Value	RPPCR Value
GLOBAL	LAMBDAD	Drilling rate per unit area.	km^{-2} yr^{-1}	0.0099	0.01389
GLOBAL	ONEPLG	Probability of having Plug Pattern 1 (full plug).	(-)	0.403	0.366
GLOBAL	TWOPLG	Probability of having Plug Pattern 2.	(-)	0.331	0.430
GLOBAL	THREEPLG	Probability of having Plug Pattern 3.	(-)	0.266	0.204

2.13 Sampling of Uncertain Parameters

Uncertain parameters are sampled with the code LHS version 3.00 in the RPPCR. With the migration of LHS to the GNU Fortran compiler on the CentOS platform (Long and King 2022), the seeded random number generator used by previous versions of LHS no longer produces the same random samples. In order to maintain the capability to directly compare analyses, LHS 3.00 has the ability to read in a list of previously generated values instead of using the values produced by a seeded random number generator. The list of values going into LHS is the uniform 0 to 1 numbers sampled by the intrinsic random number function supplied to the LHS algorithm, it is not the sampled parameter values produced by the LHS algorithm. This allows for sampling from updated distributions that maintain the same rank ordering for each parameter vector. For the RPPCR, LHS reads a table containing the same values used in the CRA-2019 PA and in the APPA. Retaining these same values enables direct comparison of the RPPCR to these previous analyses.

Four parameter distributions are changed for the RPPCR. The RPPCR calculations include an updated upper bound to the parameter distribution assigned to the permeability of the material filling a borehole from 200 years after the drilling event (BH_SAND:PRMX_LOG) (Section 2.9). The distributions for solubility uncertainty for +III and +IV actinides (SOLMOD3:SOLVAR and SOLMOD4:SOLVAR) are updated based on the thermodynamic model changes and new literature screening as described in Section 2.2 (Domski 2023a; Domski 2023b). An error was found and corrected in the PRELHS code where user supplied distributions were not forced to start at the assumed probability of zero and an incorrect ordering could occur when parameter values were repeated (SNL 2022; Docherty 2023b). The distribution for the probability of intersecting a pressurized brine pocket (GLOBAL:PBRINE) is changed as a consequence of correcting the error found in the PRELHS code. The inundated steel corrosion rate (STEEL:CORRMCO2) parameter distribution is not changed for RPPCR; however, the sampled values changed slightly from CRA-

Information Only

2019 due to the correction of the error in the PRELHS code (see Section 2.14). An impact analysis for the PRELHS error (Docherty 2023b) determined that the errors in the LHS samples were of negligible effect.

The values for sampled parameters for all vectors are written to the WIPP PA Results Database (PA_Results) for use by other WIPP PA codes. Details of the values of parameters used for RPPCR calculations are found in Kim and Feng (2023). Details of the LHS parameter sampling for the RPPCR can be found in Zeitler (2023a).

2.14 Hardware and Computational Code Updates

As discussed in Section 2.13, the LHS and PRELHS codes are updated for the RPPCR. The PRECCDFGF and CCDFGF codes are also updated in order to accommodate the additional panels, the additional panel neighboring relationships, and the additional Culebra release points.

MODFLOW6 and PEST++ IES were used to recalibrate the T-fields, as described in Section 2.11. MODFLOW6 is also used for the mining-modified Culebra flow simulations in the RPPCR, as described in Section 3.8. The PRESECOTP2D code is updated to read the MODFLOW6 output files. The PANEL code is also updated for the RPPCR to utilize the updated oxidation state model described in Section 2.2.

The RPPCR was executed on the WIPP PA HPC/Linux Cluster, which consists of Dell PowerEdge C6420 hardware running CentOS7 (Long 2020; Long and King 2022). Calculations for the CRA-2019 PA are performed on the WIPP PA Solaris Cluster, which consisted of Intel hardware running the Solaris operating system (Long 2019).

Information Only

3.0 METHODOLOGY FOR THE RPPCR

The WIPP PA calculations estimate the probability and consequence of potential radionuclide releases from the repository to the accessible environment for a regulatory period of 10,000 years after facility closure. The WIPP repository might be disturbed by exploratory drilling for natural resources during the 10,000-year regulatory period. Drilling could create additional pathways for radionuclide transport, especially in the Culebra, and could release material directly to the surface. In addition, mining for potash within the Land Withdrawal Boundary (LWB) might alter flow in the overlying geologic units and may locally accelerate transport through the Culebra. The disturbed scenarios used in PA modeling capture the range of possible releases resulting from drilling and mining (Brunell et al. 2021).

The PA methodology accommodates both aleatory (i.e., stochastic) and epistemic (i.e., subjective) uncertainty in its constituent models. Aleatory uncertainty pertains to unknowable future events such as intrusion times and locations that may affect repository performance. It is accounted for by the generation of random sequences of future events. Epistemic uncertainty concerns parameter values that are assumed to be constants; the constants' true values are uncertain due to a lack of knowledge about the system. An example of a parameter with epistemic uncertainty is the permeability of a material. Epistemic uncertainty is accounted for by sampling parameter values from assigned distributions using Latin Hypercube Sampling. One set of all sampled values required to run a WIPP PA calculation is termed a vector. Each set of 100 samples (e.g., the set of 100 vectors) is termed a replicate, and three sets of 100 samples (e.g., three replicates) are used in a full WIPP PA analysis. For each vector, 10,000 possible sequences of future events (e.g., futures) are simulated to address aleatory uncertainty. The releases for each of the 10,000 simulated futures are tabulated for each of the 100 vectors in each of the 3 replicates, totaling 3,000,000 possible futures (Helton et al. 1998).

For a random variable, the complementary cumulative distribution function (CCDF) provides the probability of the variable being greater than a particular value. By regulation, PA results are presented as a distribution of CCDFs of releases (U.S. EPA 1996). Each individual CCDF summarizes the likelihood of releases across all futures for one vector of parameter values. The uncertainty in parameter values results in a distribution of CCDFs.

3.1 Review of FEPs and Conceptual Models

A Features, Events, and Processes (FEPs) assessment was performed for the RPPCR, according to SP 9-4. The assessment determines if any of the changes implemented in this analysis affect current baseline FEP screening arguments or decisions. The FEPs assessment found that no changes to the FEP baseline were warranted (Kirkes 2023).

The RPPCR conceptual models are unchanged from those of the APPA. The primary differences between the RPPCR and the APPA are:

- The revised inventory and related parameters.
- The procedure for computing releases through the Culebra.
- Changes identified as related to new information and revised models since the CRA-2019.

Information Only

These differences do not reflect changes to the conceptual models on which the RPPCR and APPA are based.

For the APPA, the conceptual models used in the PA were reviewed to identify models that are affected by the changes due to the replacement and additional waste panels (Hansen 2021). The review concluded that 3 of the 24 conceptual models were affected:

- Disposal System Geometry
- Repository Fluid Flow
- Direct Brine Release

The Additional Panels Performance Assessment (APPA) Changed Conceptual Models Peer Review examined the changes affecting these three conceptual models and concluded that the changed conceptual models provide an adequate and reasonable representation of the repository system (Falta et al. 2021).

3.2 Salado Flow

The BRAGFLO code calculates the flow of brine and gas in the vicinity of the WIPP repository over a 10,000-year regulatory compliance period. The results of these calculations are used by other codes to calculate potential radionuclide releases to the accessible environment. Changes included in the RPPCR that were observed to most substantially affect Salado flow results, as compared to the CRA-2019 PA, are (King 2023):

- Updates to the model for creep closure of the salt onto the waste.
- Updates to the long-term borehole permeability.
- Increases to the inventory activity, iron mass, and CPR mass leading to increased gas generation and brine consumption.
- A recalculation of iron surface area.
- And additional waste areas and excavated volumes.

The following subsections summarize the approach and methodology for Salado flow modeling as described by King (2023).

3.2.1 Repository Representation in BRAGFLO

The computational grid and associated material map used by BRAGFLO for the RPPCR is modified from the grid used for the CRA-2019 PA to accommodate the additional excavated areas (King 2023). The five new east-west main drifts and their connecting cross drifts have been modeled as two new regions called the West Operations Area and West Drifts. These two new areas are modeled with the same properties as the Operations Area in the CRA-2019. A new waste area called the West Rest-of-Repository has been added to the grid to account for the additional waste Panels 11 through 19. The West Rest-of-Repository has the volume of 9 standard waste panels and is separated from the other excavated regions by a panel closure area representing the 100-foot Run-of-Mine Salt Panel Closure System (ROMPCS) that is expected to be emplaced in the access drifts of each panel.

Information Only

The BRAGFLO computational grid with modeled area descriptions and cell dimensions (meters) for the RPPCR is shown in Figure 3-1. Detailed material maps associated with the six modeling scenarios are further defined in Section 3.2 of King (2023).

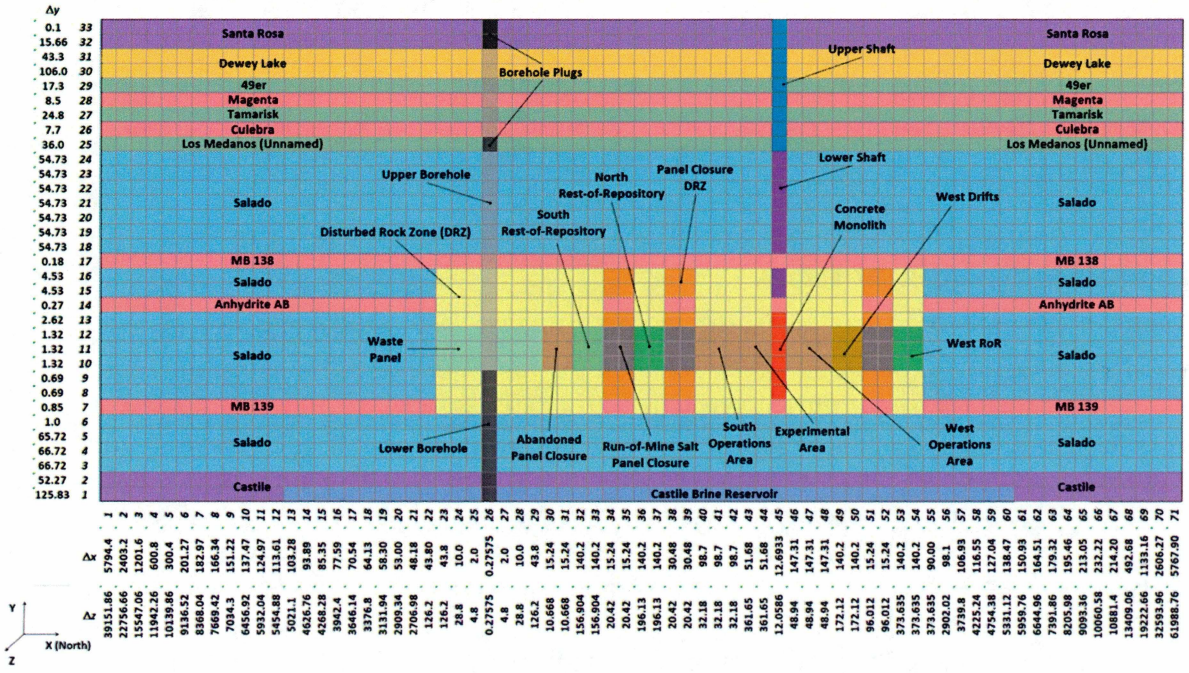

Figure 3-1. BRAGFLO Grid for the RPPCR with Modeled Area Descriptions (King 2023)

3.2.2 Panel Groups

The BRAGFLO grid (Figure 3-1) aggregates waste panels into four waste-bearing areas denoted South Waste Panel (WAS), South Rest of Repository (SRR), North Rest of Repository (NRR), and West Rest of Repository (WRR). Table 3-1 lists the panels which comprise each waste-bearing area in the BRAGFLO grid. One representative borehole is placed in the grid in the South Waste Panel area. The borehole in the South Waste Panel is considered to be a conservative representation of an intrusion into any waste panel, as the South Waste Panel tends to have higher saturation, being down dip from other panels.

Information Only

Table 3-1. Panel Groups in the RPPCR BRAGFLO Grid (Hansen et al. 2023a)

Panel Group	Repository Section	Panels in Panel Group
South Waste Panel (WAS)	South	5
South Rest of Repository (SRR)	South	3, 4, 6, 9
North Rest of Repository (NRR)	South	1, 2, 7, 8, 10
West Rest of Repository (WRR)	West	11, 12, 13, 14, 15, 16, 17, 18, 19

3.2.3 Modeling Scenarios

The six BRAGFLO modeling scenarios used in the RPPCR are unchanged from those used for the CRA-2019 PA. A single representative borehole intrusion can be used in the south repository for both south and west repository intrusions (King 2021b). Results obtained in the six scenarios are used to initialize flow and material properties in subsequent codes in the PA computational suite (e.g., in the calculation of direct brine release volumes). The scenarios include one undisturbed scenario (S1-BF), four scenarios that include a single inadvertent drilling intrusion into the repository (S2-BF to S5-BF), and one scenario investigating the effect of two intrusions into a single waste panel (S6-BF). Two types of intrusions, denoted as E1 and E2, are considered. An E1 intrusion assumes the borehole passes through a waste-filled panel and into a region of pressurized brine that may exist under the repository in the Castile formation. An E2 intrusion assumes that the borehole passes through the repository but does not encounter pressurized brine. BRAGFLO results obtained in Scenario S6-BF are only used to calculate radionuclide transport to the Culebra (Section 3.6). Table 3-2 summarizes the six scenarios used in the Salado flow calculation. A total of 1,800 separate Salado flow simulations are run (3 replicates × 6 scenarios × 100 vectors). King (2023) describes results from scenarios S1-BF, S2-BF, S4-BF, and S6-BF. Results from scenarios S2-BF and S3-BF are generally similar to each other, as are results from S4-BF and S5-BF.

Information Only

Table 3-2. BRAGFLO Modeling Scenarios for the RPPCR (King 2023)

Scenario	Description
S1-BF	Undisturbed repository.
S2-BF	E1 intrusion at 350 years.
S3-BF	E1 intrusion at 1,000 years.
S4-BF	E2 intrusion at 350 years.
S5-BF	E2 intrusion at 1,000 years.
S6-BF	E2 intrusion at 1,000 years followed by an E1 intrusion at 2,000 years.

3.3 Cuttings, Cavings, and Spallings

This section describes the calculations of the volume of solids releases from the WIPP repository from a hypothetical intrusion borehole. The PA codes CUTTINGS_S and DRSPALL are used to calculate these volumes which include cuttings, cavings, and spallings. For more information on the solids release calculation methodology, see Kicker (2023a).

Cuttings and cavings are the solid materials removed from the repository and carried to the surface by the drilling fluid during the process of drilling a borehole. Cuttings are the materials removed directly by the drill bit and cavings are the material eroded from the walls of the borehole by shear stresses from the circulating drill fluid. The volume of cuttings and cavings material removed from a single drilling intrusion is assumed to be that of a cylinder. CUTTINGS_S calculates the area of the base of this cylinder, and cuttings and cavings results in Section 4.3 are reported in terms of these areas. The volumes of cuttings and cavings removed can be calculated by multiplying these areas with the assumed initial repository height, 3.96 m (WIPP PA parameter BLOWOUT: HREPO).

The conceptual model for spallings is documented by Lord et al. (2006, Section 3) and is implemented in the code DRSPALL. A spallings event occurs during a drilling intrusion when the repository contains gas at high pressure that causes: (1) localized shear failure of the solid material surrounding the borehole; and (2) entrainment of the failed material into and up the borehole, carried ultimately to the land surface. Calculation of the spallings volume is a two-part procedure. First, DRSPALL calculates the spallings volumes from a single drilling intrusion at four "baseline" values of repository pressure (10, 12, 14, and 14.8 MPa). Next, the code CUTTINGS_S reads the time-dependent pressure for each realization from the BRAGFLO output (Section 4.2), and linearly interpolates on the DRSPALL output to compute the spallings volume for a given intrusion time.

The DRSPALL solids release volumes from Kirchner et al. (2014) and Kirchner et al. (2015) are used in the CRA-2019 PA and the RPPCR. Individual borehole spallings volumes are a function of repository conditions (i.e., pressures in waste areas). Conservative assumptions built into

Information Only

spallings volume calculations result in overestimation of spallings volumes (U.S. DOE 2019, Appendix MASS).

3.4 Radionuclide Activities for Solid Releases

Activity in waste encountered during a hypothetical drilling event is quantified using the metric of EPA units. The activity in EPA units for a radionuclide is the initial source term activity (in Ci) of that radionuclide divided by the product of the waste unit factor (WUF) and the release limit (in Ci/unit of waste) for the same radionuclide (Sanchez et al. 1997). Release limits and the number of Ci in an EPA unit vary by radionuclide.

The activity in EPA units at each time interval for interest of each of the major radionuclides in each waste stream is calculated by the WIPP PA code EPAUNI. EPAUNI also calculates the activity of the entire waste stream in EPA units (at each of the time intervals) and the probability of encountering each waste stream during a drilling intrusion.

Ten radionuclides (^{241}Am, ^{244}Cm, ^{137}Cs, ^{238}Pu, ^{239}Pu, ^{240}Pu, ^{241}Pu, ^{90}Sr, ^{233}U, and ^{234}U) are modeled in the PA code EPAUNI. These ten radionuclides account for 99.61% of the EPA units at the time of repository closure in the RPPCR inventory. For a full description of the EPAUNI calculation, see Kicker (2023b).

3.5 Direct Brine Release Volumes

If the WIPP repository were to be penetrated by a borehole while under conditions of sufficient repository brine pressure and saturation, brine could migrate up through the intruding borehole to reach the land surface. Such an event is defined as a direct brine release (DBR). As with previous WIPP PAs, the BRAGFLO DBR analysis uses the BRAGFLO code to numerically evaluate the volumetric flux of brine that enters the borehole over the duration of the release.

Changes included in the RPPCR that are observed to affect DBR results most substantially as compared to the CRA-2019 PA are (Docherty and King 2023):

- Changes to DBR grid representation to account for new waste areas.
- Updated model for creep closure of the salt onto the waste.

Pressure and saturation from the Salado flow simulations are initial conditions in the DBR calculation. Changes in the RPPCR that affect these initial conditions strongly affect both the number of DBRs and the volume of brine released in a DBR.

3.5.1 Model Representation in BRAGFLO_DBR

The DBR numerical grid and material map used in the CRA-2019 PA calculations are shown in Figure 3-2 and the DBR numerical grid and material map used in the RPPCR calculations are shown in Figure 3-3.

The DBR numerical grid for the RPPCR takes a conceptual deviation from the CRA-2019 DBR grid. In the CRA-2019 and previous analyses, the DBR grid modeled the entire waste volume. For the RPPCR, the intruded waste panel volume and any volume not separated by a panel closure to

Information Only

the intruded waste panel are modeled; however, not all of the volume of the waste area is modeled. Analyses have shown that direct brine release volumes are primarily determined by the conditions in the intruded panel; other areas in the DBR grid have little to no effect on DBRs (Shumaker 2021). This is due to the short duration of DBR events, which results in very little communication across panel closures. Consequently, the grid volume used in the CRA-2019 to represent the NRR has been split into two regions to represent the NRR and the WRR.

In addition to the three drilling locations considered in the CRA-2019 PA, a fourth intrusion location is considered in the RPPCR. An "O" (for other) intrusion location has been added to the existing locations "U" (for upper, since it is up-dip), "M" (for middle), and "L" (for lower since it is down-dip). These intrusion locations are shown in Figure 3-3. The calculations for scenarios S2-DBR and S3-DBR (Section 3.5.3) represent a drilling intrusion preceded by an E1 intrusion in either the same or a different waste panel. The effects of a prior E1 intrusion are incorporated into the calculations by specifying pressure at a boundary condition well, denoted by the red oval in Figure 3-2 and Figure 3-3.

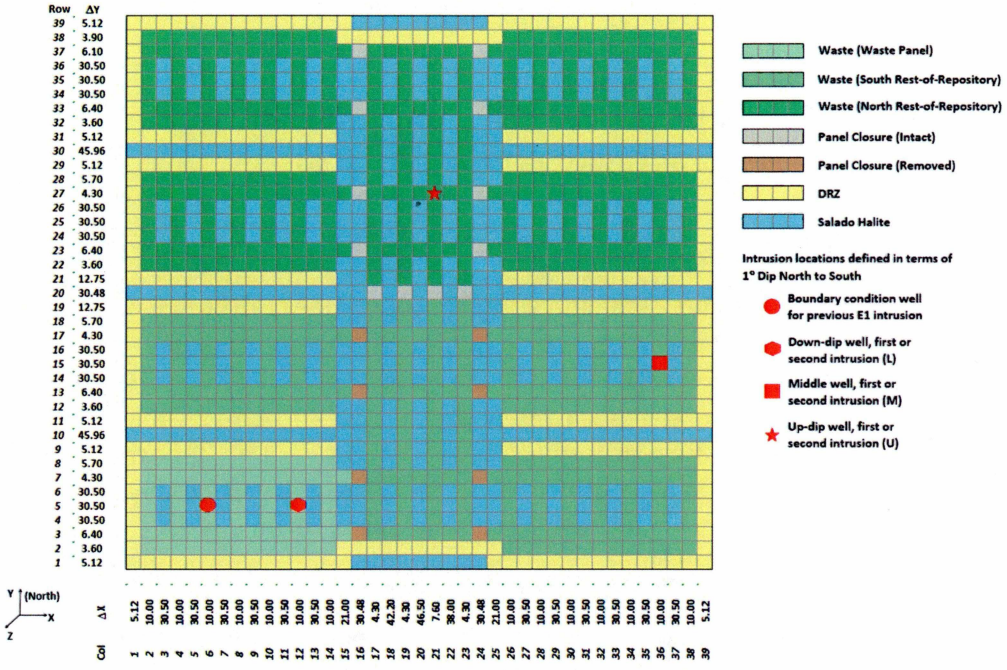

Figure 3-2. CRA-2019 DBR Grid with Simulated Intrusion Locations (Docherty and King 2023)

Information Only

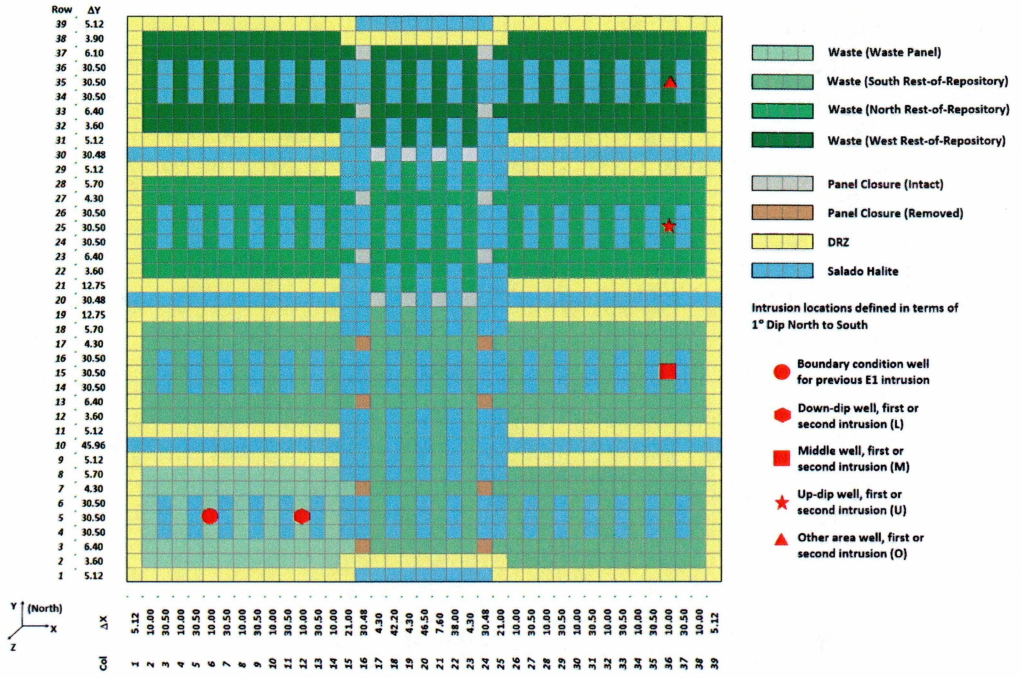

Figure 3-3. RPPCR DBR Grid with Simulated Intrusion Locations (Docherty and King 2023)

3.5.2 Initial Conditions

Brine pressures and brine saturations calculated during the BRAGFLO Salado flow simulations (King 2023) are volume-averaged and used as initial conditions in the DBR simulations. Figure 3-4 illustrates the method used to transfer initial conditions in the RPPCR. The BRAGFLO grid aggregates waste panels into four waste-bearing regions, as described in Table 3-1: Waste Panel, South Rest of Repository, North Rest of Repository, and West Rest of Repository. In Figure 3-4, these regions are denoted Waste Panel, SRoR, NRoR and WRoR, respectively. At the time of the intrusion, the volume-averaged pressure and saturation from the four waste-filled regions in the BRAGFLO grid are used as the initial pressure and saturation for corresponding waste regions in the DBR grid. Consistent with the designations L, M, U and O for the intrusion locations, the DBR grid waste regions will be referred to as Lower, Middle, Upper, and Other. As indicated in Figure 3-4 conditions in the BRAGFLO Waste Panel map to the Lower waste region in the DBR grid; likewise, BRAGFLO SRoR conditions map to the Middle DBR region, NRoR to the Upper DBR region, and WRoR to the Other DBR region. Note that pressure and saturation are allowed to evolve during the DBR simulations.

Information Only

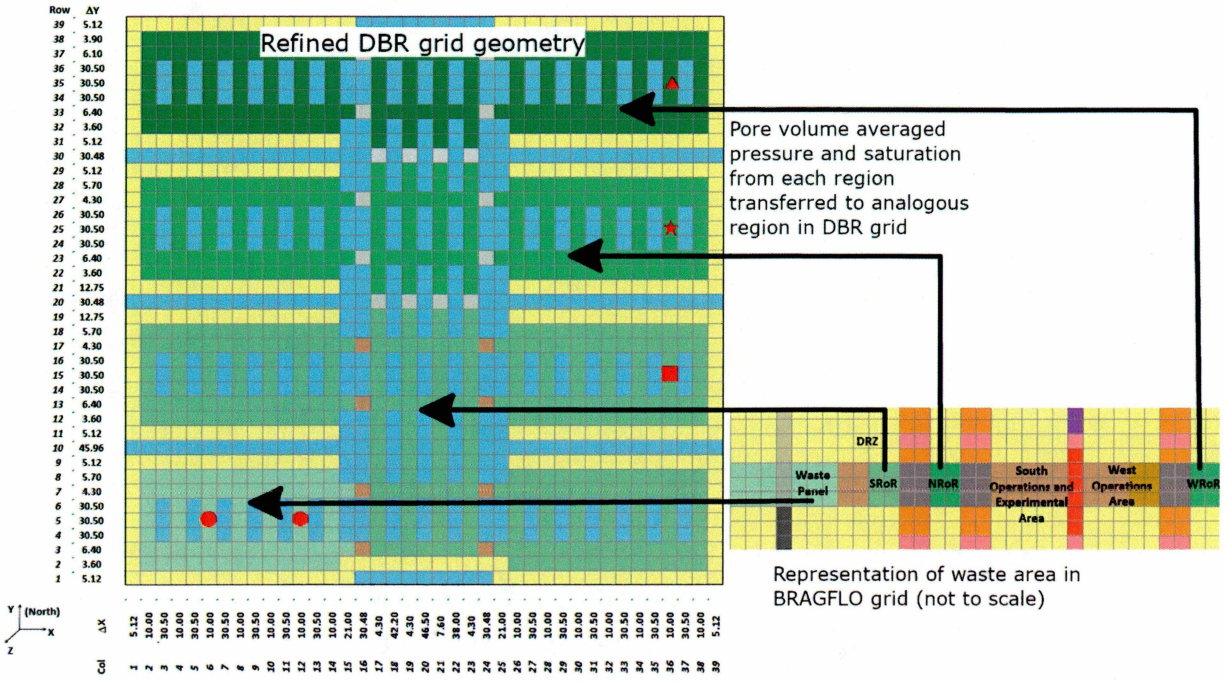

Figure 3-4. Transfer of Initial Pressure and Saturation from the BRAGFLO Salado Flow Grid to the DBR Grid (Docherty and King 2023)

3.5.3 Modeling Scenarios

In performing DBR calculations, five of the BRAGFLO Salado flow model scenarios, S1-BF to S5-BF, are used to set the initial conditions for the DBR calculations at the time of intrusion. As described by King (2023), the five BRAGFLO Salado flow scenarios capture the long-term behavior of the repository under three different conditions: undisturbed (E0); intersected by a borehole that continues down to a hypothetical pressurized brine reservoir below the repository (E1); and intersected by a borehole that does not intersect pressurized regions below the repository (E2). DBR calculations map the resulting BRAGFLO pressure and saturation conditions at a suite of intrusion times onto the DBR model grid and simulate flow to the intrusion. The scenarios and intrusion times used for the RPPCR, presented in Table 3-3, are the same as those used for the CRA-2019 PA. Note that the addition of the O intrusion location in the RPPCR results in a total of 104 combinations, or DBR simulations, for each parameter vector. In the CRA-2019, with only L, M, and U Intrusion locations, there were 78 DBR simulations per parameter vector.

Information Only

Table 3-3. DBR Scenarios (Docherty and King 2023)

Scenario	Description
S1-DBR	Initially undisturbed repository (E0 conditions). Intrusion at the L, M, U, or O location at 100; 350; 1,000; 3,000; 5,000; or 10,000 years: 24 combinations.
S2-DBR	Initial E1 intrusion at 350 years followed by a second intrusion at the L, M, U, or O location at 550; 750; 2,000; 4,000; or 10,000 years: 20 combinations.
S3-DBR	Initial E1 intrusion at 1,000 years followed by a second intrusion at the L, M, U, or O location at 1,200; 1,400; 3,000; 5,000; or 10,000 years: 20 combinations.
S4-DBR	Initial E2 intrusion at 350 years followed by a second intrusion at the L, M, U, or O location at 550; 750; 2,000; 4,000; or 10,000 years: 20 combinations.
S5-DBR	Initial E2 intrusion at 1,000 years followed by a second intrusion at the L, M, U, or O location at 1,200; 1,400; 3,000; 5,000; or 10,000 years: 20 combinations.

3.6 Mobilized Radionuclide Concentrations

The code PANEL simulates the radionuclide inventory in the repository waste panels over the 10,000-year regulatory period, both as the radionuclides decay and as they are mobilized in brine. To reduce computational cost, decay chains have been abridged where intermediate radionuclides with short half-lives (i.e., less than 2 years) are excluded. The abridged decay chains were formulated to include radionuclides deemed potentially significant to releases based on criteria set forth in the CCA Appendix WCA (U.S. DOE 1996, pg. WCA-23). The abridged decay chains are shown in Figure 2-1 of Kim (2023). PANEL models the decay and ingrowth of 30 radionuclides subject to the abridged decay chains..

The RPPCR analysis employs the WIPP thermodynamic database DATA0.FM6, created by Domski (2023c), to assess the baseline solubilities of actinides with the +III, +IV, and +V oxidation states. The EPA-specified solubility of 1.0×10^{-3} M is used for the baseline solubility of U(VI) in Salado and Castile brines in the RPPCR. The baseline solubilities of actinides with +III and +V oxidation states are increased in the RPPCR compared to the CRA-2019, while those for actinides with +IV oxidation state are slightly decreased.

There is no uncertainty modeled in the +V and +VI oxidation state solubilities; the solubility uncertainty exponent for actinides in the +V and +VI oxidation states has been set to zero for all realizations (Brush and Garner 2005; U.S. DOE 2019, Appendix GEOCHEM). The sampled solubility uncertainties of actinides with +III oxidation state, An(III), are shifted to lower values with narrower distributions in the RPPCR (Figure 4-11 in Kim 2023). Like An(III), the sampled solubility uncertainties of An(IV) are shifted to lower values with narrower distributions in the RPPCR (Figure 4-12 in Kim 2023).

Intrinsic and microbial colloidal enhancement parameters are changed in the RPPCR. Changes in colloidal parameters increase the fractional contribution of microbial colloids for Am(III), Th(IV), Np(IV), and Np(V), and decrease fractional contributions for Pu(III) and Pu(IV). While microbial

Information Only

colloid enhancement parameters are changed for U(IV) and U(VI), microbial colloid contributions remain a small fraction of U(IV) and U(VI) mobilization.

As discussed in Section 2.2, the likelihood of selecting the Pu(III) oxidation state has decreased from 0.5 in the CRA-2019 to 0.25 in the RPPCR based on Lucchini and Swanson (2023). This means that 25% of the realizations in the RPPCR assume the +III state-controlled Pu solubility and 75% of the realizations assume the +IV state-controlled Pu solubility.

PANEL performs the decay and mass balance calculations on the full set of 30 individual radionuclides. PANEL also reports concentrations and discharges in terms of 5 "lumped" radionuclides that represent 10 of the 30 (Table 3-4). PANEL performs this lumping procedure internally at each time step.

Table 3-4. Lumped and Represented Radionuclides (Kim 2023)

Lumped Radionuclide	Constituent Radionuclides (in Curies)[1, 2]
AM241L	$AM241L = Ci^{AM241} + Ci^{PU241}\left(t_{1/2}^{PU241}/t_{1/2}^{AM241}\right)$
PU239L	$PU239L = Ci^{PU239} + Ci^{PU240} + Ci^{PU242}\left(t_{1/2}^{PU242}/t_{1/2}^{PU239}\right)$
PU238L	$PU238L = Ci^{PU238}$
U234L	$U234L = Ci^{U234} + Ci^{U233}$
TH230L	$TH230L = Ci^{TH230} + Ci^{TH229}$

[1] $t_{1/2}$ is the half-life of a constituent radionuclide.
[2] Ci represents a radionuclide in curies.

PANEL computes the total mobilization potential for each actinide of interest, both individual and lumped. Total mobilization potential is the amount of an actinide that could be mobilized either by dissolving in brine or by associating with mobile colloids. The total mobilization potentials are constant throughout the course of a simulation for a given model realization (U.S. DOE 2019, Appendix MASS) but vary between realizations due to the solubility uncertainty factor, oxidation state of an actinide, and brine source. The total mobilization potentials are used by both PANEL and NUTS to calculate releases via Salado transport as a function of time.

For the concentration calculations used for the DBRs, PANEL assumes that brine volume in the waste panels is constant over time and the waste panels behave as a closed system. The PA consequently runs the code PANEL multiple times with a set of predefined brine volumes. For a full discussion of the PANEL calculation, see Kim (2023).

3.7 Salado Transport

The codes NUTS and PANEL are used to simulate transport of lumped radionuclides in the Salado formation. Cumulative radionuclide discharges through the (conceptually combined) shaft and borehole are assumed to flow into the overlying Culebra member of the Rustler formation. These cumulative radionuclide discharges versus time results are used by the code CCDFGF to calculate radionuclide releases reaching the LWB through the Culebra.

Information Only

NUTS (used for the undisturbed scenario, E1 intrusion scenario, and E2 intrusion scenario) uses the same two-dimensional grid as the BRAGFLO code and relies on the BRAGFLO results for the brine flux fields and other fluid and rock properties. For disturbed scenarios (scenarios S2 – S5), NUTS utilizes BRAGFLO's Salado flow field output and a non-sorbing tracer in order to identify ("screen in") realizations with potential to transport more than a minimal mass (1.0×10^{-7} kg) of radionuclides across defined boundaries. Full NUTS transport simulations for the screened-in vectors then calculate cumulative radionuclide discharges. Cumulative discharges are tabulated at the intersection of the borehole and the Culebra formation. PANEL (used for the E1E2 intrusion scenario) performs a mass balance calculation over a fixed number of waste panels, and similarly relies on the BRAGFLO results for brine volume and brine discharge inputs. For a full description of the Salado transport calculation used in the RPPCR, see Kim (2023).

3.8 Flow and Transport in the Culebra

Culebra radionuclide transport calculations are performed for three replicates of 100 vectors each for two potash mining scenarios (600 unique flow fields) and four mass release locations (2,400 total transport simulations). In each simulation, Culebra transport simulations calculate the cumulative mass discharge at the WIPP LWB over the 10,000-year regulatory period due to a discrete source located over waste panel area. The source releases 1 kg for each of the radionuclides Am-241, U-234, Th-230, and Pu-239, over the first 50 years of the simulation. Transport of the Th-230 daughter product of U-234 decay is also calculated and tracked as a separate species.

The five steps in estimating radionuclide transport through the Culebra and changes for the RPPCR include:

Step 1. Construction of 1,000 base geostatistical realizations of Culebra hydraulic transmissivity (T), anisotropy, storativity, and recharge fields (collectively referred to as "T-fields"). The base T-fields documented in Hart et al. (2008) are used in both the CRA-2019 PA and RPPCR.

Step 2. Calibration of the T-fields to observed head and pumping drawdowns. The updates to the T-field calibrations are described in Section 2.11 and documented in Bowman et al. (2023).

Step 3. Modification of the T-fields to account for potential subsidence due to potash mining beneath the Culebra. The two mining scenarios include partial mining, which assumes extraction of all potash reserves outside the LWB, and full mining, which assumes extraction of all potash reserves both inside and outside the LWB. The mining modification scripts are updated for the RPPCR to interface with the MODFLOW 6 input files (Bethune 2023).

Step 4. Calculation of steady-state groundwater flow-fields for each mining-modified T-field using MODFLOW. Groundwater flow simulations are migrated from MODFLOW-2000 to MODFLOW 6 for the RPPCR (Bethune 2023).

Step 5. Calculation of radionuclide transport through the Culebra to the LWB for each simulated flow field and release location using SECOTP2D. As described in Section 2.10, the radionuclide transport calculations are updated with additional mass release locations over the replacement and additional waste panels of the RPPCR repository layout (Bethune 2023). The

Information Only

release points include the centroid of the 10 waste panels used in the CRA-2019 calculations (CRP1), and three new release points (CRP2 through CRP4) over the proposed additional and replacement waste panel region.

Analysis of the RPPCR Culebra flow and transport calculations, including a comparison to the CRA-2019 are provided in Bethune (2023). The output of Step 5 is used by the WIPP software CCDFGF to calculate potential radionuclide releases through the Culebra to the accessible environment (see Section 4.8.4 and Brunell and Zeitler 2023).

3.9 Calculation of CCDFs for Releases

The conceptual structure of the CCDFGF calculation in the RPPCR remains the same as for the CRA-2019. For each member of a sample of uncertain parameters, many 10,000-year futures are randomly generated. Each future comprises a sequence of simulated drilling intrusions and mining events. Drilling location, whether a brine pocket is penetrated, and the type of plugging pattern are randomly determined, and the simulation of many possible realizations, or futures, characterizes the aleatory uncertainty of the results. For each drilling intrusion, direct releases are tabulated using output from the other models described in Section 3.0 and, over the course of the entire future, releases through the Salado and Culebra to the LWB are recorded using output from the Salado and Culebra transport models. The switch from partial mining to full mining conditions occurs randomly with a probability of 1% per 100 years. The total of these various releases at the end of the 10,000-year period yields a datum for total releases; the collection of total release data points, over all futures, comprises one complementary cumulative distribution function (CCDF) of releases. The code CCDFGF generates the random futures and constructs the CCDFs. For a full description of the CCDFGF calculation in the RPPCR, see Brunell and Zeitler (2023). The following subsections summarize the updates to the CCDFGF approach and methodology described in Brunell and Zeitler (2023).

3.9.1 Panel Neighboring Assignments

The CRA-2019 classified each pair of waste panels into one of three groups as determined by the number of panel closures separating the waste panels: same, adjacent, and non-adjacent (Brunell 2019). For the RPPCR, the panel neighbor groups are extended to same, connected, adjacent, and non-adjacent, which required a change to the CCDFGF code (Brunell 2022). Same panel connections are used for multiple intrusions into the same panel. Two panels are connected if there are no intervening panel closures, e.g., Panel 4 and Panel 5 are connected. Two panels are adjacent if both panels are in the same half of the repository (i.e., both panels are either in the south or in the west) but are separated by one or more intervening panel closures, e.g., Panel 1 and Panel 5 are adjacent. Two panels are non-adjacent if the panels are in different halves of the repository. The path between panels is traced through excavated areas only. Table 3-5 summarizes the panel neighbor scheme and intrusion probabilities for the RPPCR; Table 3-6 shows the same information for the CRA-2019.

Information Only

Table 3-5. Panel Neighbor Relationships for RPPCR (Hansen et al. 2023a)

Intruded Panel[1]	Connected Panels	Adjacent Panels
1	-	2 – 10
2	-	1, 3 – 10
3	4, 5, 6, 9	1, 2, 7, 8, 10
4	3, 5, 6, 9	1, 2, 7, 8, 10
5	3, 4, 6, 9	1, 2, 7, 8, 10
6	3, 4, 5, 9	1, 2, 7, 8, 10
7	-	1 – 6, 8, 9, 10
8	-	1 – 7, 9, 10
9	3, 4, 5, 6	1, 2, 7, 8, 10
10	-	1 – 9
11	-	12 – 19
12	-	11, 13 – 19
13	-	11, 12, 14 – 19
14	-	11 – 13, 15 – 19
15	-	11 – 14, 16 – 19
16	-	11 – 15, 17 – 19
17	-	11 – 16, 18, 19
18	-	11 – 17, 19
19	-	11 – 18

[1]The intrusion probability of Panel 9 is 0.042, Panel 10 is 0.046, and all other panels is 0.054.

Information Only

Table 3-6. Panel Neighbor Relationships for CRA-2019

Intruded Panel[1]	Adjacent Panels
1	10
2	10
3	4, 5, 6, 9, 10
4	3, 5, 6, 9, 10
5	3, 4, 6, 9, 10
6	3, 4, 5, 9, 10
7	10
8	10
9	3, 4, 5, 6, 10
10	1, 2, 3, 4, 5, 6, 7, 8, 9

[1]The intrusion probability of Panel 9 is 0.079, Panel 10 is 0.086, and all other panels is 0.104.

3.9.2 Method for Determining Confidence Intervals

Two methods have been used in WIPP PA to calculate the confidence interval for the mean CCDF of total releases. The first method uses the mean CCDF of each replicate as an estimate of true mean, and a t-distribution using the number of replicates minus one as the degrees of freedom to place the confidence interval (Helton et al. 1998, Section 6.4). The second method used in more recent PA calculations, including the CRA-2019, uses all vector CCDFs from all replicates and the t-distribution with the number of total vectors minus one as the degrees of freedom.

The second calculation has an underlying assumption that the vector CCDFs are normally distributed about the (unknown) population mean. Because of this assumption, the first method for calculating the confidence interval using the replicate means is deemed more appropriate and is used in the RPPCR. To provide a direct comparison between analyses, the confidence intervals for the mean total releases presented in Section 4.8 and Section 4.9 for both the CRA-2019 PA and the RPPCR are calculated using the first method. This calculation is described in detail in Brunell and Zeitler (2023).

3.10 Run Control

The WIPP PA codes have been migrated to the WIPP PA HPC/Linux Cluster, which consists of the login node FWM and 24 Dell PowerEdge C6420 compute nodes running CentOS 7 (Long 2020; Long and King 2022). A full description of the run control for the RPPCR analysis, including names and locations of input and output files, can be found in Long (2023).

Information Only

Input files were prepared by individual analysts and the run control coordinator prepared the run scripts. The RPPCR was performed using qualified code versions on the WIPP PA Linux cluster (Table 3-7). As described in AP-204 (Hansen et al. 2023a), the DRSPALL and MERGESPALL codes were not run for the RPPCR; instead, results from a previous analysis were used as input (Kirchner et al. 2014; Kirchner et al. 2015).

The WIPP PA Parameter Database (PAPDB), ParamDB, is used as the source for parameter values. The results of the LHS sampling and CCDFGF release calculations were written to the WIPP PA Results Database PA_Results. Parameter specifications and sampled values can be found in Kim and Feng (2023). Input and output files for the RPPCR analysis are archived in the WIPP CVS repository $CVSLIB/WIPP_ANALYSES/RPPCR.

Information Only

Table 3-7. WIPP PA Codes Used for the RPPCR (Long 2023)

Code	Version	Executable[1]	Build Date
ALGEBRACDB	2.37	algebracdb	8/17/20
BRAGFLO	7.01	bragflo	9/17/20
CCDFGF	8.01	ccdfgf	7/28/22
CCDFVECTORSTATS	1.02	ccdfvectorstats	8/19/20
CUTTINGS_S	6.04	cuttings_s	11/13/20
DTRKMF	1.02	dtrkmf	1/13/21
EPAUNI	1.20	epauni	8/19/20
GENMESH	6.11	genmesh	8/20/20
GROPECDB	2.14	gropecdb	6/16/20
ICSET	2.24	icset	8/20/20
LHS	3.00	lhs	11/1/21
MATSET	9.25	matset	9/8/20
MODFLOW6	6.2.2	modflow6	5/16/22
NUTS	2.08	nuts	11/16/21
PANEL	5.02	panel	8/16/22
POSTBRAG	4.03	postbrag	9/8/20
POSTLHS	4.12	postlhs	9/17/20
POSTSECOTP2D	1.06	postsecotp2d	8/17/20
PREBRAG	9.01	prebrag	8/20/20
PRECCDFGF	3.01	preccdfgf	7/28/22
PRELHS	2.46	prelhs	8/29/22
PRESECOTP2D	1.25	presecotp2d	1/25/23
RELATE	1.46	relate	8/20/20
SCREEN_NUTS	1.03	screen_nuts	8/19/20
SECOTP2D	1.44	secotp2d	8/20/20
STEPWISE	2.23	stepwise	10/28/20
SUMMARIZE	3.03	summarize	8/17/20

[1] Executables are located in $CVSLIB/WIPP_CODES/PA_CODES/*CODE*/Build/Linux

Information Only

This page intentionally left blank.

Information Only

4.0 RESULTS

This section summarizes the RPPCR process model results and release calculations detailed in each of the analysis reports (Bethune 2023; Brunell and Zeitler 2023; Docherty and King 2023; Kicker 2023a; Kicker 2023b; Kim 2023; King 2023). The PA process model results are shown for the inventory, repository conditions, direct release mechanisms, and subsurface transport mechanisms. Results of PA process models are primarily compared to the CRA-2019 PA, and selectively to the APPA. Finally, CCDFs of cumulative releases for each release mechanism, total releases, and the sensitivity analysis for the total releases are discussed. Release calculations are compared to the CRA-2019 PA, APPA, and EPA's CRA-2019_COMB analysis (U.S. EPA 2022a).

4.1 Inventory

This section summarizes the inventory analysis detailed in Kicker (2023a) and Kicker (2023b) for the RPPCR. The half-lives of important radionuclides in the WIPP inventory are listed in Table 4-1.

Table 4-1. Half-lives of important WIPP Radionuclides

Radionuclide	Half-life (y)[1]
Am-241	432.7
Cm-244	18.1
Cs-137	30.07
Pu-238	87.7
Pu-239	24,100
Pu-240	6,560
Pu-241	14.29
Sr-90	28.8
U-233	159,200
U-234	246,000

[1] International Commission on Radiological Protection (ICRP 2008, Table A.1).

4.1.1 Total Waste Volume

The individual waste stream volumes of TRU waste shown in Table 4-2 (scaled to a full repository) illustrate which waste streams are the primary contributors to total waste volume in the RPPCR inventory. Table 4-2 shows that in the RPPCR inventory, 10 wastes streams (out of a total of 591 waste streams) contribute approximately 54% of the waste volume. The top two RPPCR waste streams by volume, SR-CH-PP and RL200-02, provide 27.11% of the total RPPCR volume.

Information Only

Table 4-2. WIPP CH- and RH-TRU Waste Streams by Total Scaled Volume from RPPCR Inventory (Kicker 2023b)

Rank Order	Waste Stream ID	Stream Type	Volume (m^3)	% of Total	Cumulative %
1	SR-CH-PP	CH	3.57E+04	20.33%	20.33%
2	RL200-02	CH	1.19E+04	6.78%	27.11%
3	WP-BN510	CH	9.63E+03	5.48%	32.60%
4	LA-MHD01-Pits	CH	7.74E+03	4.41%	37.00%
5	LA-MHD01.001	CH	6.94E+03	3.95%	40.96%
6	RLPFP-01	CH	6.34E+03	3.61%	44.57%
7	WP-ID-SDA-SLUD	CH	5.19E+03	2.96%	47.52%
8	WP-RF029.01	CH	4.31E+03	2.45%	49.98%
9	WP-BNINW216	CH	3.47E+03	1.98%	51.96%
10	WP-BN510.1	CH	3.42E+03	1.95%	53.90%
…	…	…	…	…	…
591	WP-LA-OS-00-04	CH	2.69E-03	0.00%	100.00%
	Total:		175,574	100.00%	

4.1.2 Inventory by EPA Units

The waste stream inventory in EPA units in Table 4-3 illustrates which waste streams are the primary contributors to the total number of EPA units. The table identifies the 10 waste streams that comprise about 83% of the total inventory in EPA units at closure. The top two waste streams, SR-KAC-PuOx and SR-CH-PP, respectively provide 41.36% and 21.51% of the total EPA units at closure in the waste inventory. Waste stream SR-KAC-PuOx has the highest activity with a total of 2.48E+06 Ci, which includes 1.15+06 Ci of ^{239}Pu, 6.84E+05 Ci of ^{241}Am, 3.87E+05 Ci of ^{240}Pu, 1.59E+05 Ci of ^{241}Pu, and 9.67E+04 Ci of ^{238}Pu (Van Soest 2022, Table 5-1).

The total number of EPA units in the RPPCR waste inventory at the closure year of 2083 is 10,025 (Table 4-3). As discussed in Kicker (2023b), the conversion of activity in Ci to EPA units is a function of the WUF and the EPA release limit.

By 10,000 years post-closure, the total number of EPA units in the RPPCR inventory decreases to 3,344 (Table 4-4). The top two waste streams at 10,000 years are still SR-KAC-PuOx and SR-CH-PP, providing 73.12% of the total EPA units. Ten waste streams account for approximately 87% of the repository activity at the end of the regulatory time period.

Information Only

streams account for approximately 87% of the repository activity at the end of the regulatory time period.

Table 4-3. WIPP CH- and RH-TRU Waste Streams by Total EPA Units (calendar year 2083) from RPPCR Inventory (Kicker 2023b)

Rank Order	Waste Stream ID	Stream Type	EPA Units	% of Total	Cumulative %
1	SR-KAC-PuOx	CH	4.15E+03	41.36%	41.36%
2	SR-CH-PP	CH	2.16E+03	21.51%	62.87%
3	LA-MHD01.001	CH	5.60E+02	5.58%	68.45%
4	LA-MHD01-Pits	CH	3.00E+02	2.99%	71.44%
5	WP-LA-MHD01.00	CH	2.79E+02	2.79%	74.23%
6	WP-RF009.01	CH	2.36E+02	2.36%	76.59%
7	WP-RF118.01	CH	1.86E+02	1.86%	78.44%
8	WP-SR-W027-221	CH	1.68E+02	1.68%	80.12%
9	WP-SR-MD-PAD1	CH	1.17E+02	1.17%	81.29%
10	WP-INW216.001	CH	9.79E+01	0.98%	82.27%
…	…	…	…	…	…
591	WA-LA-MHD08.00	CH	2.25E-08	0.00%	100.00%
	Total:		10,025	100.00%	

Information Only

Table 4-4. WIPP CH- and RH-TRU Waste Streams by Total EPA Units (calendar year 12083) from RPPCR Inventory (Kicker 2023b)

Rank Order	Waste Stream ID	Stream Type	EPA Units	% of Total	Cumulative %
1	SR-KAC-PuOx	CH	1.78E+03	53.29%	53.29%
2	SR-CH-PP	CH	6.63E+02	19.83%	73.12%
3	WP-RF118.01	CH	1.00E+02	3.00%	76.12%
4	WP-RF009.01	CH	8.20E+01	2.45%	78.57%
5	LA-MHD01.001	CH	8.13E+01	2.43%	81.00%
6	LA-MHD01-Pits	CH	8.13E+01	2.43%	83.43%
7	WP-LA-MHD01.00	CH	7.81E+01	2.34%	85.77%
8	WP-BN510	CH	2.01E+01	0.60%	86.37%
9	WP-RF003.01	CH	1.89E+01	0.57%	86.93%
10	LL-M001	CH	1.68E+01	0.50%	87.44%
…	…	…	…	…	…
591	ND-T002	CH	6.76E-10	0.00%	100.00%
	Total:		3,344	100.00%	

4.1.3 Waste Stream Activity Concentration

The EPAUNI code calculates the activity concentration for each waste stream. The activity concentrations for the top 10 contributing RPPCR waste streams at closure are provided in Table 4-5. Waste stream concentrations are used in cuttings and cavings release calculations (Section 4.8.1). In those calculations, waste streams are randomly selected based on waste type (contact-handled [CH] or remote-handled [RH]); within each waste type a waste stream's intersection probability is equal to the waste stream's fraction of total waste type volume. In Figure 4-1, the probability of intersecting any waste stream is calculated on the waste stream volume fraction. The RPPCR activity concentrations in an intersected waste stream are compared to the CRA-2019 concentrations as shown in Figure 4-1.

At 10,000 years post-closure, while the concentration of EPA units has decreased due to decay (see Figure 4-2 and Table 4-6), the CCDFs of the RPPCR and CRA-2019 activity concentrations remain similar. Comparing Figure 4-1 and Figure 4-2, the two curves shifting left in Figure 4-2 relative to Figure 4-1 is the impact of inventory decay. The subtle increase in the RPPCR curve relative to the CRA-2019 curve from Figure 4-1 to Figure 4-2 is an indication that inventory decay is less impactful in the RPPCR due to the inventory having a larger fraction of long half-life radionuclides.

Information Only

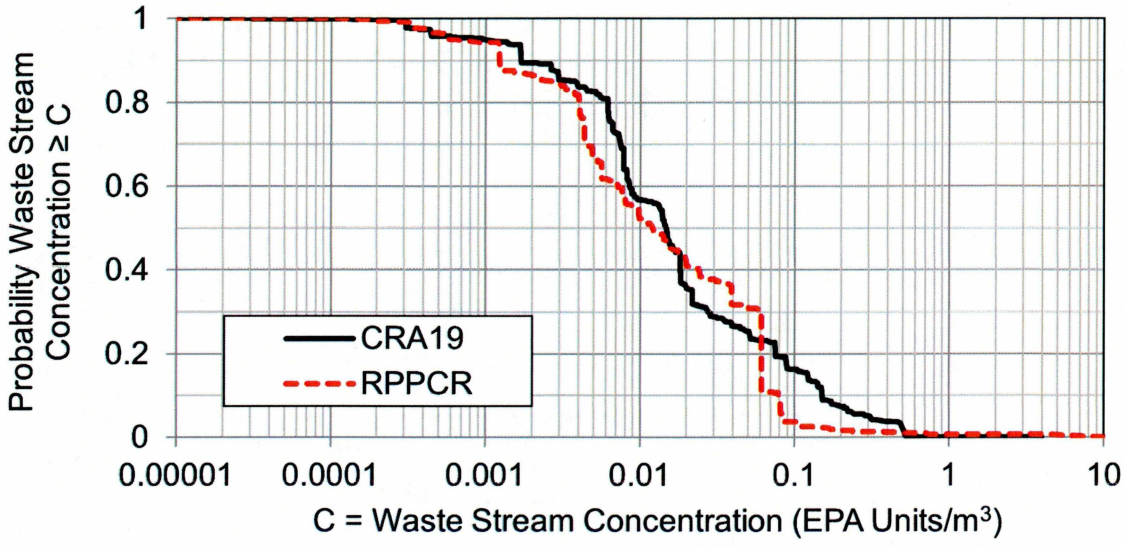

Figure 4-1. CCDFs for Waste Stream Concentration in an Intersected Waste Stream, EPA Units per m^3 at Closure (Calendar Year 2083) from Figure 1 of Kicker (2023b)

Information Only

Table 4-5. WIPP CH- and RH-TRU Waste Streams Ordered by Concentration at Closure (Calendar Year 2083) from RPPCR Inventory (Kicker 2023b)

Rank Order	Waste Stream ID	Stream Type	Volume (m^3)	EPA Units per m^3	Fraction of Stream Type Volume	Overall Intersection Probability	Cumulative Probability
1	WA-LA-OS-00-01	CH	1.14E-02	1.00E+01	6.77E-08	6.31E-08	6.31E-08
2	OR-OXIDE-CH-HE	CH	6.48E-01	8.86E+00	3.85E-06	3.59E-06	3.65E-06
3	SR-KAC-PuOx	CH	9.29E+02	4.46E+00	5.51E-03	5.14E-03	5.14E-03
4	WP-LA-OS-00-01	CH	2.12E+01	2.04E+00	1.26E-04	1.17E-04	5.26E-03
5	WP-LA-OS-00-04	CH	2.69E-03	1.60E+00	1.60E-08	1.49E-08	5.26E-03
6	LA-OS-00-01.00	CH	2.22E+01	1.47E+00	1.32E-04	1.23E-04	5.38E-03
7	WP-RF005.02	CH	1.84E+01	9.31E-01	1.09E-04	1.02E-04	5.49E-03
8	WP-RLHMOX.001	CH	4.55E+01	8.76E-01	2.70E-04	2.52E-04	5.74E-03
9	SR-RH-235F.01	RH	1.05E+00	8.23E-01	1.48E-04	1.01E-05	5.75E-03
10	SR-RH-MNDPAD1.	RH	2.94E+00	8.18E-01	4.16E-04	2.82E-05	5.78E-03
…	…	…	…	…	…	…	…
591	WA-LA-MHD08.00	CH	4.88E-02	4.61E-07	2.90E-07	2.70E-07	1.00E+00
	Total:		175,574	5.76E+01	2.00E+00	1.00E+00	

NOTES:
1. Total CH stream type volume = 168,502 m^3; total RH stream type volume = 7,072 m^3.
2. CH area = 216,952 m^2; RH area = 15,760 m^2; CH stream type area probability = 0.932; RH stream type area probability = 0.068; stream type probability = waste stream volume/total stream type volume; overall probability = stream type probability × stream type area probability.

Information Only

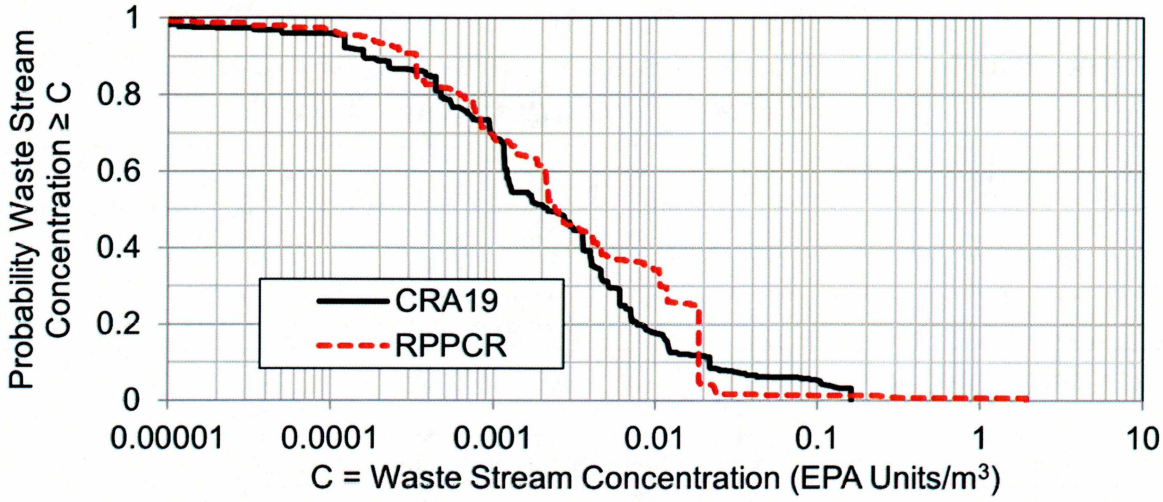

Figure 4-2. CCDFs for Waste Stream Concentration in an Intersected Waste Stream at 10,000 Years after Closure (Calendar Year 12083) (Kicker 2023b)

Information Only

Table 4-6. WIPP CH- and RH-TRU Waste Streams Ordered by Concentration at 10,000 Years after Closure (Calendar Year 12083) from RPPCR Inventory (Kicker 2023b)

Rank Order	Waste Stream ID	Stream Type	Volume (m^3)	EPA Units per m^3	Fraction of Stream Type Volume	Overall Intersection Probability	Cumulative Probability
1	SR-KAC-PuOx	CH	9.29E+02	1.92E+00	5.51E-03	5.14E-03	5.14E-03
2	OR-OXIDE-CH-HE	CH	6.48E-01	9.89E-01	3.85E-06	3.59E-06	5.14E-03
3	WP-LA-OS-00-04	CH	2.69E-03	9.34E-01	1.60E-08	1.49E-08	5.14E-03
4	WP-RLRFETS.001	CH	1.50E+01	3.66E-01	8.90E-05	8.30E-05	5.23E-03
5	LA-OS-00-01.00	CH	2.22E+01	3.26E-01	1.32E-04	1.23E-04	5.35E-03
6	WP-RF118.01	CH	3.37E+02	2.97E-01	2.00E-03	1.86E-03	7.21E-03
7	WP-RLHMOX.001	CH	4.55E+01	2.81E-01	2.70E-04	2.52E-04	7.47E-03
8	WP-RF128.01	CH	4.65E+01	2.72E-01	2.76E-04	2.57E-04	7.72E-03
9	WP-RF121.01	CH	1.08E+01	2.71E-01	6.41E-05	5.98E-05	7.78E-03
10	WP-RLMSSC.001	CH	1.52E+01	2.70E-01	9.02E-05	8.41E-05	7.87E-03
…	…	…	…	…	…	…	…
591	ND-T002	CH	1.68E+00	4.03E-10	9.97E-06	9.29E-06	1.00E+00
	Total:		175,574	1.27E+01	2.00E+00	1.00E+00	

NOTES: Total CH stream type volume = 168,502 m^3; total RH stream type volume = 7,072 m^3. See Note 2 in Table 4-5 for probability definitions.

4.1.4 Total Radionuclide Activity

Figure 4-3 compares the total activity in both EPA units and curies as a function of time for the CH and RH waste inventories. RH waste provides a minimal contribution in terms of either EPA units or curies. The higher activities over time for the RPPCR compared to the CRA-2019 can be attributed to increased inventory of ^{239}Pu, which has a relatively long half-life. Figure 4-4 compares the overall activity concentration as a function of time for the RPPCR and CRA-2019 waste inventories. Overall activity concentration is determined as the total EPA units for all waste streams divided by the total volume of the waste. As seen in Figure 4-4, RH waste provides a small fraction of the overall activity concentration. The CH overall activity concentration at closure in

Information Only

both the RPPCR and CRA-2019 is approximately 0.059 EPA units/m^3. Inventory activity decays less in the RPPCR such that activity concentration for RPPCR CH waste remains higher over time compared to CRA-2019. The increased ^{239}Pu inventory increases direct solids releases for RPPCR calculations.

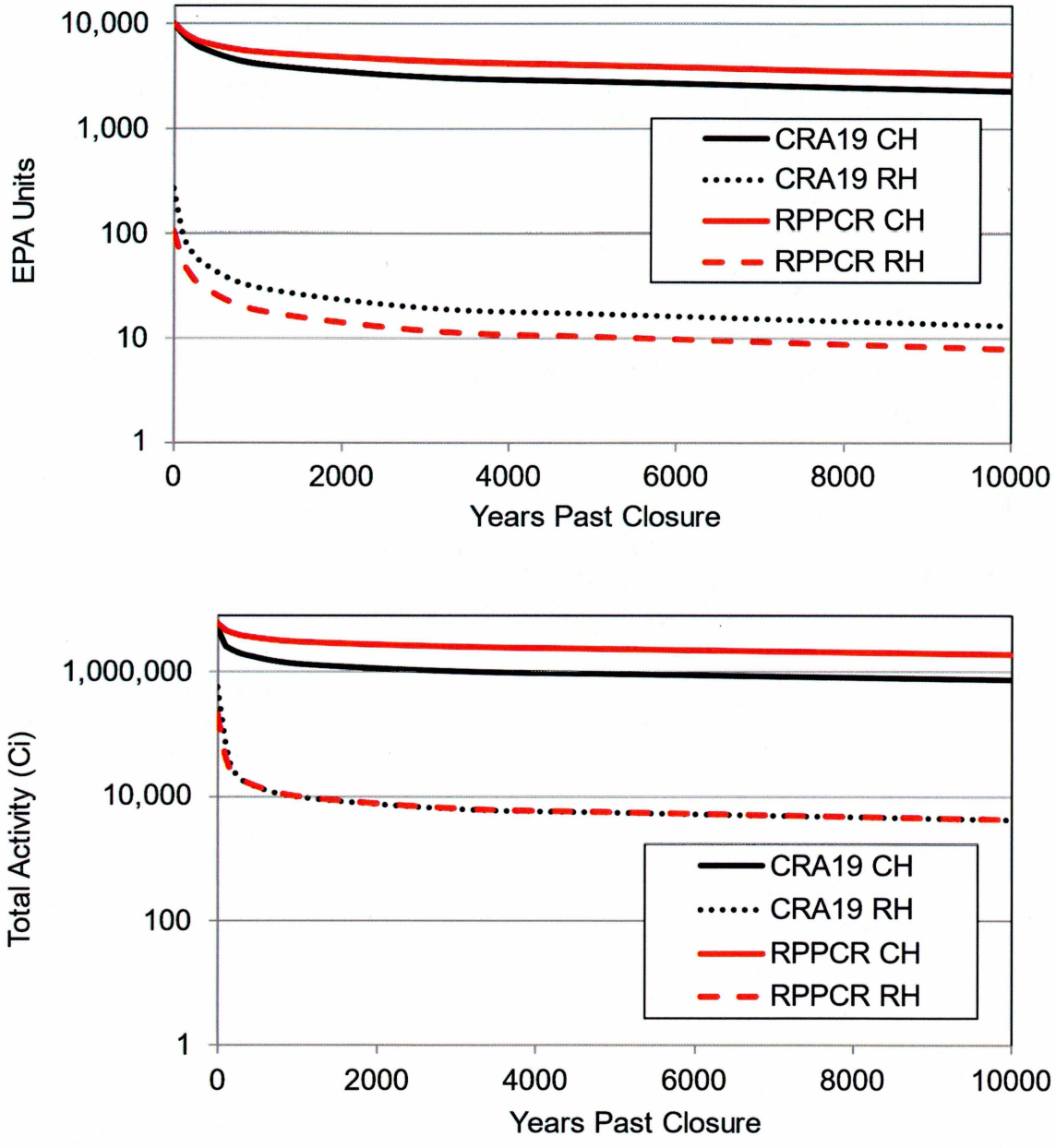

Figure 4-3.Total Activity in EPA Units (top) and Curies (bottom) for WIPP CH- and RH-TRU Waste from Closure to 10,000 Years After Closure (Kicker 2023b)

Information Only

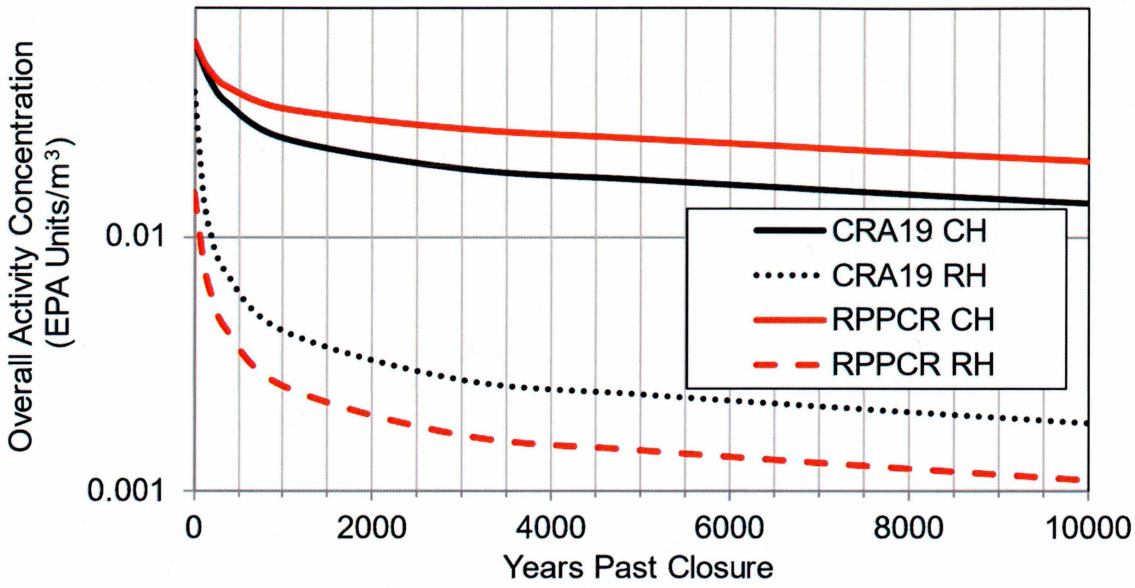

Figure 4-4. Overall Activity Concentrations in WIPP CH- and RH-TRU Waste from Closure to 10,000 Years After Closure (Kicker 2023b)

The highest activity isotopes in the WIPP waste are shown in Table 4-7 at closure and at 10,000 years post-closure. Figure 4-5 shows the total activity (in EPA units and Ci) as a function of time, along with the highest activity radionuclides that contribute to the overall total. The initial activity of the inventory is dominated by ^{241}Am, ^{238}Pu, ^{239}Pu, and ^{240}Pu (Figure 4-5). The ^{241}Am and ^{238}Pu inventories decay rapidly. The total activity of the inventory is dominated at later times (> 2,000 years) by mainly ^{239}Pu with a smaller contribution from ^{240}Pu. The radionuclides ^{244}Cm, ^{137}Cs, ^{241}Pu, ^{90}Sr, ^{233}U, and ^{234}U do not appreciably contribute to the total activity at any time throughout the 10,000-year regulatory period. The increase in ^{239}Pu in the RPPCR results in a higher total activity, as shown in Figure 4-3.

Information Only

Table 4-7. Highest Activity Isotopes in WIPP CH- and RH-TRU Waste at Closure and After 10,000 Years (Kicker 2023b)

Radionuclide	Half-life (y)	RPPCR Inventory				CRA-2019 Inventory			
		Activity at Closure		Activity after 10,000 Years		Activity at Closure		Activity after 10,000 Years	
		Ci	EPA Units	Ci	EPA Units	Ci	EPA Units	Ci	EPA Units
Am-241	432.7	1.42E+06	2.55E+03	1.56E-01	2.79E-04	1.14E+06	3.46E+03	1.31E-01	3.97E-04
Cm-244	18.1	9.85E+03	—	0.00E+00	—	3.94E+04	—	0.00E+00	—
Cs-137	30.07	9.20E+04	1.65E+01	0.00E+00	0.00E+00	2.51E+05	7.60E+01	0.00E+00	0.00E+00
Pu-238	87.7	1.30E+06	2.32E+03	6.41E-29	1.15E-31	9.65E+05	2.92E+03	4.76E-29	1.44E-31
Pu-239	24,100	2.17E+06	3.88E+03	1.63E+06	2.91E+03	8.74E+05	2.65E+03	6.56E+05	1.99E+03
Pu-240	6,560	6.93E+05	1.24E+03	2.40E+05	4.29E+02	3.19E+05	9.67E+02	1.11E+05	3.35E+02
Pu-241	14.29	4.38E+05	—	0.00E+00	—	1.87E+06	—	0.00E+00	—
Sr-90	28.8	6.19E+04	1.11E+01	0.00E+00	0.00E+00	1.97E+05	5.96E+01	0.00E+00	0.00E+00
U-233	159,200	5.30E+02	9.49E-01	5.08E+02	9.08E-01	1.27E+02	3.85E-01	1.22E+02	3.69E-01
U-234	246,000	6.78E+02	1.21E+00	1.11E+03	1.99E+00	4.86E+02	1.47E+00	8.09E+02	2.45E+00
Total		6.19E+06	1.00E+04	1.87E+06	3.34E+03	5.66E+06	1.01E+04	7.67E+05	2.32E+03

NOTE: Half-life taken from ICRP (2008). EPA units are calculated for each radionuclide based on EPAUNI output activity (Ci), radionuclide release limits (Kicker 2023c), and the waste unit factor (Kicker 2023c). CRA-2019 results are provided by Kicker (2019).

Information Only

This page intentionally left blank.

Information Only

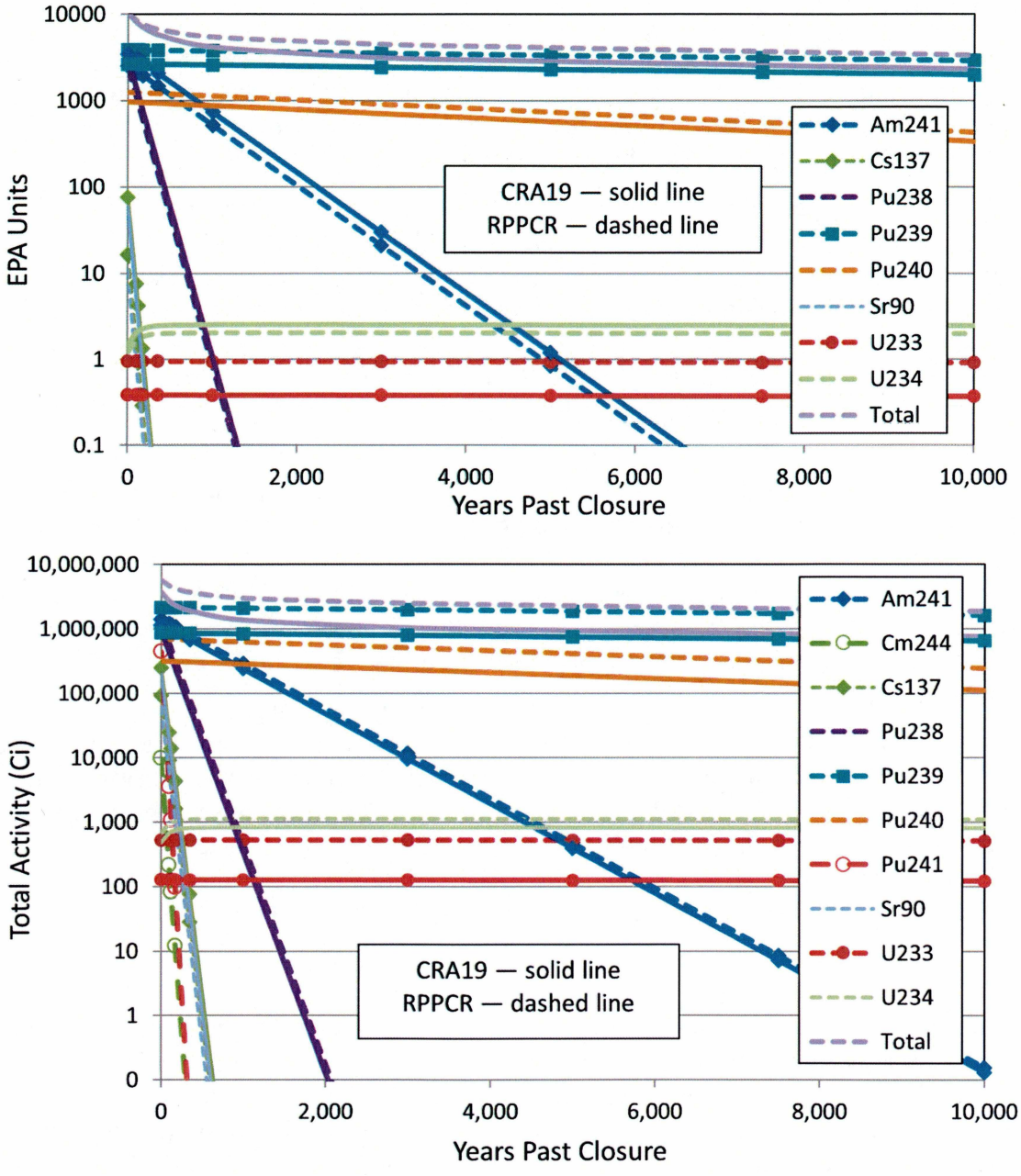

Figure 4-5. Total Activity in EPA Units (top) and Curies (bottom) for Dominant Isotopes in WIPP CH and RH-TRU Waste from Closure to 10,000 Years (Kicker 2023b)

Information Only

4.2 Salado Flow

Repository conditions influencing releases are summarized and compared with corresponding results from the CRA-2019. These conditions include pressures and brine saturations within the waste areas of the repository. Only differences in the mean results are shown and discussed here. King (2023) explores more differences in the overall distribution of results.

Brine saturations through time are shown in Figure 4-6. Brine saturations increase at early times due to the inflow of brine from the DRZ and marker beds. At late times, brine saturations slowly decrease due to the gas generation and brine consumption reactions. In scenarios with a Castile brine reservoir intrusion, a rapid increase in brine saturations can be seen at the time of the intrusion. Brine saturations have increased in scenarios without an E1 intrusion and decreased in scenarios with an E1 intrusion (Figure 4-6). The new porosity surface, increased gas generation, and the updated long-term borehole permeability are seen as the largest drivers for the changes in brine saturation.

Pressures through time are shown in Figure 4-7. Pressures increase rapidly at early times due to the creep closure of the salt. Gas generation provides a slower, more consistent source for pressure increases at later times. Scenarios with Castile brine intrusions have a rapid pressure increase at the time of intrusion. Mean and median pressures increased in the RPPCR over the CRA-2019 values (Figure 4-7). Maximum pressures decreased. The new porosity surface, increased gas generation, and the updated long-term borehole permeability are the major drivers for the changes to the pressure results.

The increase in the RPPCR inventory (in terms of mass of iron, mass of CPR, and activity of the waste) have increased the moles of gas generated and brine consumed in cases without an E1 intrusion. The decrease in brine saturations have decreased the moles of gas generated and brine consumed in cases with an E1 intrusion (Figure 4-8). In the RPPCR 92% of BRAGFLO simulations have more than 10% of the initial iron in the repository remaining at 10,000 years, this has decreased from the 98% of simulations in the CRA-2019 (Table 4-8).

Brine flows up the borehole, toward the Culebra, have decreased significantly with the decrease in long-term borehole permeability (Figure 4-9). The updated porosity surface discussed in Section 2.7 has resulted in a decrease in mean waste area porosities (Figure 4-10). The decrease in porosity, and therefore pore volume, has had a significant impact on brine pressures and saturations. The increased excavated volume and new panels is not a major driver for any of the differences in the repository behavior shown in the Salado flow results. See King (2023) for a full discussion of the Salado flow model and results.

Information Only

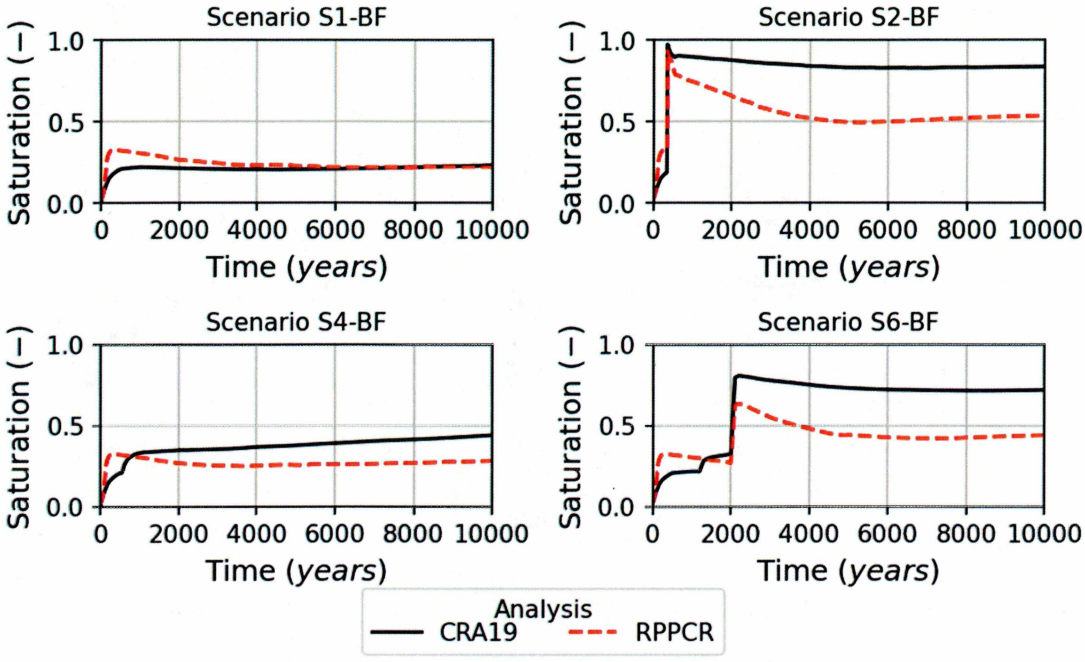

Figure 4-6. Mean Brine Saturation in the Waste Panel (King 2023)

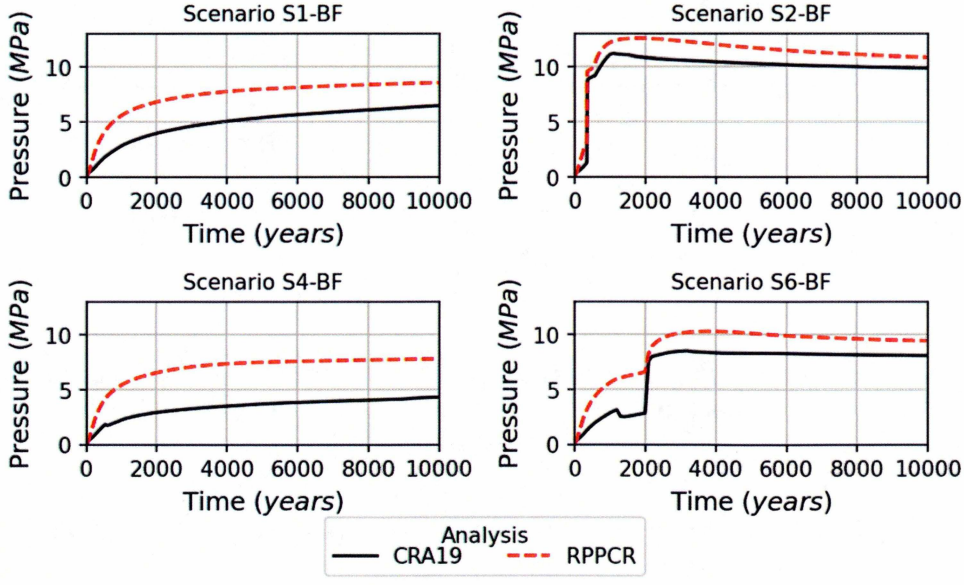

Figure 4-7. Mean Brine Pressure in the Waste Panel (King 2023)

Information Only

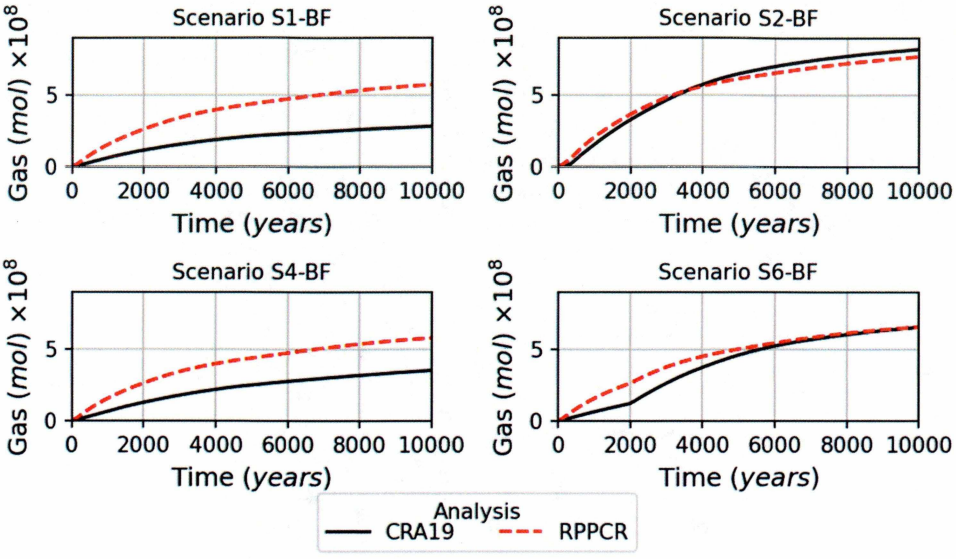

Figure 4-8. Mean Cumulative Total Gas Generation (King 2023)

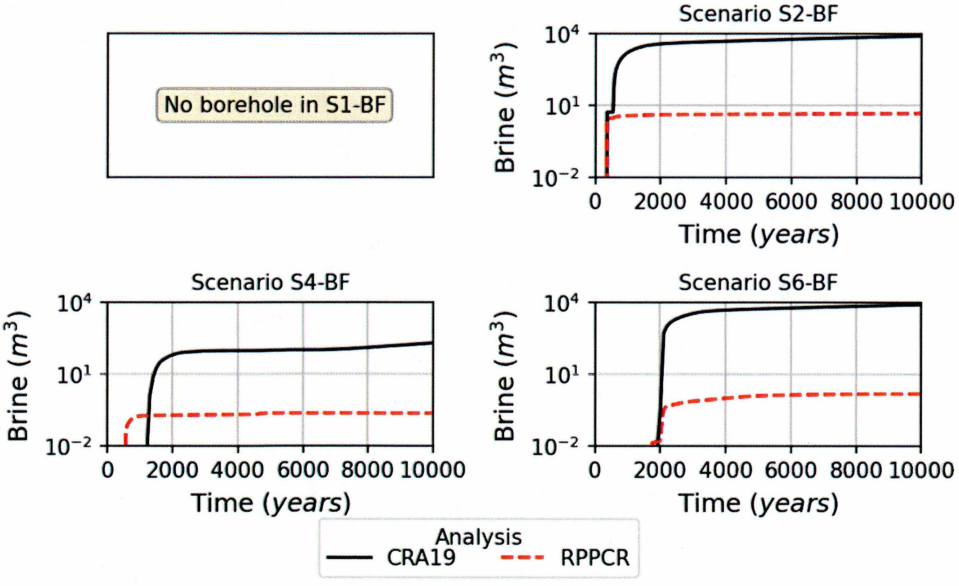

Figure 4-9. Mean Cumulative Brine Flow up the Borehole (King 2023)

Information Only

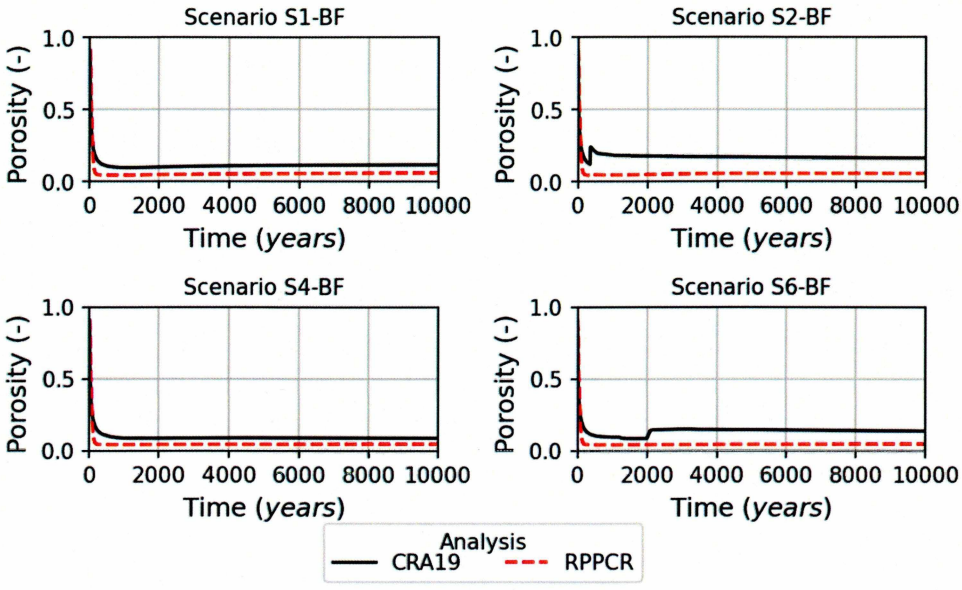

Figure 4-10. Mean Waste Panel Porosity (King 2023)

Table 4-8. Fraction of Realizations with more than 10% of Initial Iron Remaining Uncorroded After 10,000 Years (King 2023)

Scenario	Representative Waste Panel		Total Waste Area	
	CRA19	RPPCR	CRA19	RPPCR
S1-BF	91%	80%	98%	92%
S2-BF	15%	44%	98%	92%
S4-BF	79%	81%	98%	92%
S6-BF	32%	66%	98%	92%

4.3 Cuttings, Cavings, and Spallings

The CUTTINGS_S code calculates the quantity of material brought to the surface from a radioactive waste disposal repository as a consequence of an inadvertent human intrusion through drilling, either as cuttings and cavings or as spallings releases.

The RPPCR uses CUTTINGS_S version 6.04. CUTTINGS_S calculates an area for cuttings and cavings and a spallings volume for each combination of replicate, vector, scenario, drilling location, and intrusion time. A total of 31,200 areas (3 replicates × 100 vectors × 4 drilling locations × 26 intrusion times) and 31,200 volumes were determined. CUTTINGS_S uses sampled parameters for waste shear strength and drill string angular velocity, as well as a set of constant inputs providing waste material, borehole, and drilling mud parameters (Kicker 2023a, Tables 2 and 3).

Information Only

4.3.1 Cuttings and Cavings

Cuttings and cavings parameters and results are the same for the RPPCR and the CRA-2019 PA. The drill bit diameter is specified to be 0.311150 m, which corresponds to a cuttings area of 0.0760 m^2 for all realizations. The variation in cavings area arises primarily from uncertainty in the shear strength of the waste (parameter BOREHOLE:TAUFAIL). Lower shear strengths tend to result in larger cavings areas (Figure 4-11). In Figure 4-11, the lowest attainable cuttings and cavings area is 0.0760 m^2, which corresponds to a release due only to cuttings (i.e., a release with zero cavings area). Statistics for cavings area are shown in Table 4-9.

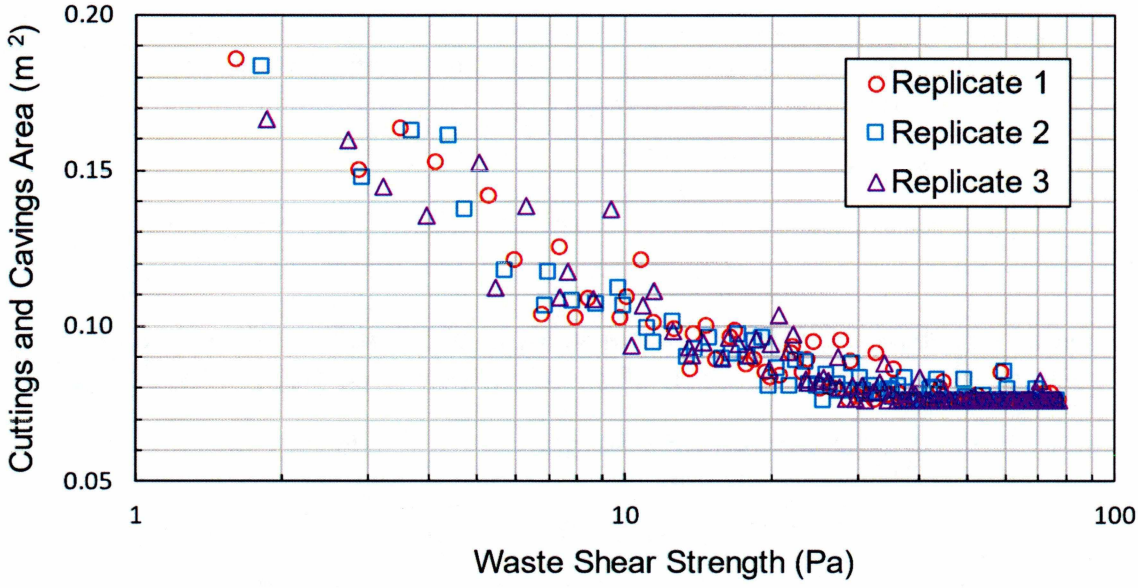

Figure 4-11. Cuttings and Cavings Area as a Function of Waste Shear Strength for RPPCR (Kicker 2023a)

Information Only

Table 4-9. Cavings Area Statistics for the RPPCR and CRA-2019 (Kicker 2023a)

Material	Mean Cavings Area (m^2)	Maximum Cavings Area (m^2)	Number of Vectors without Cavings
R1	0.011	0.110	49
R2	0.010	0.107	44
R3	0.011	0.090	49

4.3.2 Spallings

Spallings volumes are calculated based on pressure conditions in the repository waste areas and are discussed in Section 4.3.2.1. Average CH-TRU waste concentration (activity/volume) is discussed in Section 4.3.2.2.

4.3.2.1 Spallings Volume

Time-dependent spallings volumes are determined by interpolating the spallings volumes calculated by DRSPALL to the time-dependent repository pressures calculated by BRAGFLO. Intrusion scenarios and times used in the calculation of spallings volumes are shown in Table 4-10. Summary statistics of spallings volumes for each intrusion scenario are shown in Table 4-11 for all 3 replicates of the RPPCR and the CRA-2019 PA. These statistics are assessed over all replicates, scenarios, intrusion times, vectors, and drilling locations. As seen in Table 4-11, the maximum spallings volumes are higher in the RPPCR compared to the CRA-2019 PA, except for scenario S3-DBR, where they are the same. The likelihood of spallings and the means (of non-zero) spallings volumes are higher in the RPPCR compared to the CRA-2019 for all intrusion scenarios.

For the CRA-2019 PA, spallings were calculated for three intrusion locations: 1) the Upper Region (which corresponds to the North RoR region from BRAGFLO calculations); 2) the Middle Region (South RoR); and 3) Lower Region (South Waste Panel). The RPPCR adds a fourth intrusion location: the Other Region (which corresponds to the West RoR region from BRAGFLO calculations). Spallings by intrusion location are shown in Table 4-12. Spallings releases in each region are similar, with the highest maximum spallings volumes and highest number of nonzero spallings volumes occurring in the lower intrusion location.

Information Only

Table 4-10. Intrusion Scenarios used in Calculating Direct Brine and Spallings Releases (Kicker 2023a)

DBR/ Spallings Scenario[1]	BRAGFLO Scenario for Initial Conditions	Previous Intrusion Type and Time (year)	Subsequent Intrusion Times – (year)
S1-DBR	S1-BF	None (Undisturbed Repository)	100, 350, 1000, 3000, 5000, 10000
S2-DBR	S2-BF	E1 intrusion at 350	550, 750, 2000, 4000, 10000
S3-DBR	S3-BF	E1 intrusion at 1,000	1200, 1400, 3000, 5000, 10000
S4-DBR	S4-BF	E2 intrusion at 350	550, 750, 2000, 4000, 10000
S5-DBR	S5-BF	E2 intrusion at 1,000	1200, 1400, 3000, 5000, 10000

[1]The S*x*-DBR (*x*=1-5) scenario uses the S*x*-BF scenario results (waste area pressures and saturations) as initial conditions for a subsequent intrusion at the times given in the last column.

Table 4-11. Summary Spallings Results by Intrusion Scenario (Kicker 2023a)

Scenario	Maximum Volume (m^3)		Mean Nonzero Volume (m^3)		Number (and Percentage) of Realizations with Nonzero Spallings Volume	
	RPPCR	CRA19	RPPCR	CRA19	RPPCR	CRA19
S1-DBR	12.09	7.47	1.24	0.72	1085 (15.1%)	258 (4.8%)
S2-DBR	12.76	10.23	0.99	0.83	2021 (33.7%)	1254 (27.9%)
S3-DBR	10.23	10.23	0.92	0.68	1988 (33.1%)	1063 (23.6%)
S4-DBR	11.38	7.47	0.98	0.59	951 (15.9%)	105 (2.3%)
S5-DBR	9.97	7.47	1.02	0.56	1217 (20.3%)	135 (3.0%)

Information Only

Table 4-12. Summary Spallings Results by Intrusion Location (Kicker 2023a)

Location	Maximum Volume (m^3)		Mean Nonzero Volume (m^3)		Number (and Percentage) of Nonzero Volumes	
	RPPCR	CRA19	RPPCR	CRA19	RPPCR	CRA19
Lower Region (South Waste Panel)	12.76	10.23	1.01	0.76	2304 (29.5%)	1135 (14.6%)
Middle Region (South ROR)	12.69	10.23	1.01	0.75	2294 (29.4%)	1128 (14.5%)
Upper Region (North ROR)	12.59	9.85	1.09	0.71	1688 (21.6%)	552 (7.1%)
Other Region (West ROR)	10.13	—	0.86	—	976 (12.5%)	—

The cumulative frequency of nonzero spallings volumes for the RPPCR (Replicates 1, 2, and 3) is shown in Figure 4-12, together with the CRA-2019 PA. Figure 4-12a considers only those simulations in which nonzero spallings occur, showing higher spallings volumes in the RPPCR compared to the CRA-2019 at corresponding cumulative frequency levels. Figure 4-12b plots the cumulative distribution of spallings volume including all simulations. The shift in the cumulative frequency of occurrence curve for the RPPCR spallings volumes compared to the CRA-2019 (Figure 4-12b) is the result of more simulations with spallings across all intrusion locations.

The new porosity surface has the largest effect on pressure behavior (King 2023, Section 4.2). The increase in radionuclide and steel inventory will also drive more gas generation leading to increased pressures. The increased excavated volume of the new panels is not seen as a major driver for the pressure prediction (Section 4.2), and therefore not a major driver for the increase in spalling volumes.

Information Only

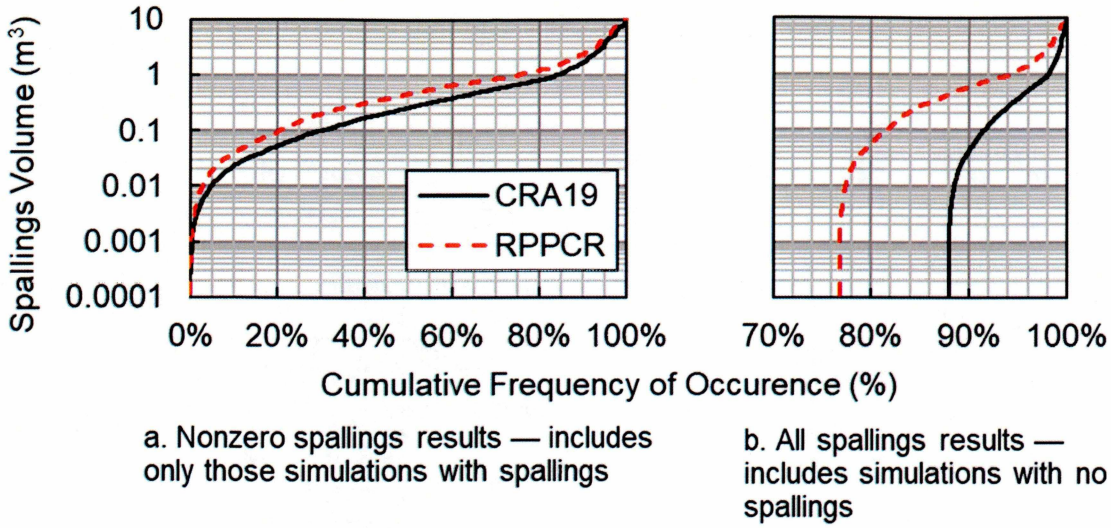

Figure 4-12. Cumulative Frequency of Spallings Volume in the RPPCR and the CRA-2019 (Kicker 2023a)

4.3.2.2 Spallings Concentration

For spallings releases in PA calculations, concentrations of radionuclides are calculated by the PRECCDFGF code from EPAUNI output as the volume-weighted average concentration in all CH-TRU waste streams. Spallings concentration (EPA units/m^3 of waste) throughout the 10,000-year regulatory period is shown in Figure 4-13. Compared to the CRA-2019 inventory, the RPPCR inventory shows consistently higher concentrations over time.

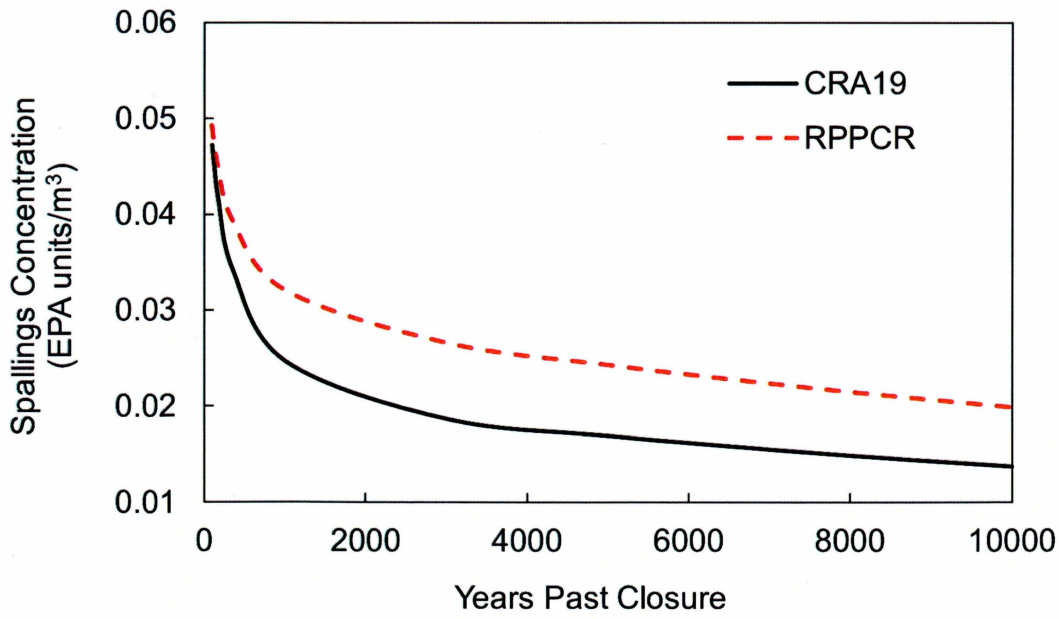

Figure 4-13. Spallings Concentration from Closure to 10,000 Years (Kicker 2023a)

Information Only

4.4 Direct Brine Release Volumes

Combined direct brine volume results for all three replicates of the CRA-2019 and the RPPCR are discussed in this section. Compared to the CRA-2019, the fraction of DBR simulations with non-zero releases is greater in the RPPCR (Table 4-13). Most releases are, however, small in magnitude; the number of large magnitude releases in the RPPCR is decreased compared to the CRA-2019 (Figure 4-14 and Figure 4-15).

Mean, median, and maximum non-zero release volumes are all decreased for the RPPCR (Figure 4-16). Note also that mean, median and maximum release volumes are comparable across the five intrusion scenarios in the RPPCR (Figure 4-17); in the CRA-2019, scenarios S2-DBR and S3-DBR dominated these measures. Considering all scenarios, intrusion times, vectors and locations, the mean volume of brine released in the RPPCR is only about one third of the volume released in the CRA-2019 (Table 4-13).

For both the CRA-2019 and the RPPCR, the largest fraction of non-zero DBRs, and the mean non-zero release volume, occur at the L intrusion location; these quantities decrease as the intrusion location moves to the north, that is, up dip (Table 4-13). Releases from the O intrusion location, which was not included in the CRA-2019, contribute to RPPCR DBRs; however, O intrusion releases are less frequent and mean volumes are smaller compared to the L, M and U intrusion locations in the RPPCR.

As described by King (2023), the RPPCR Salado flow results show an increase in mean and median brine pressures and, for scenarios without a previous E1 intrusion (i.e., S1-DBR, S4-DBR and S5-DBR), an increase in brine saturation; these are effects that would tend to increase the number of non-zero DBRs. King (2023) also points out that maximum brine pressure is reduced in the RPPCR and, for scenarios with a previous E1 intrusion (i.e., S2-DBR and S3-DBR), there is a decrease in brine saturation relative to CRA-2019; these are effects that will tend to reduce the largest DBR volumes.

The updated porosity surface has the largest effect on DBR volumes from the CRA-2019 to the RPPCR is the updated porosity surface used in the Salado flow calculations to determine pressure and brine saturation in the waste, which are initial conditions for DBR simulations. The new porosity surface significantly reduces porosity in the waste compared to the CRA-2019 (King 2023), affecting both initial waste pressure and brine saturation in the RPPCR DBR simulations.

Information Only

Table 4-13. DBR Volume Summary (Docherty and King 2023)

Intrusion Location	Mean Brine Released (m^3)		Fraction of Simulations with Non-Zero Releases		Mean of Non-Zero Brine Releases (m^3)	
	CRA19	RPPCR	CRA19	RPPCR	CRA19	RPPCR
S1-DBR	0.26	0.58	2.54%	9.58%	10.11	6.03
L	0.70	1.51	5.44%	15.67%	12.87	9.66
M	0.07	0.34	1.17%	7.22%	5.62	4.74
U	0.00	0.34	1.00%	8.89%	0.30	3.88
O	-	0.11	-	6.56%	-	1.66
S2-DBR	8.29	2.18	47.22%	37.90%	17.55	5.76
L	15.64	5.46	73.53%	74.27%	21.27	7.35
M	9.21	2.56	66.07%	55.40%	13.94	4.61
U	0.00	0.57	2.07%	14.40%	0.15	3.99
O	-	0.14	-	7.53%	-	1.88
S3-DBR	5.23	1.43	40.44%	33.22%	12.94	4.31
L	10.83	3.73	66.60%	66.33%	16.27	5.63
M	4.86	1.18	52.93%	40.60%	9.19	2.9
U	0.00	0.61	1.80%	15.40%	0.22	3.98
O	-	0.2	-	10.53%	-	1.92
S4-DBR	0.07	0.78	1.04%	12.72%	7.14	6.11
L	0.22	1.84	2.27%	19.40%	9.83	9.51
M	0.00	0.66	0.40%	11.67%	0.18	5.65
U	0.00	0.47	0.47%	12.33%	0.01	3.82
O	-	0.14	-	7.47%	-	1.81
S5-DBR	0.12	1.02	1.62%	14.88%	7.70	6.84
L	0.36	2.43	3.60%	22.33%	10.10	10.86
M	0.01	0.81	0.80%	12.87%	1.38	6.27
U	0.00	0.64	0.47%	13.93%	0.01	4.58
O	-	0.2	-	10.40%	-	1.96
All Scenarios						
L	5.37	2.94	29.33%	38.68%	18.29	7.6
M	2.72	1.08	23.38%	24.85%	11.65	4.34
U	0.00	0.52	1.15%	12.83%	0.18	4.06
O	-	0.16	-	8.42%	-	1.86
L, M, and U	2.70	1.51	17.96%	25.45%	15.02	5.94
ALL	2.70	1.17	17.96%	21.20%	15.02	5.54

Information Only

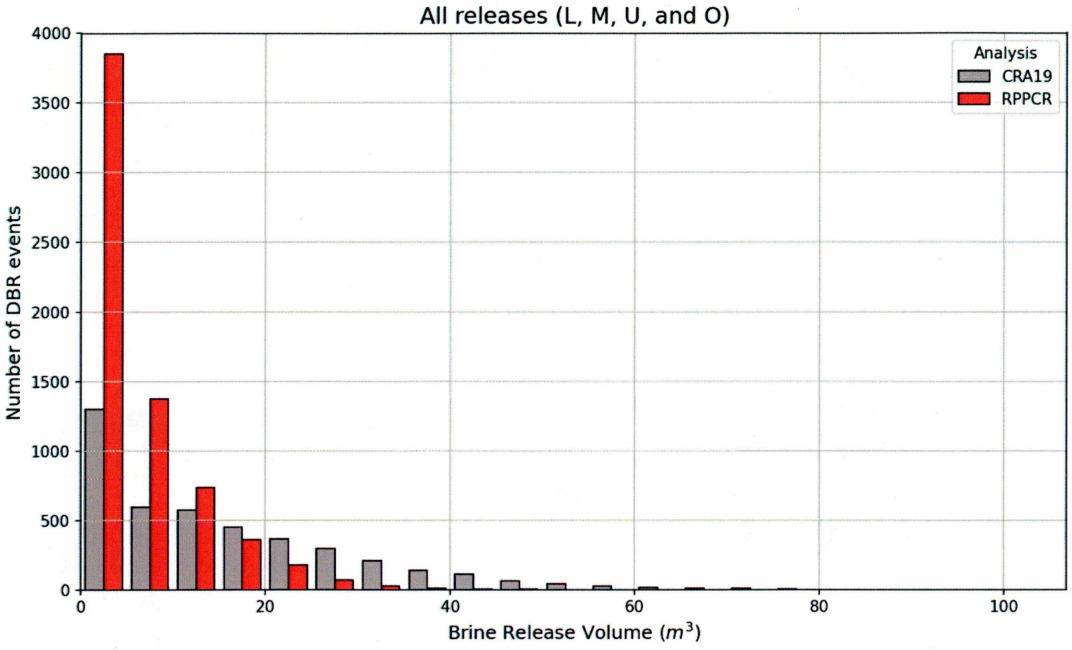

Figure 4-14. Release Volume Frequency, All Non-zero Releases (Docherty and King 2023)

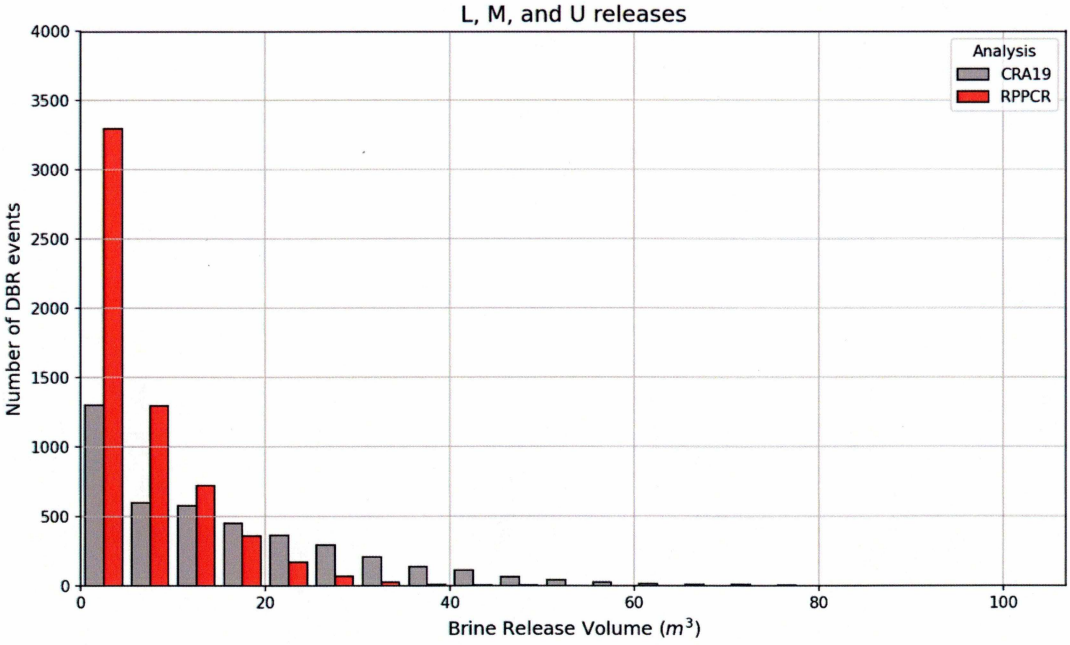

Figure 4-15. Release Volume Frequency, L, M, and U Non-zero Releases Only (Docherty and King 2023)

Information Only

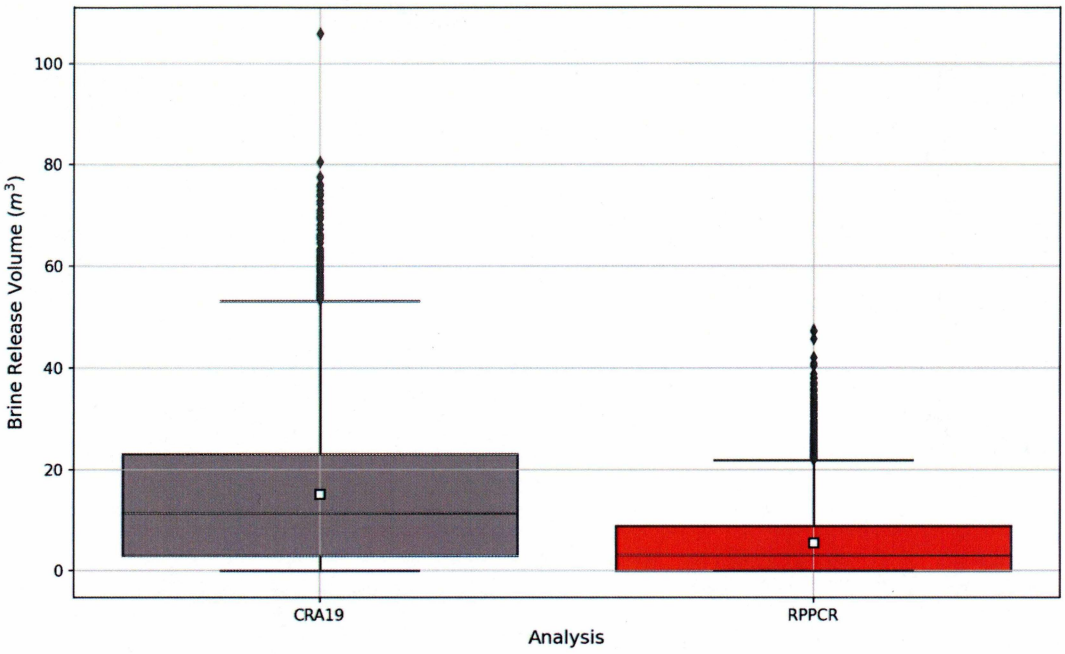

Figure 4-16. Release Volumes, All Non-zero Releases (Docherty and King 2023)

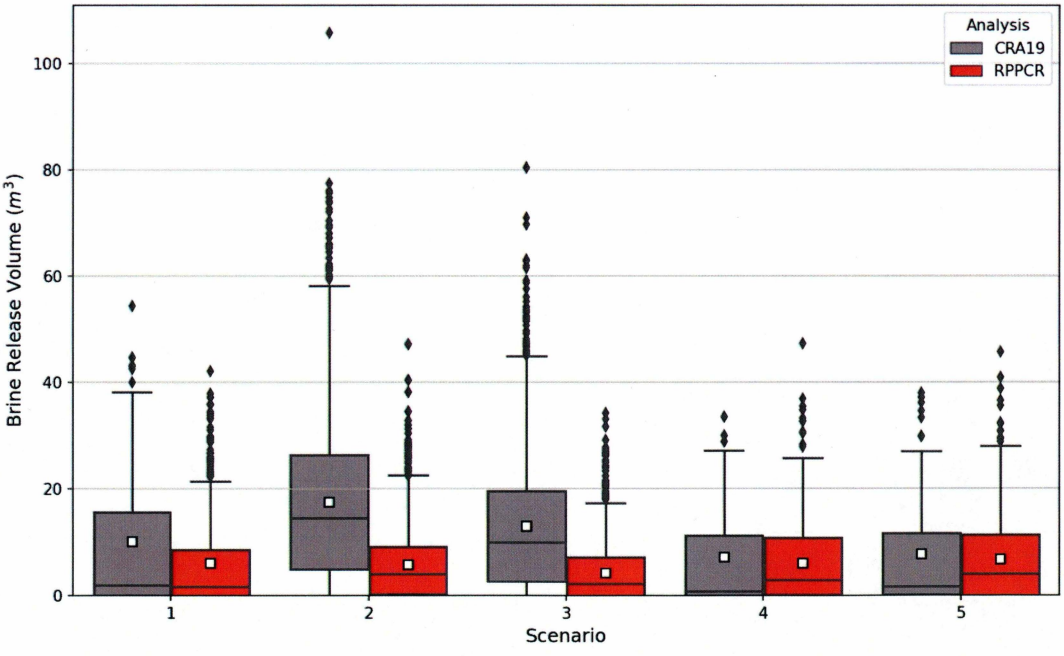

Figure 4-17: Release Volumes by Scenario, All Non-zero Releases (Docherty and King 2023)

Information Only

4.5 Mobilized Radionuclide Concentrations

Changes in the baseline solubilities, solubility uncertainty distributions, intrinsic and microbial colloid enhancement parameters, and the likelihood of selecting the Pu(III) oxidation state have affected total mobilization potentials for actinide elements in the RPPCR (Kim 2023, Section 4.2). Because the solubilities of lumped radionuclides are calculated with the total mobilization potential for actinide elements and the fixed (in time) lumped-isotopes-to-element mole fraction (LSOLDIF) parameters, the impact of these changes can be observed in Figure 4-18. This figure shows distributions of the solubilities of lumped radionuclides that are used by both PANEL and NUTS to calculate their transport within the Salado formation. Mean solubilities of AM241L and TH230L are increased in the RPPCR, while those of PU239L, PU238L, and U234L are decreased.

A decrease in the likelihood of Pu(III) to 0.25 from 0.5 means that more realizations are represented by Pu(IV), which has lower total mobilization potential for 96% of realizations in the RPPCR. As the likelihood of selecting the Pu(III) oxidation state decreases, mean total mobilization potential for Pu is decreased within the same analysis. As such, a decrease in the likelihood of selecting the Pu(III) oxidation state from 0.5 (in the CRA-2019) to 0.25 (in RPPCR) decreases the mean total mobilization potential for Pu (Kim 2023, Section 4.2).

The instantaneous concentrations for lumped radionuclides are determined as a function of time by PANEL. Figure 4-19 shows mean instantaneous concentrations in Castile brine for lumped radionuclides with the lowest assumed brine volume. Mean instantaneous concentrations for lumped radionuclides except TH230L are decreased in the RPPCR. AM241L is the dominant contributor to mean total instantaneous concentration at earlier times, while PU239L is the dominant contributor at later times. Total radionuclide concentrations in Castile brine for all realizations are shown in Figure 4-20. Activity from Am-241 is the primary component of total concentrations early times. A noticeable change in activity concentration occurs as Am-241 decays and becomes inventory limited. At late times, Pu-239 becomes the primary component of total activity concentrations.

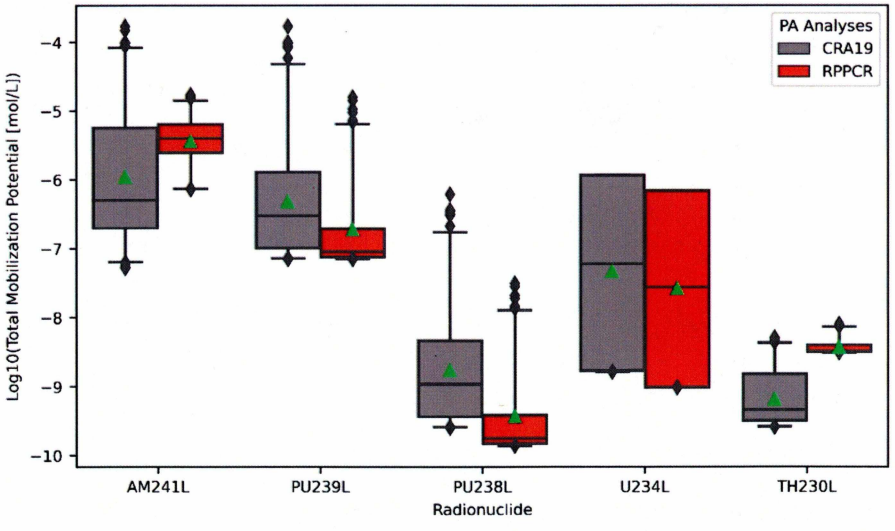

Figure 4-18. Log10 of the Solubility for the Lumped Radionuclides in Castile Brine (Kim 2023)

Information Only

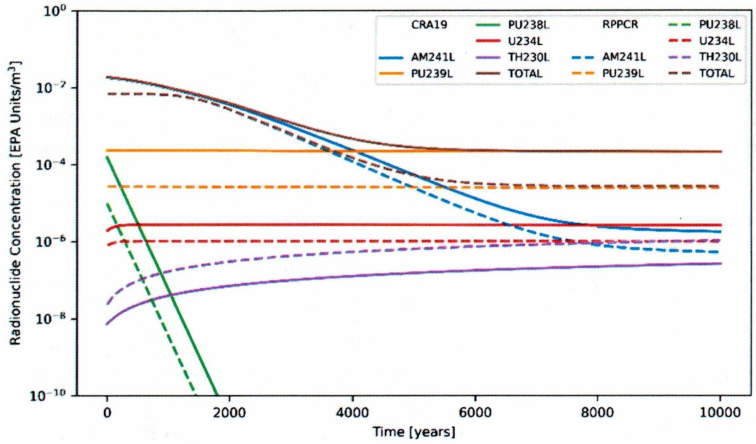

Figure 4-19. Means Radionuclide Concentrations of Lumped and Total Actinides in 33,804 m^3 Castile Brine over Time (Kim 2023)

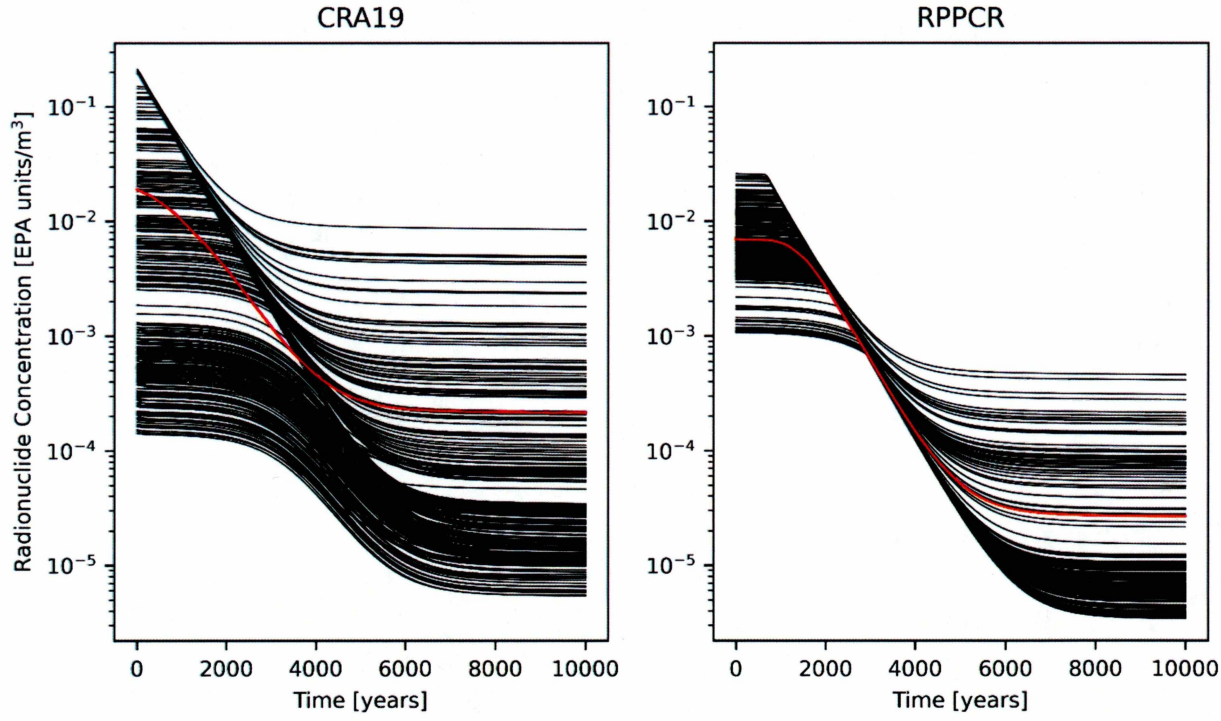

Figure 4-20. Total Activity Concentration in Castile Brine vs Time for 3 Replicates (Kim 2023)

4.6 Salado Transport

Radionuclide transport up an intruding borehole is the primary pathway for radionuclide mass transport through the Salado. The large decrease in brine discharges through the borehole, discussed in Section 4.2, greatly reduces the radionuclide mass transport through the Salado.

Information Only

Table 4-14 summarizes the number of screened-in vectors for scenarios S2 – S5. As discussed in Section 3.7, screened-in vectors are those with the potential to transport a significant mass of radionuclides (exceeding the cutoff of 1.0×10^{-7} kg) and are thus selected to undergo the full transport simulation. Vectors that are screened in for scenarios S2 – S5 are automatically screened in for scenario S1, so the number of the screened-in vectors for scenario S1 is not shown in this table. The number of screened-in vectors in the RPPCR are considerably decreased compared to the CRA-2019. The updated borehole permeability significantly decreases brine flow up the borehole (Section 4.2) which decreases radionuclide transport up the borehole. The updated long-term borehole permeability is considered to be the dominant factor decreasing the number of vectors exceeding the screening criteria.

Table 4-14. Number of the Screened-in Vectors (Kim 2023)

Scenario	CRA19				RPPCR			
	R1	R2	R3	Total	R1	R2	R3	Total
S2	67*	69	71	207	25	25	22	72
S3	60*	62	59	181	17	15	19	51
S4	8*	7	7	22	2	2	1	5
S5	8*	7	6	21	1	1	1	3

* Vector 53 in the CRA19 showed that the cumulative tracer release through the Marker Beds to the LWB (but not a borehole to the Culebra) exceeded 1×10^{-7} kg.

Table 4-15 shows that mean cumulative lumped radionuclide discharges to the Culebra are decreased in the RPPCR by several orders of magnitude compared to the CRA-2019. Mean cumulative discharges of TOTAL (= AM241L + PU239L + PU238L + U234L + TH230L) lumped radionuclides through a borehole to the Culebra at 10,000 years for the E1 intrusion scenarios (scenarios S2 and S3) are decreased in RPPCR by a factor of $\sim 10^4$, for the E2 intrusion scenarios (scenarios S4 and S5) by a factor of $\sim 10^3$, and for the E1E2 intrusion scenario (scenario S6) by a factor of $\sim 10^3$.

Information Only

Table 4-15. Mean Cumulative Lumped Radionuclides Discharges (in EPA Units) Through a Borehole to the Culebra at 10,000 Years (Kim 2023)

Analysis	Scenario	AM241L	PU239L	PU238L	U234L	TH230L	TOTAL
CRA19	2	5.89E+00	1.54E+00	2.86E-02	9.80E-03	8.23E-04	7.46E+00
	3	1.44E+00	8.39E-01	9.56E-05	5.45E-03	5.81E-04	2.28E+00
	4	5.08E-02	6.37E-02	7.02E-06	3.93E-04	1.27E-05	1.15E-01
	5	2.39E-02	6.08E-02	7.53E-09	3.59E-04	1.10E-05	8.50E-02
	6	2.77E+00	5.43E+00	5.53E-08	1.94E-02	8.67E-04	8.22E+00
RPPCR	2	7.48E-04	1.67E-05	3.66E-08	2.80E-06	1.06E-06	7.68E-04
	3	2.76E-04	1.26E-05	2.71E-09	2.24E-06	6.64E-07	2.92E-04
	4	1.49E-04	1.18E-06	1.69E-09	2.48E-07	6.56E-08	1.50E-04
	5	5.89E-05	3.01E-07	1.01E-11	1.82E-07	4.33E-08	5.94E-05
	6	3.99E-03	2.69E-05	2.40E-11	3.98E-06	1.23E-06	4.02E-03

4.7 Culebra Flow and Transport

This section presents the Culebra flow and transport results first using particles tracks from a non-sorbing particle, then using radionuclide transport simulations from a 1 kg source term placed at the release point. Total discharge of radionuclides across the LWB at the Culebra for random futures is calculated with the code CCDFGF (see Section 4.8.4) using the radionuclide transport simulations presented here. Results for Replicate 1 of the RPPCR Culebra flow and transport for the full and partial mining scenarios and mass release points CRP1, CRP2, CRP3, and CRP4 (Figure 2-4) will be summarized. Results from Replicates 2 and 3 are similar to those from Replicate 1. Bethune (2023) presents the full set of results and in more detail. CRP1 results are compared to the CRA-2019. CRP2 through CRP4 are new to the RPPCR.

The WIPP software DTRKMF is used to track non-sorbing particles from the mass release locations to the LWB in the full mining scenario (Figure 4-21) and partial mining scenario (Figure 4-22). In these figures, subplots show the spatial distribution of the particle tracks for the RPPCR, with the mining-impacted area shown in gray for reference. The exceedance probability subplots describe the likelihood of a particle crossing the LWB within the range of observed particle travel times.

The results show distinct travel behavior of particles released at CRP4 in the full mining scenario, wherein particles travel west then turn sharply to the south near the western edge of the LWB. Particles released into CRP4 in the full mining scenario also cross the LWB significantly earlier than in the other release points and mining scenarios across all probability levels. In contrast, particles released into CRP1, CRP2, or CRP3 generally travel to the south. For all release points, in the partial mining particle tracks are more broadly distributed across the east-west direction (i.e., not focused by any persistent features across realizations), but are generally oriented toward the south.

Information Only

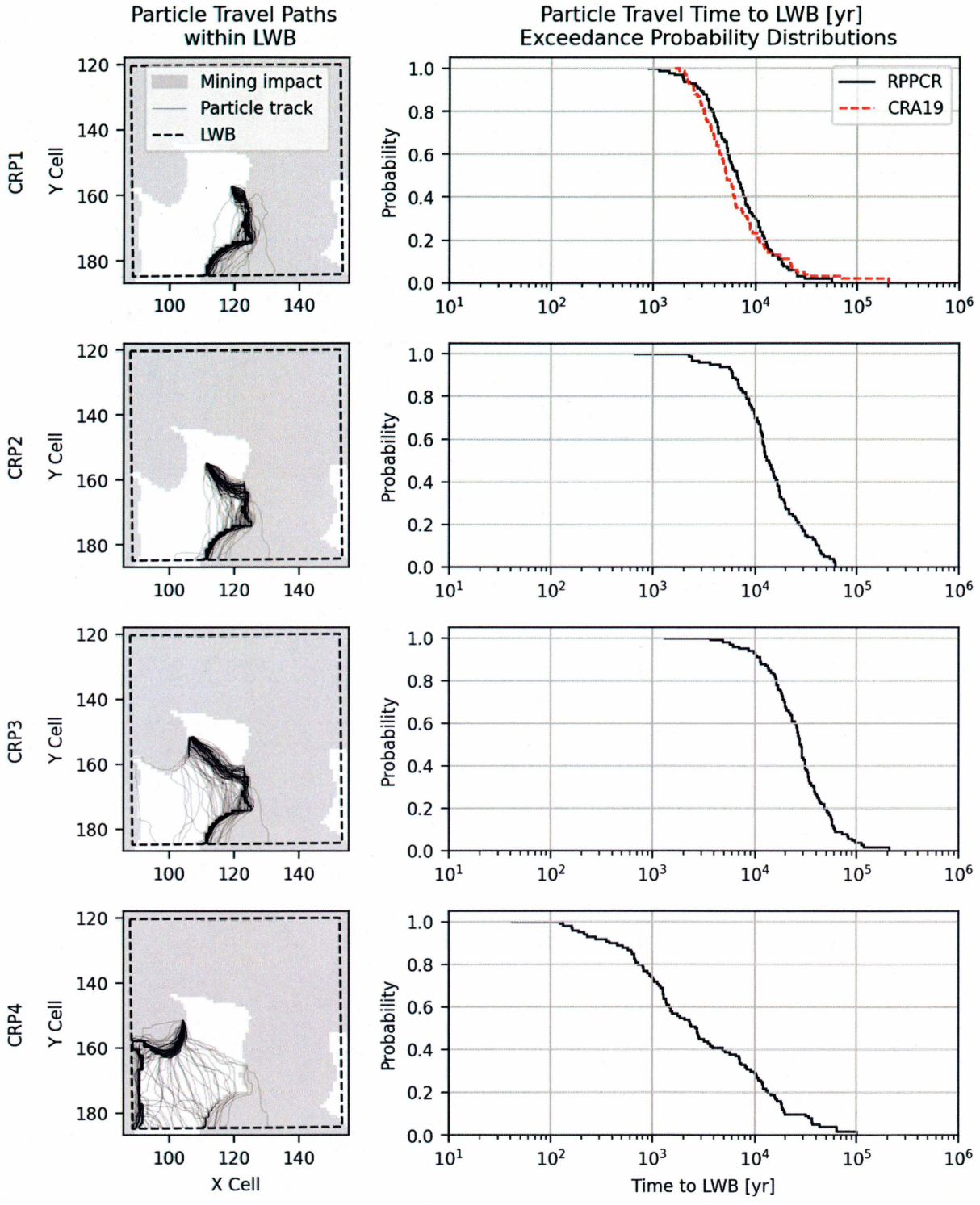

Figure 4-21. Particle Travel Paths and Travel Time to the LWB Exceedance Probabilities, Full Mining Scenario (Bethune 2023)

Information Only

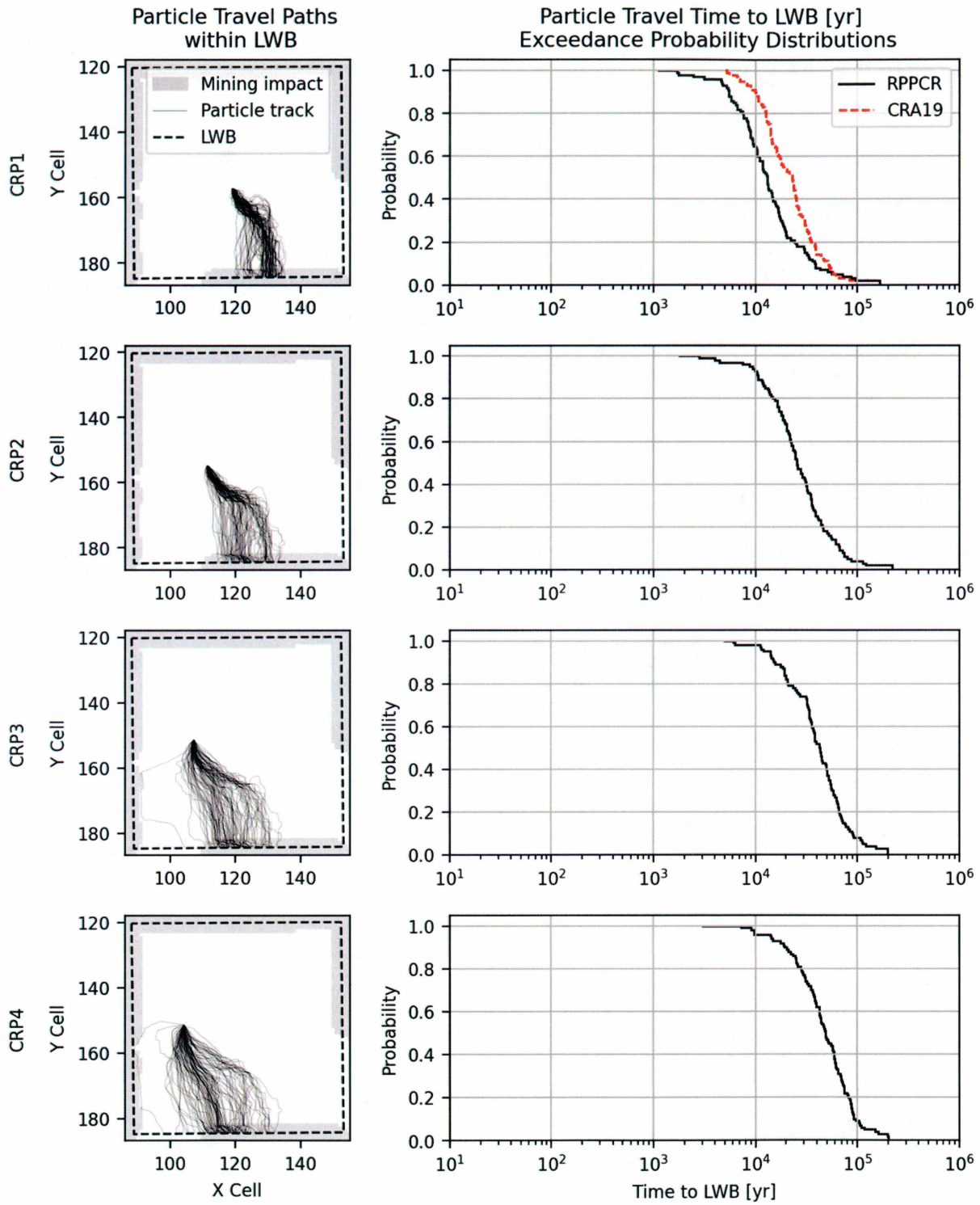

Figure 4-22. Particle Travel Paths and Resultant Travel Time to the LWB Exceedance Probabilities, Partial Mining Scenario (Bethune 2023)

Information Only

The radionuclide transport simulations account physical processes not modeled int the particle track simulations. Culebra transport results are summarized into exceedance probability curves of cumulative mass reaching the LWB by 10,000 years model time for the full mining scenario (Figure 4-23) and partial mining scenario (Figure 4-24). Results are shown for radionuclides Am-241, Pu-239, Th-230, and U-234. Consistent with Bethune (2023), the notation Th-23A refers to Th-230 released that enters the Culebra as Th-230. The notation Th-230 refers to the daughter product of U-234 which decays inside of the Culebra. Only the Th-23A results are summarized in this report. The CCDFs are shown on a logarithmic abscissa from 10^{-10} to 1 kg. Results below the plotting limits are not shown on the figures, resulting in some figures displaying few data points.

Consistent with the particle tracking results, mass released into CRP4 in full mining flow conditions results in earlier and higher radionuclide discharge to the LWB at all visible probability levels than for other combinations of mining scenario and release point. Mass discharge of U-234 and Pu-239 is highest and occurs most frequently, while discharge of Am-241 is lowest. Mass discharge to the LWB in the partial mining scenario is relatively low on average from all displayed release points and isotopes, though maximum mass discharge is above 0.1 kg in the Pu-239 and U-234 simulations. The CRA-2019 mass discharge to the LWB is comparable to the RPPCR CRP1 mass discharge result for all isotopes and mining scenarios.

Information Only

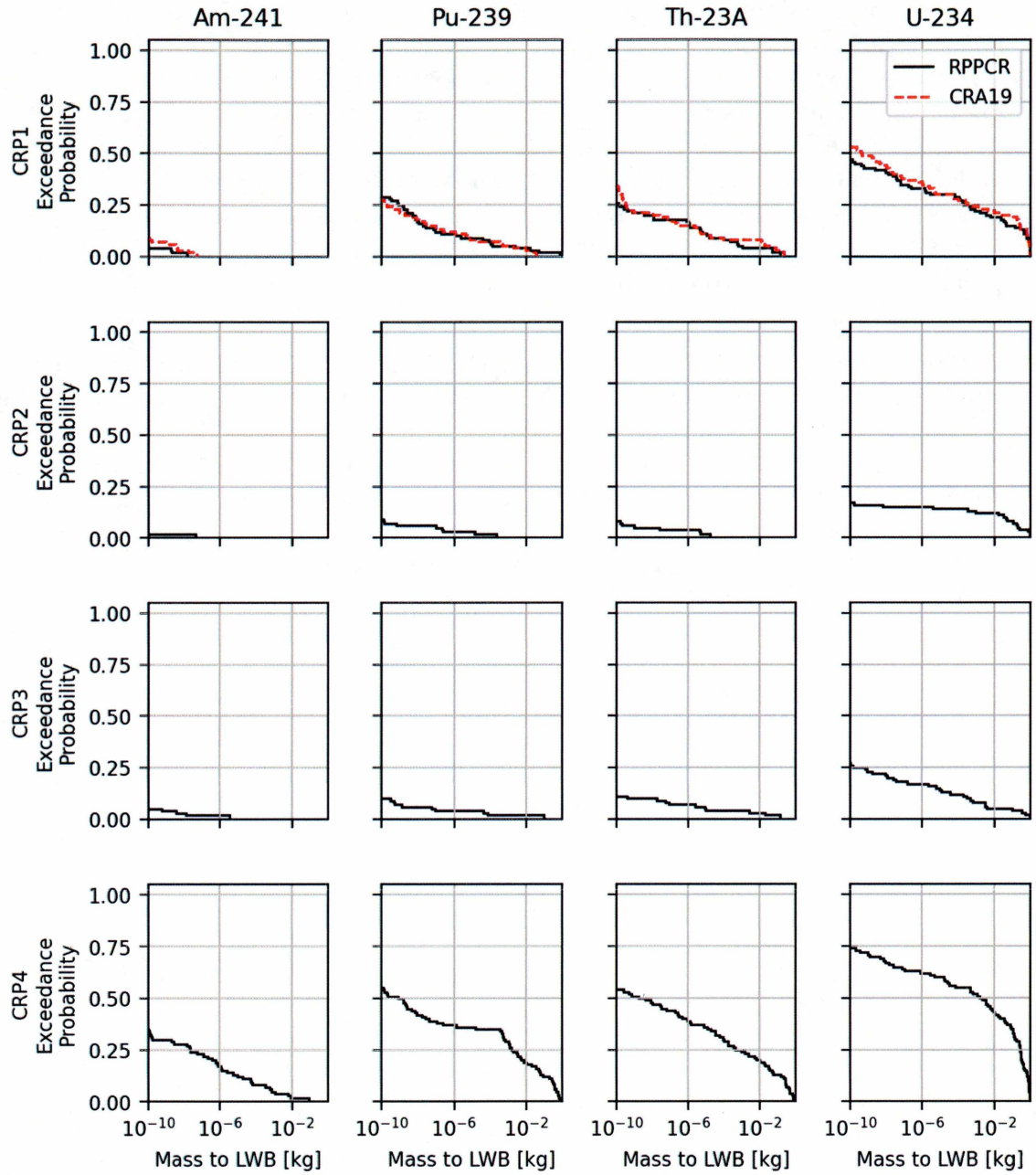

Figure 4-23. Exceedance Probabilities of Cumulative Mass Discharge to the LWB by 10,000 Years by Release Point (rows) and Radionuclide (columns), Full Mining Scenario (Bethune 2023)

Information Only

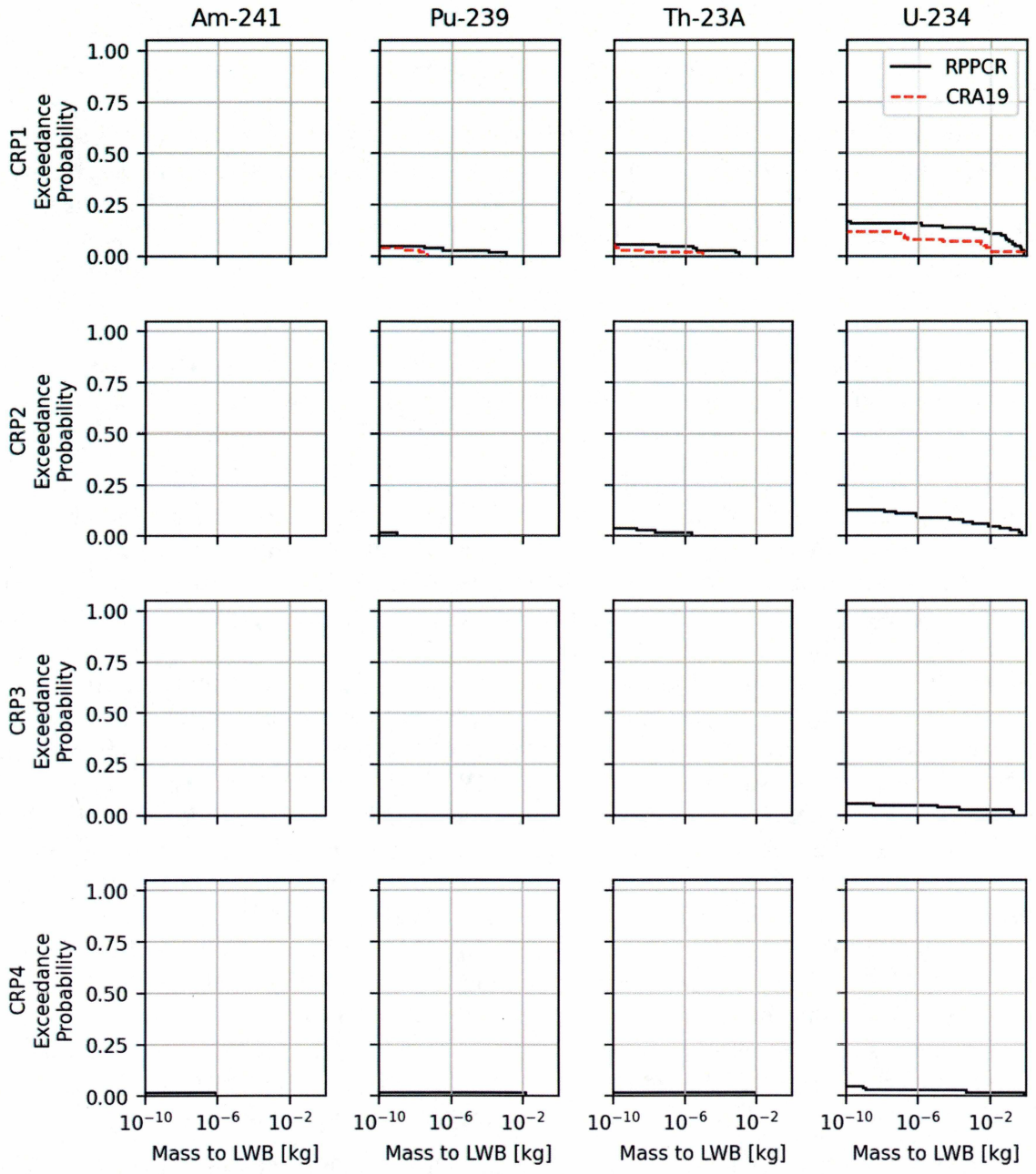

Figure 4-24. Exceedance Probabilities of Cumulative Mass Discharge to the LWB by 10,000 Years by Release Point (rows) and Radionuclide (columns), Partial Mining Scenario (Bethune 2023)

Information Only

4.8 Releases by Release Mechanism

This section presents releases for each of the four release mechanisms (cuttings and cavings, spallings, DBRs, and releases from the Culebra) that contribute to total releases, followed by total releases. In the results that follow, the CCDFs of releases for each release pathway are compared to results from the CRA-2019 PA. Sensitivities of total releases to uncertain parameters in the WIPP PA are also summarized. For a full description of CCDFGF results and the sensitivity analysis for each release mechanism, see Brunell and Zeitler (2023).

4.8.1 Cuttings and Cavings Releases

For each intrusion, cuttings and cavings releases are calculated from the cuttings volume, cavings volume, and radionuclide concentrations of the waste. Figure 4-25 shows the CCDFs for cuttings and cavings releases and the mean CCDF for Replicate 1 of the RPPCR. Figure 4-26 compares the cuttings and cavings volumes for the RPPCR with the CRA-2019 and the APPA.

While the cuttings and cavings results reported in Section 4.3 for individual boreholes in the RPPCR are unchanged from the CRA-2019, the larger repository footprint and the increased drilling frequency result in a greater number of boreholes per future in the RPPCR as compared to the CRA-2019. As a result of the greater number of boreholes, the cuttings and cavings volumes increased from the CRA-2019 to the RPPCR (Figure 4-26); however, the volumes represented in Figure 4-26 are excavated volumes rather than waste volumes. The waste volume in cuttings and cavings releases is computed by multiplying the excavated volume by either the parameter REFCON:FVW (FVW), which represents the fraction of the repository volume that contains contact-handled waste, or the parameter REFCON:FVRW (FVRW), which represents the fraction of the repository volume that contains remote-handled waste. A decrease in either FVW or FVRW will therefore cause a corresponding decrease in waste release volumes from each intrusion. Figure 4-27 shows the estimated cuttings and cavings waste release volumes for CRA-2019 and RPPCR, i.e., release volumes scaled by their respective values of FVW (0.385 for CRA-2019 and 0.197 for RPPCR; see Section 2.4). The effect of reducing the value of FVW is to reduce the waste mass in the cuttings and caving release volume; on average, the reduction is the same proportion as the increase in waste area footprint. Therefore, a comparison between Figure 4-26 and Figure 4-27 isolates the impact of the increased repository footprint. Note that the CCDFGF code outputs a combined volume for releases of CH and RH waste. The combined volume of CH and RH waste has been scaled by the value of FVW in Figure 4-27 for comparison purposes only.

In contrast to the smoothly decreasing CCDFs for cuttings and cavings releases in the CRA-2019, the CCDFs for cuttings and cavings in the RPPCR have a shelf-like plateau at a probability of approximately 0.4 (Figure 4-25). The plateau represents the probability of a future having at least one drilling intrusion that intersects the SR-KAC-PuOx waste stream which contains a relatively high activity concentration (Section 4.1.3). The probability of at least one borehole intersecting the SR-KAC-PuOx waste stream in a future is roughly 38% as calculated by Brunell and Zeitler (2023).

For the CRA-2019 and the APPA, the per-container volume of waste was calculated based on the volume of the container measured from the outermost container face. For the RPPCR, the per-container volume of waste is calculated based on the volume of the container measured from the

Information Only

inner container face (Table 1 of Kicker 2023c; NMED 2023). In the CRA-2019 the SR-KAC-PuOx waste stream had an activity concentration of 324 Ci/m^3 at closure, a single order of magnitude higher than the average activity concentration of 30 Ci/m^3. Due to this change in container volume measurement, in the RPPCR, the SR-KAC-PuOx activity concentration is 2.67 × 10^3 Ci/m^3 at closure, nearly two orders of magnitude greater than the average of 37.0 Ci/m^3, meaning the difference in releases between futures with a SR-KAC-PuOx intersection and those without is more dramatic in the RPPCR than in CRA-2019. Also due to the outer container volume being used for CRA-2019, the SR-KAC-PuOx waste represents 4% of the total waste volume. This gives the chance that a future does not include a borehole that intersects the SR-KAC-PuOx waste stream at roughly 28% in the CRA-2019, compared to 62% in the RPPCR. The combination of lower activity concentration and higher chance of at least one future with an intrusion intersecting the waste stream in CRA-2019 led to no observation of a plateau in cuttings and cavings releases for the CRA-2019 analysis.

Overall, as seen in Figure 4-28, the mean CCDF for cuttings and cavings releases in the RPPCR has increased at all release levels when compared to the CRA-2019. Cuttings and cavings releases in the APPA are overall similar to those in the CRA-2019, demonstrating that the additional repository volume has a minor effect on the cuttings and cavings releases seen in the RPPCR. The increase in cuttings and cavings is largely due to the increase in drilling frequency.

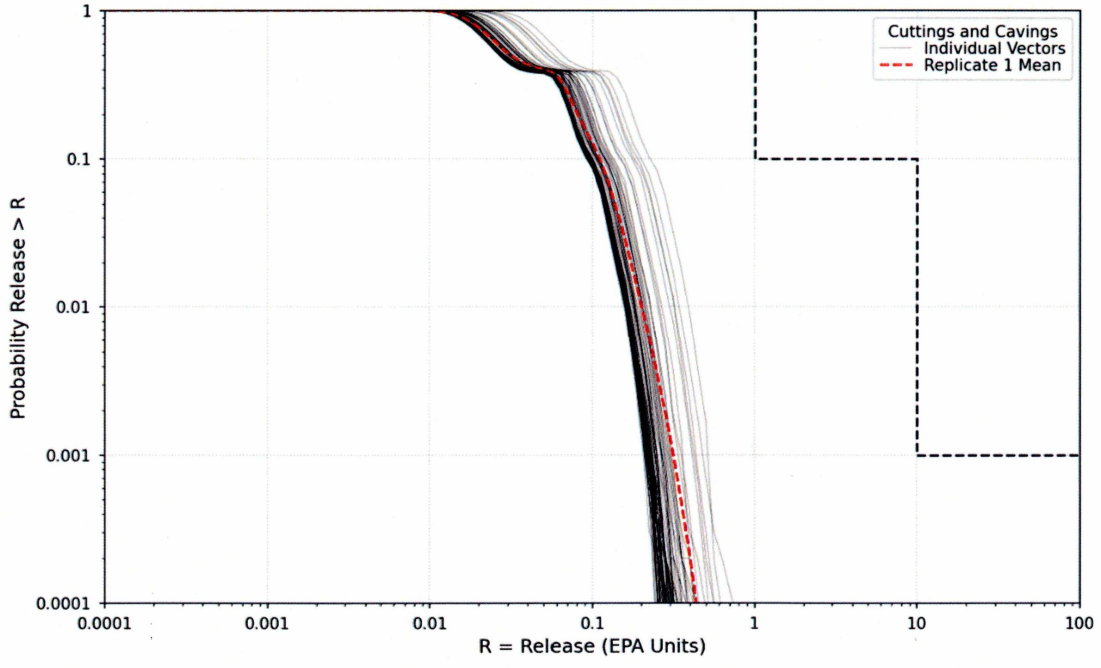

Figure 4-25. Cuttings and Cavings Releases for Replicate 1 of the RPPCR

Information Only

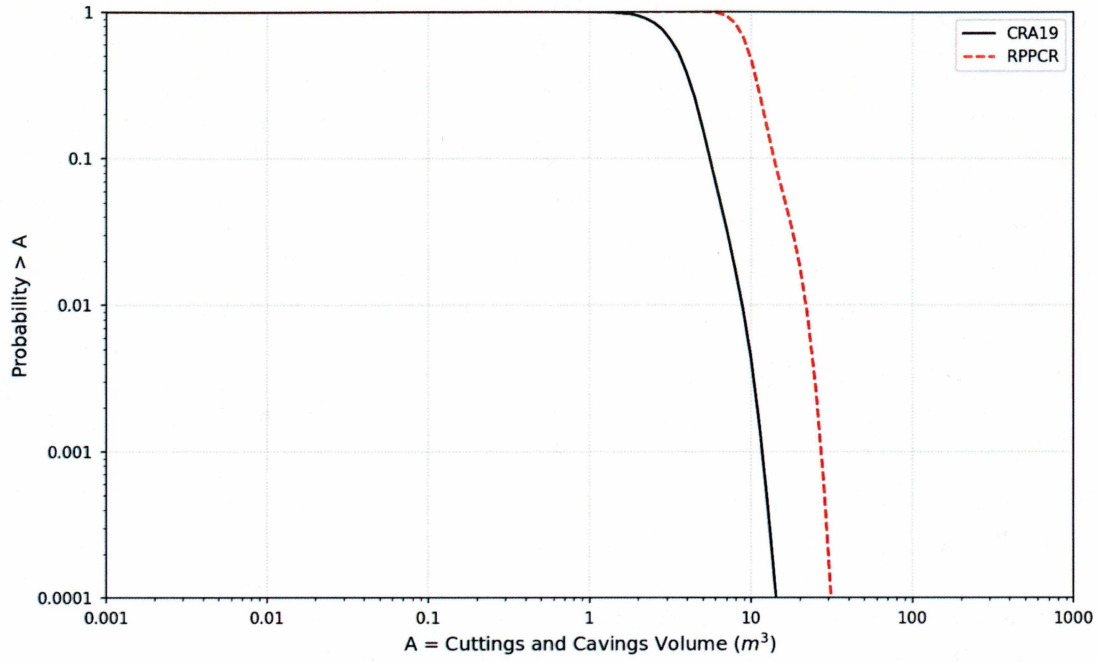

Figure 4-26. 3-Replicate Mean CCDFs for Cuttings and Cavings Release Volumes

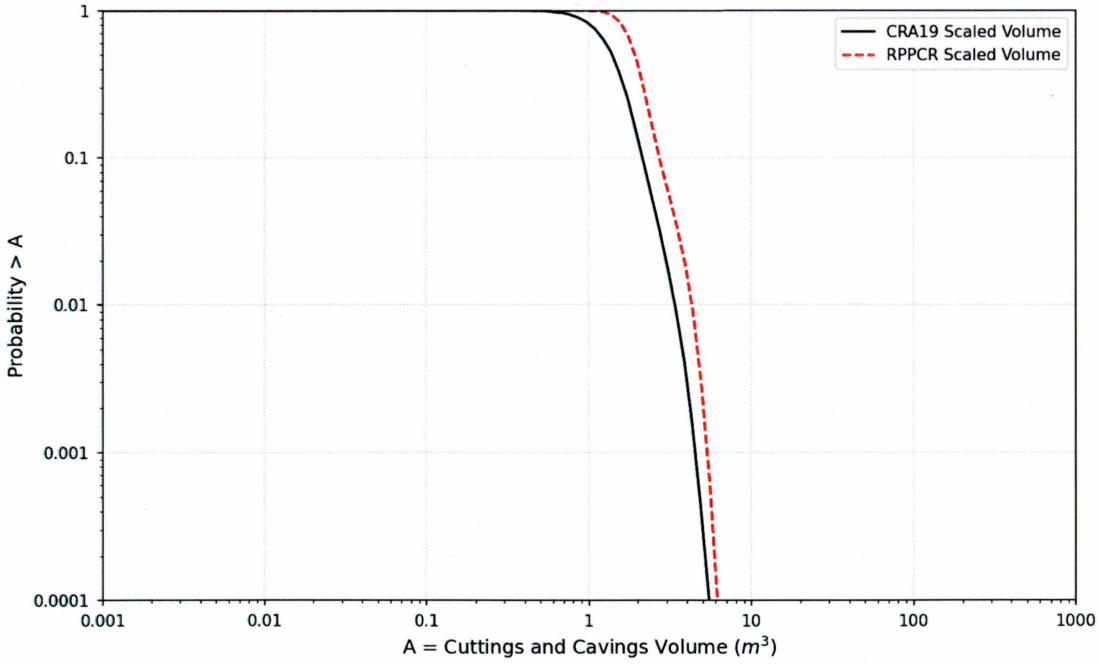

Figure 4-27. Three-Replicate Mean CCDFs for Waste Volume in Cuttings and Cavings Release Volumes

Information Only

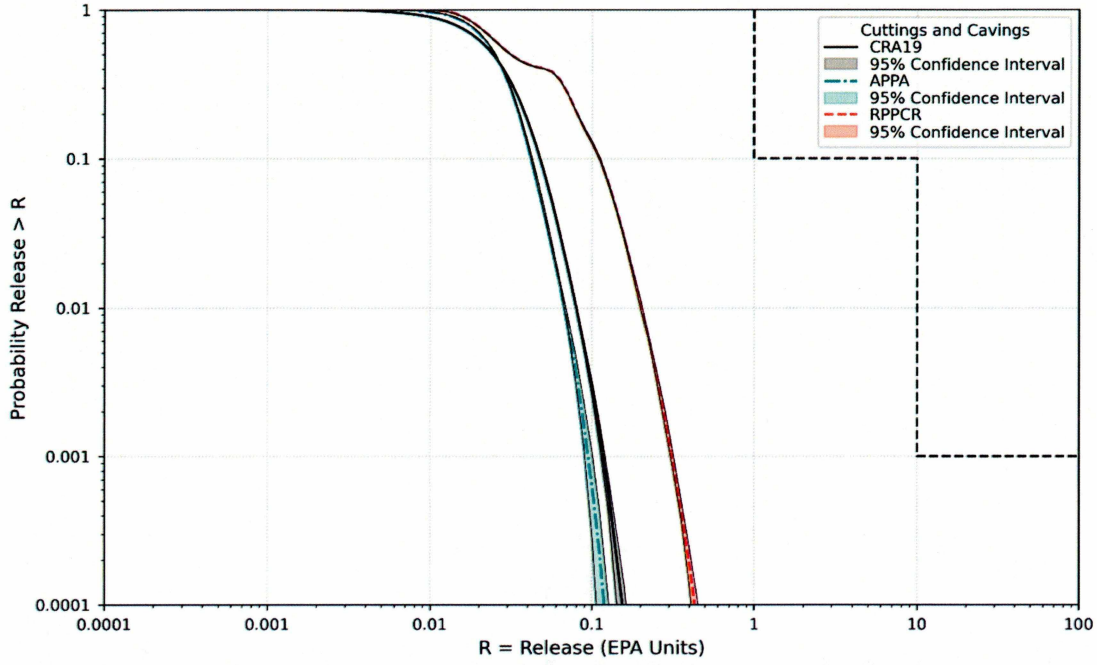

Figure 4-28. Three-Replicate Means for Cuttings and Cavings Releases with Confidence Limits

4.8.2 Spallings Releases

Spallings releases are calculated from spallings volumes and spallings concentrations. Spallings volumes from individual intrusions and the likelihood that an intrusion will result in spallings have both increased compared to CRA-2019 (Section 4.3.2.1) due to an increase in repository pressures (Section 4.2). Additionally, the increased drilling frequency and consequent increased number of boreholes in a future contributes to larger total volumes of spallings in the RPPCR (Figure 4-29). The volumes comprising spallings are scaled by the parameter REFCON:FVW (FVW) in Figure 4-30 to calculate the waste volume in spallings. Overall, the FVW-scaled spallings volumes increase in comparison to the CRA-2019 volumes (Figure 4-30).

Information Only

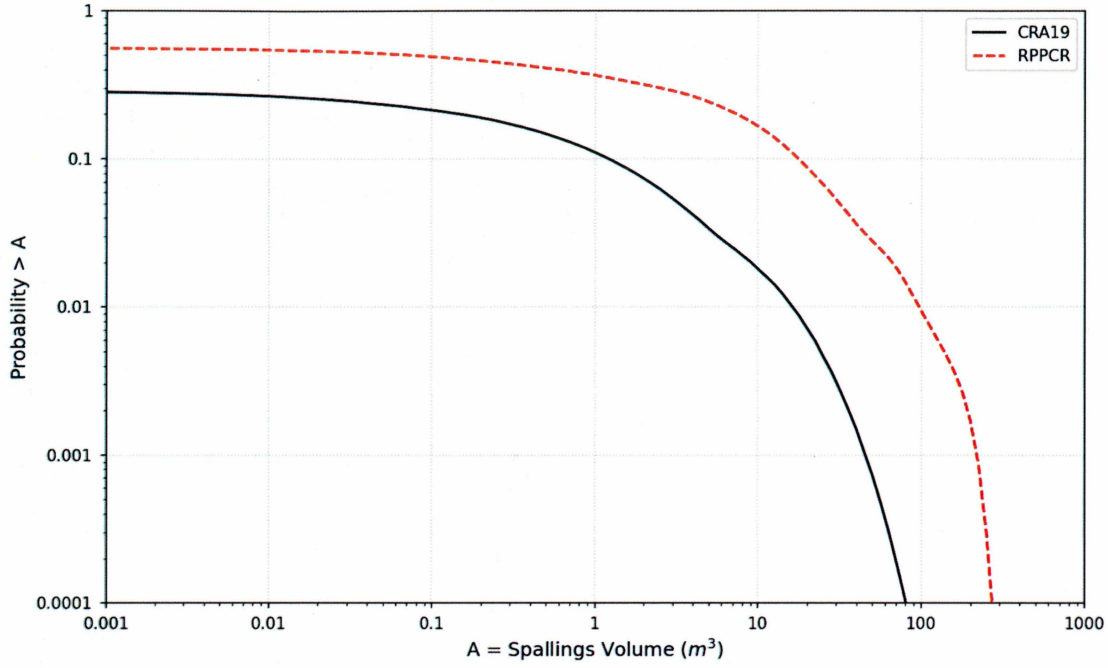

Figure 4-29. Three-Replicate Mean CCDFs for Spallings Volumes

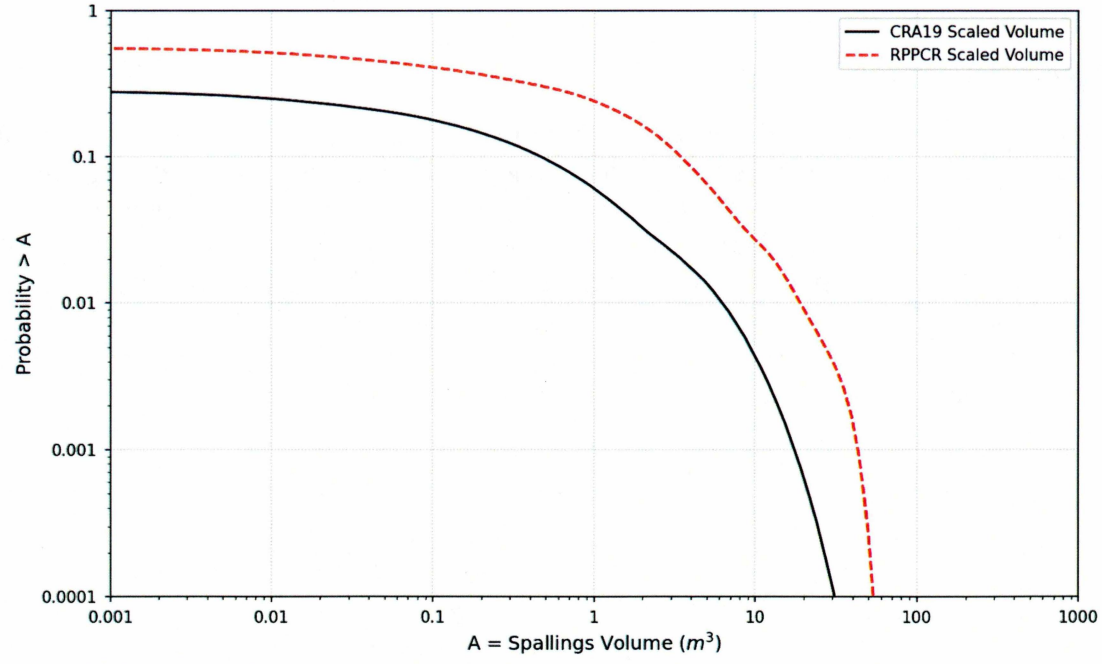

Figure 4-30. Three-Replicate Mean CCDFs for Waste Volume in Spallings Volumes

Information Only

Figure 4-31 shows the CCDFs for spallings releases and the mean CCDFs for Replicate 1 of the RPPCR. As discussed in Section 4.3.2.2, the spallings concentrations in the RPPCR are greater than those seen in the CRA-2019 at all time periods due to an increase in inventory activity. Greater spallings concentrations combined with larger spallings volumes results in larger releases at all probabilities as compared with the CRA-2019 and the APPA (Figure 4-32). Spallings releases in the APPA decreased compared with the CRA-2019 due to a decrease in maximum pressures in the repository (King 2021a), demonstrating that the additional repository volume does not contribute to the increased releases due to spallings in the RPPCR. Note that the method of calculating the confidence interval on the three-replicate means (Section 3.9.2) produces pinch points where the three replicate means cross, as seen at several points in Figure 4-32 for the RPPCR and APPA.

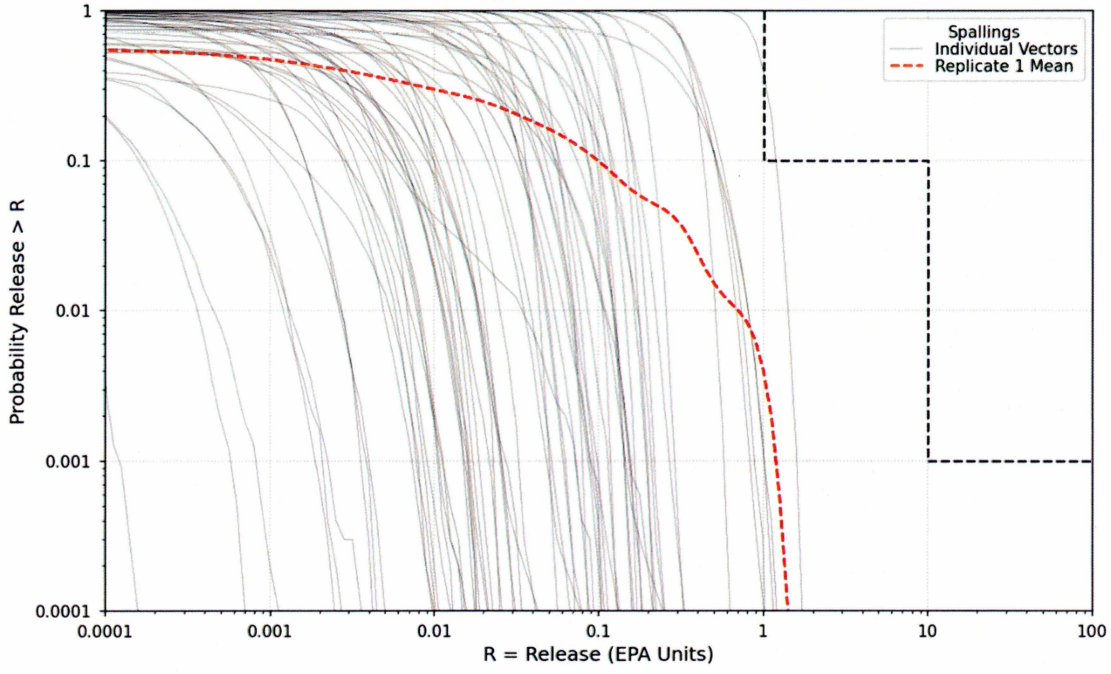

Figure 4-31. Spallings Releases for Replicate 1 of the RPPCR

Information Only

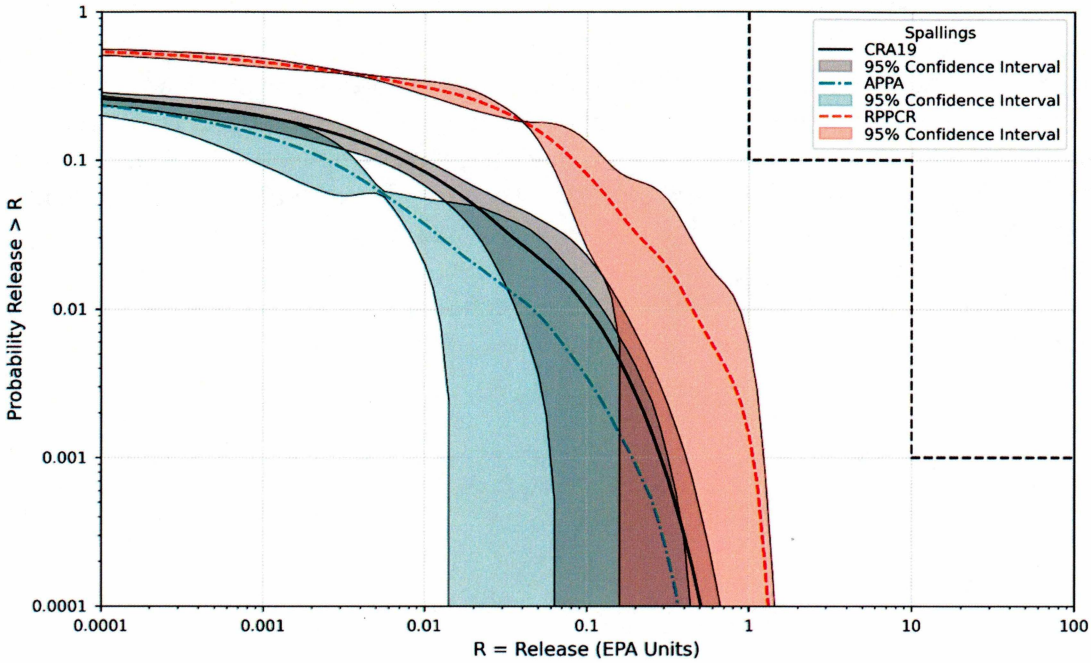

Figure 4-32. Three-Replicate Means for Spallings Releases with Confidence Limits

4.8.3 Direct Brine Releases

Direct brine releases are calculated from DBR volumes and mobilized actinide concentrations in brine. Compared to the CRA-2019 PA, mean DBR volumes in the RPPCR are increased at all probabilities (Figure 4-33). As seen in Figure 4-33, DBR volumes were similar between the APPA and the CRA-2019 (Brunell et al. 2021). As discussed in Section 4.8.1, the APPA results effectively isolate the impact of the additional repository volume. Therefore, the increased DBR volumes seen in the RPPCR are attributable to other factors.

As shown in Table 4-13, the mean DBR volume and the frequency of large magnitude DBR volumes decreased in the RPPCR compared to the CRA-2019. These changes are both due to a reduction in maximum brine pressure and, in scenarios with a previous E1 intrusion, a reduction in brine saturation in the Salado flow model. In contrast, the number of non-zero DBRs and the frequency of small magnitude DBR volumes increased significantly in the RPPCR compared to the CRA-2019. This is attributed by Docherty and King (2023) to increases in brine pressures and, in scenarios without a previous E1 intrusion, an increase in brine saturation. These pressure changes are largely a result of the updated model for salt creep closure onto the waste utilized in the Salado flow calculations (Section 4.2).

Mobilization is predominantly limited by solubility (as it was in CRA-2019). Radionuclide concentrations in brine are decreased overall (Section 4.5) due to the changes in the baseline solubilities and solubility uncertainty distributions.

Information Only

The increased number of DBRs, the reduction in mobilized radionuclides, and the increased likelihood of smaller DBR volumes from each intrusion culminate in an increased likelihood of direct brine releases and an increase in the mean direct brine release. Figure 4-35 shows the CCDFs for direct brine release and the mean CCDF for Replicate 1 of the RPPCR. Overall mean direct brine releases have increased at all probabilities compared to the CRA-2019 (Figure 4-34).

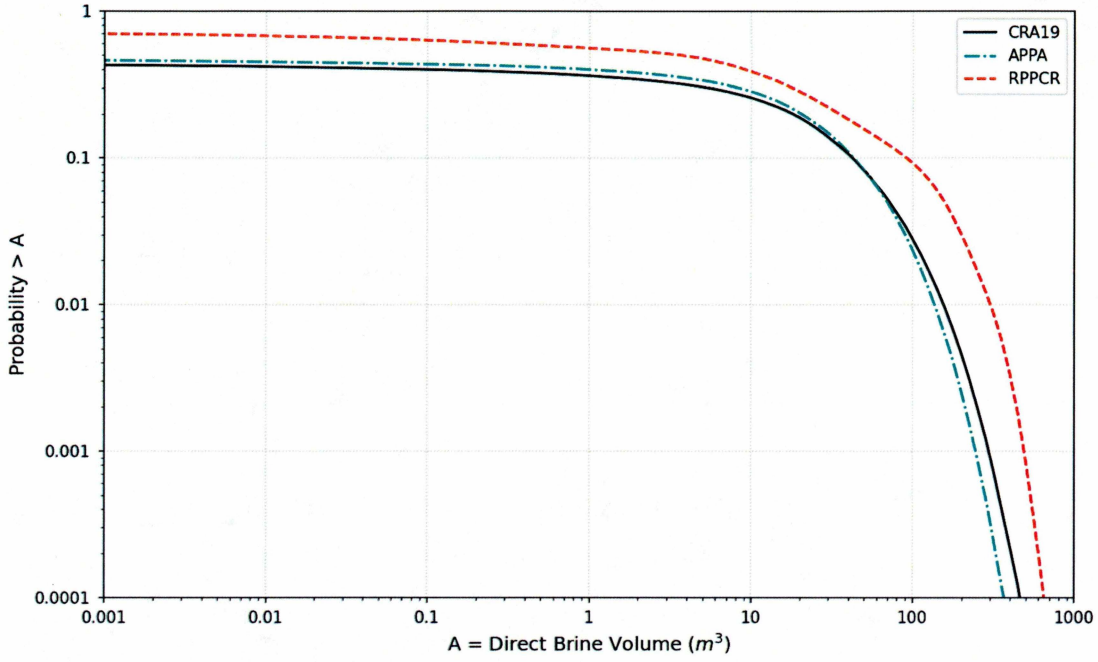

Figure 4-33. Three-Replicate Mean CCDFs for Direct Brine Volumes

Information Only

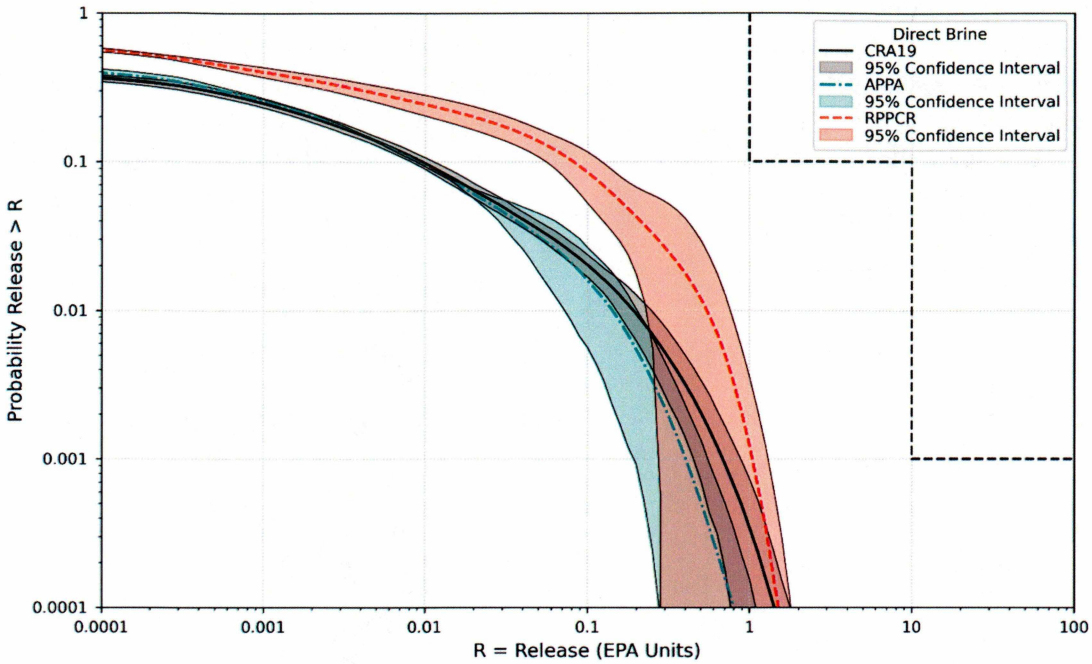

Figure 4-34. Three-Replicate Means for Direct Brine Releases with Confidence Limits

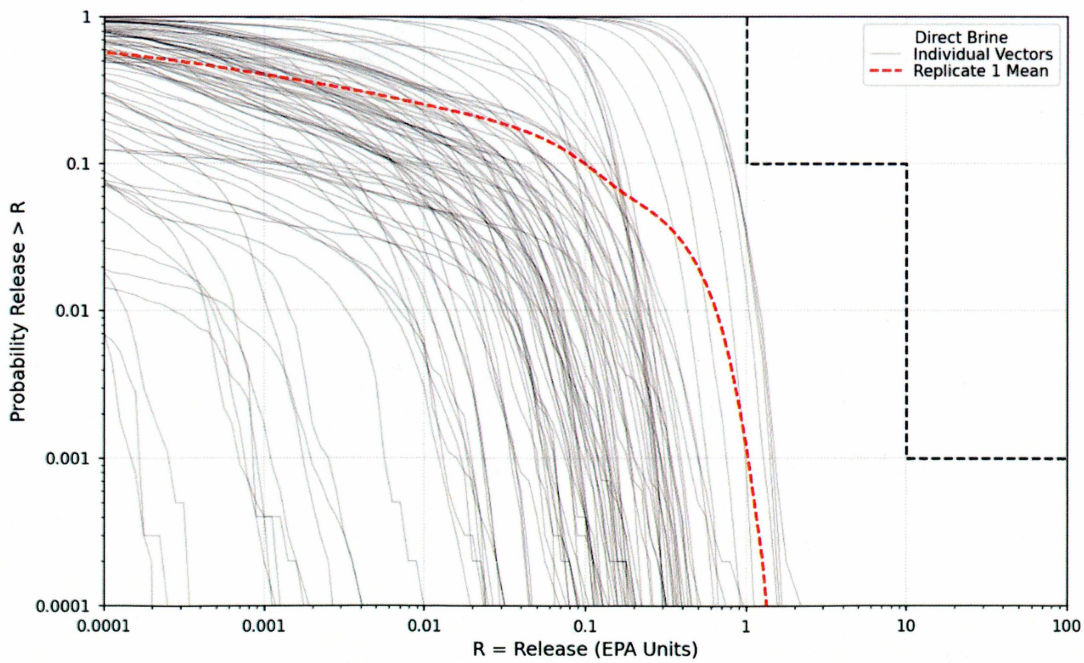

Figure 4-35. Direct Brine Releases for Replicate 1 of the RPPCR

Information Only

4.8.4 Culebra Releases

The CCDFs of releases from the Culebra at the LWB are calculated via a convolution of the cumulative radionuclide discharges to the Culebra (Section 4.6) and the results of Culebra transport calculations with a one kg source term (Section 4.7).

Figure 4-36 shows the individual and the mean CCDFs for radionuclide transport to the Culebra for Replicate 1 of the RPPCR. Note that radionuclide transport to the Culebra comprises the source term for releases through the Culebra and is not by itself a part of the total releases used to determine regulatory compliance. Transport of radionuclides to the Culebra is decreased at all probabilities in the RPPCR compared to the CRA-2019 and the APPA (Figure 4-37). The slight increase in the APPA from the CRA-2019 is due to the increased number of boreholes resulting from the increased area of the repository. The decrease in the RPPCR is due to the updated distribution for BH_SAND:PRMX_LOG, the logarithm of the permeability of a borehole after plug failure and degradation of borehole materials described in Gjerapic et al. (2023). Due to this update, brine flow up the borehole is significantly reduced (Section 4.2).

Figure 4-38 shows the CCDFs for releases from the Culebra and the mean CCDF for Replicate 1 of the RPPCR. Note the extended x-axis in Figure 4-38 in order to show low magnitude releases.

As seen in Figure 4-39 and Figure 4-40, releases from the Culebra are dominated by U234 in both analyses, but the contribution of Am241 to total releases from the Culebra increased in the RPPCR. The three-replicate mean release for each Culebra release point for all radionuclides are shown in Figure 4-41. Overall, mean releases from the Culebra have decreased in the RPPCR analysis for all probabilities compared to the CRA-2019 and the APPA (Figure 4-42). Since the Culebra transport calculations are identical for the APPA and the CRA-2019, the increase in releases from the Culebra seen in the APPA is due to the increase in radionuclide transport to the Culebra.

The mean releases from the Culebra are driven mainly by the release of U234 and Am241 from CRP4. As discussed in Bethune (2023), the particle travel times in the RPPCR for the full mining scenario from CRP4 are significantly shorter than from other release points at all probabilities.

Information Only

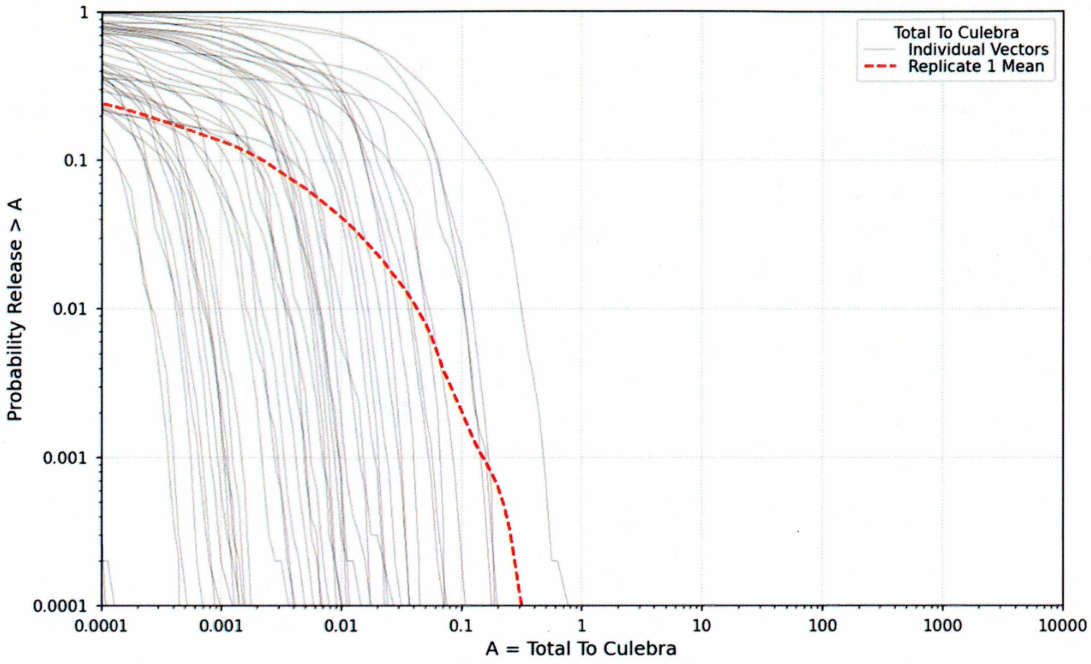

Figure 4-36. Radionuclide Transport to the Culebra for Replicate 1 of the RPPCR

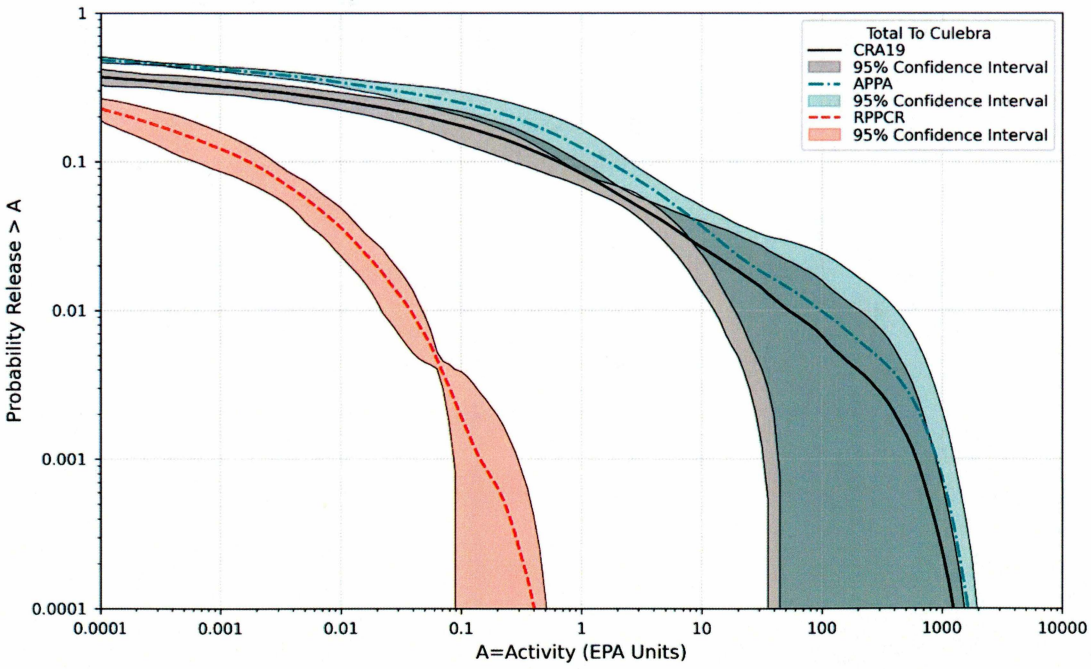

Figure 4-37. Three-Replicate Means for Radionuclide Transport to the Culebra with Confidence Limits

Information Only

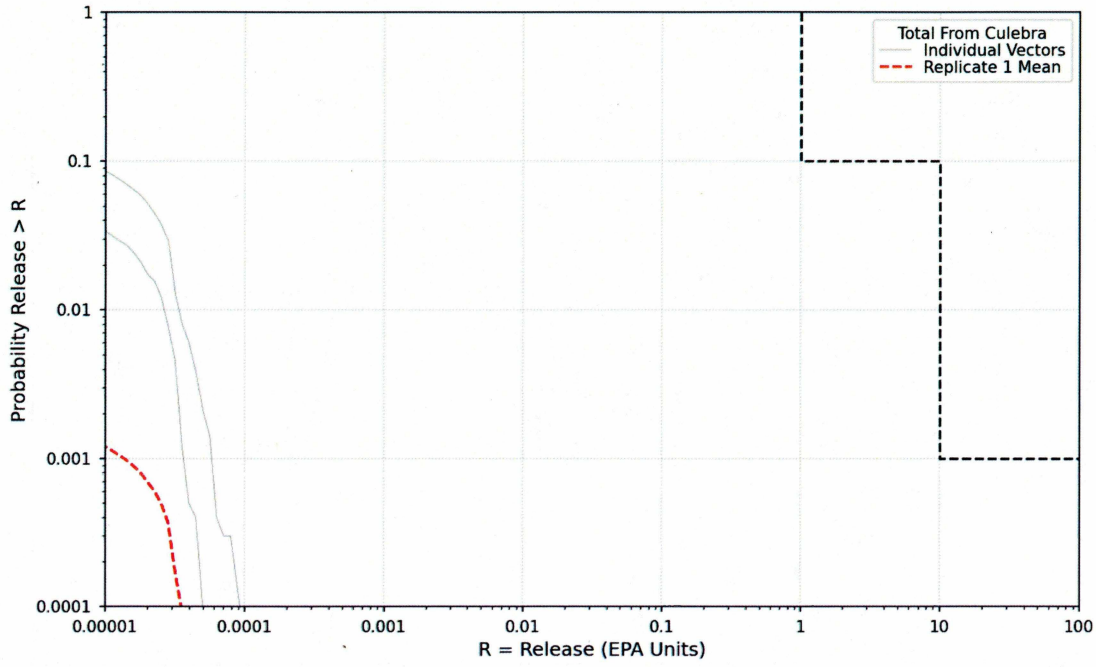

Figure 4-38. Releases from the Culebra for Replicate 1 of the RPPCR

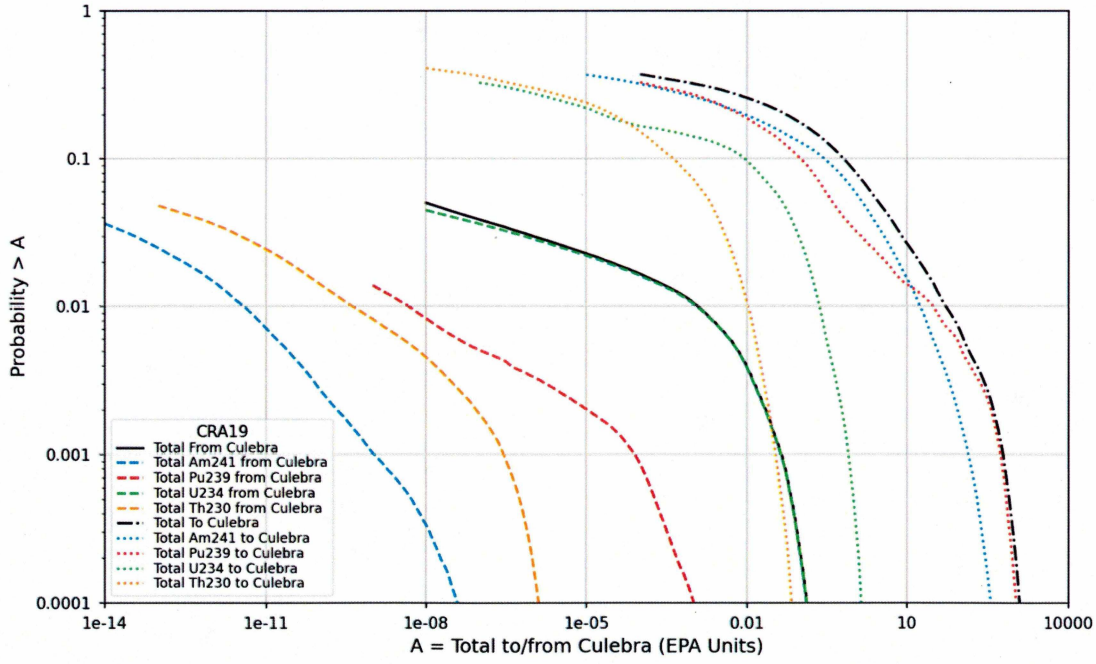

Figure 4-39. Total Releases to and from the Culebra by Radionuclide for the CRA-2019 (Three-Replicate Means)

Information Only

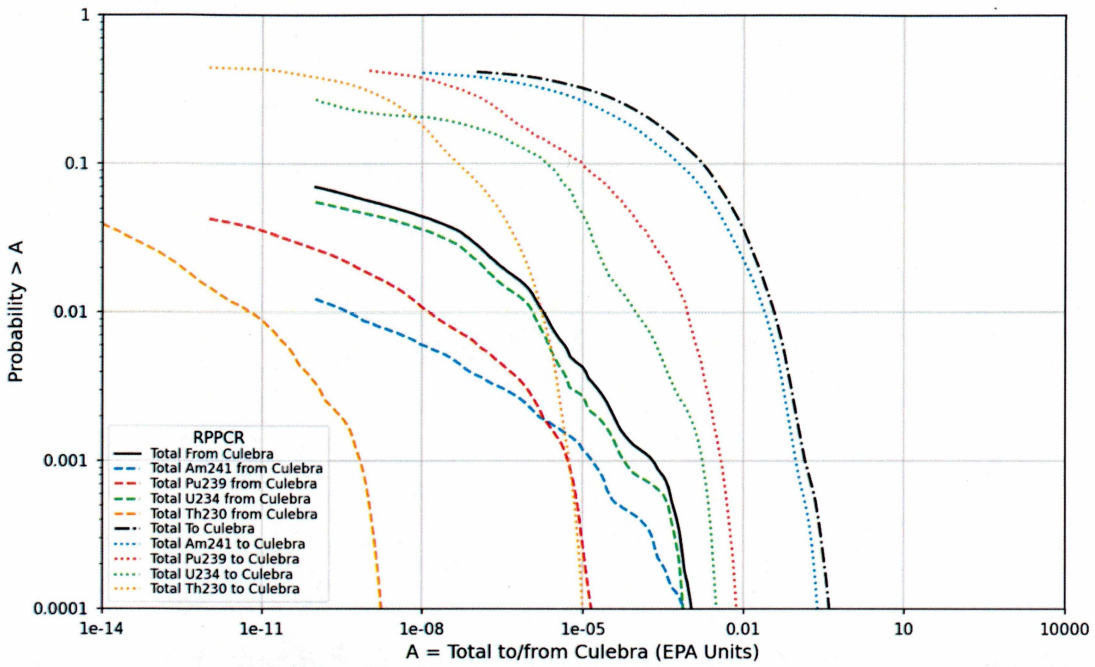

Figure 4-40. Releases to and from the Culebra by Radionuclide for the RPPCR (Three-Replicate Means)

Information Only

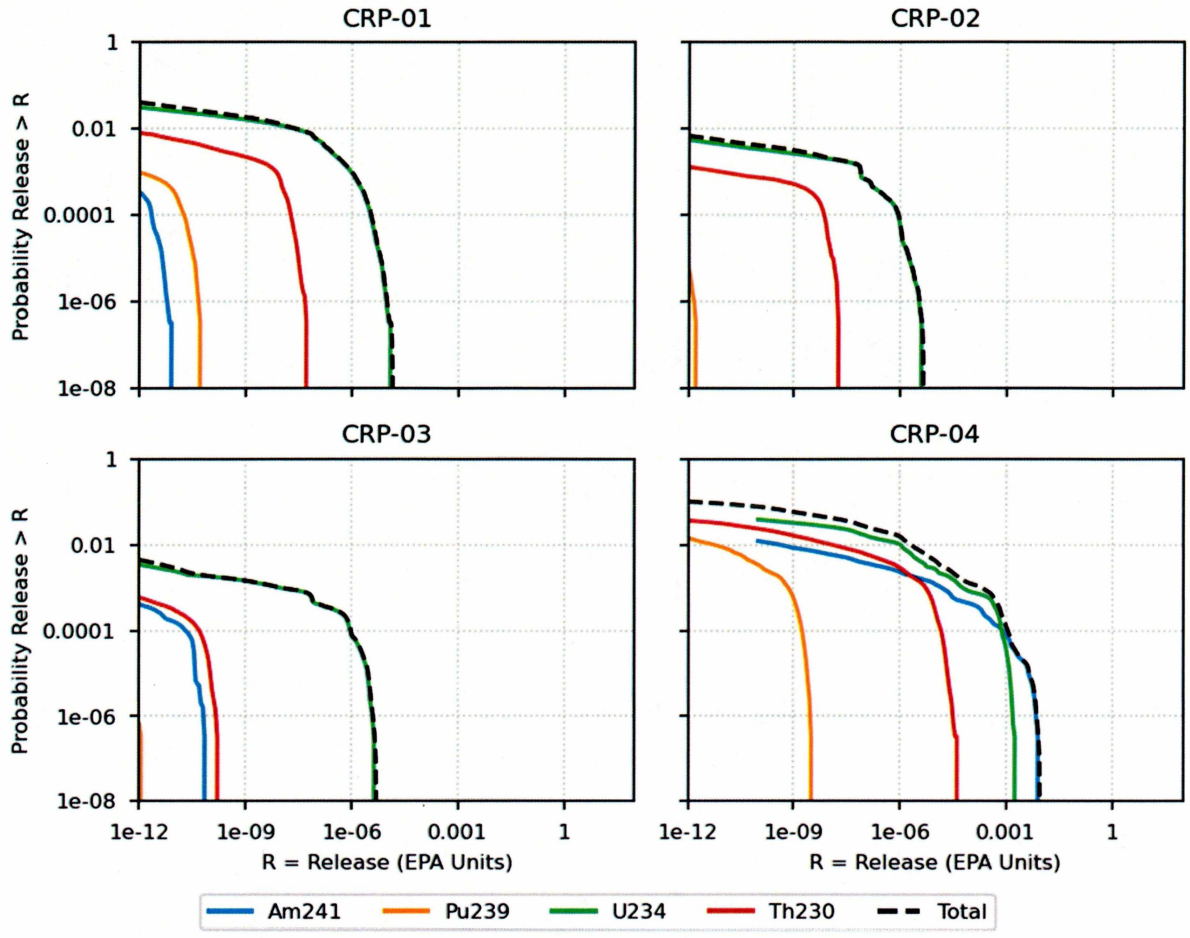

Figure 4-41. Radionuclide Releases from the Culebra by Release Point for the RPPCR (Three-Replicate Means)

Information Only

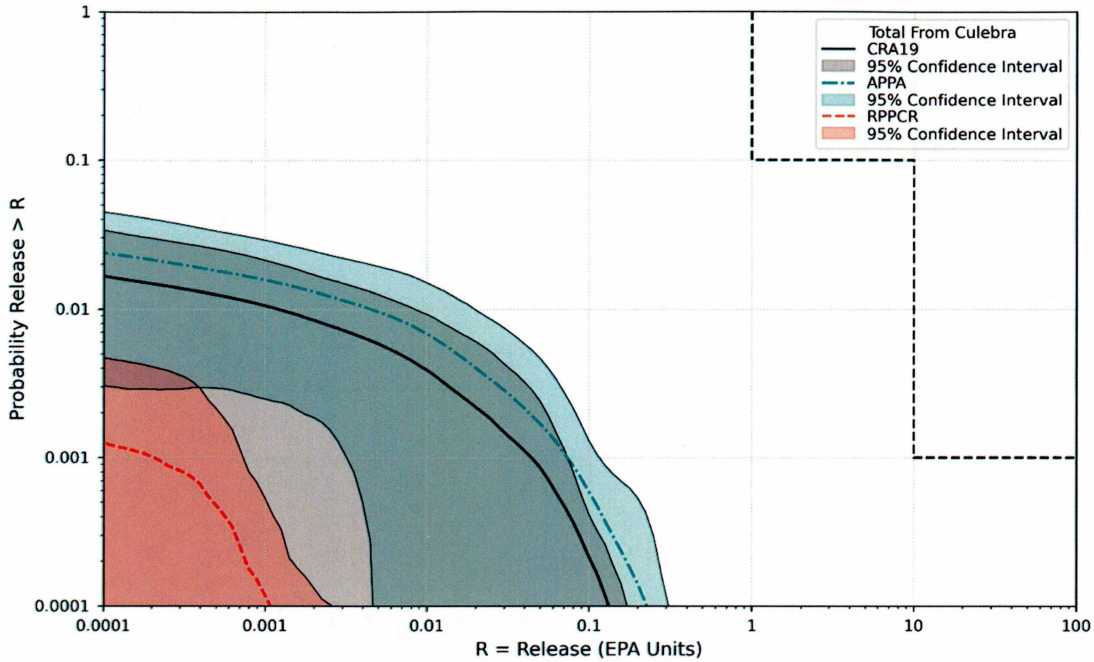

Figure 4-42. Three-Replicate Means for Transport Releases from the Culebra with Confidence Limits

4.8.5 Total Releases

Individual horsetail plots and the mean CCDF of total releases for Replicate 1 of the RPPCR analysis are shown in Figure 4-43. Similar to the CRA-2019 and the APPA, mean total releases for the RPPCR analysis are dominated by cuttings and cavings releases at high probabilities (Figure 4-44 and Figure 4-45). However, unlike previous analyses where mean total releases at low probabilities are dominated by DBRs, spallings and direct brine releases contribute equally to mean total releases at lower probabilities. Figure 4-46 compares mean total release between the CRA-2019, the APPA, and the RPPCR, while Table 4-16 contains the statistics on the overall mean for total releases and its lower/upper 95% confidence limits for the CRA-2019, the APPA, and the RPPCR, calculated using the method described in Section 3.9.2.

Of the updates incorporated in the RPPCR discussed in Section 2.0, the changes in total releases mainly result from the changes to the borehole permeability, the model for salt creep closure onto the waste, the inventory, and the increased drilling frequency. The increased repository volume of the additional and replacement panels results in a decrease in probability of releases at most release levels, as seen in the APPA results in Figure 4-46. The updated borehole permeability combined with the updated Culebra transmissivity fields and updated procedure for calculating Culebra transport result in a significant decrease in releases from the Culebra. Although total releases are increased in the RPPCR compared to the CRA-2019, the releases displayed in Figure 4-46 and Table 4-16 are below regulatory release limits. Accordingly, with the proposed replacement and additional waste panels, the WIPP remains in compliance with the containment requirements of 40 CFR Part 191.

Information Only

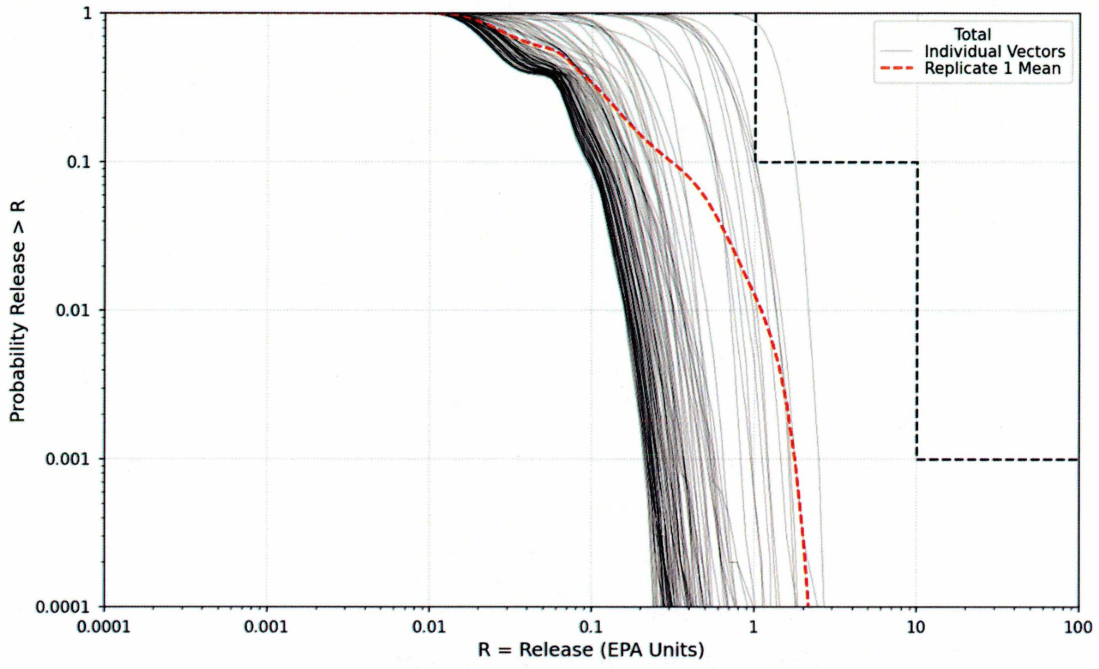

Figure 4-43. Total Releases for Replicate 1 of the RPPCR

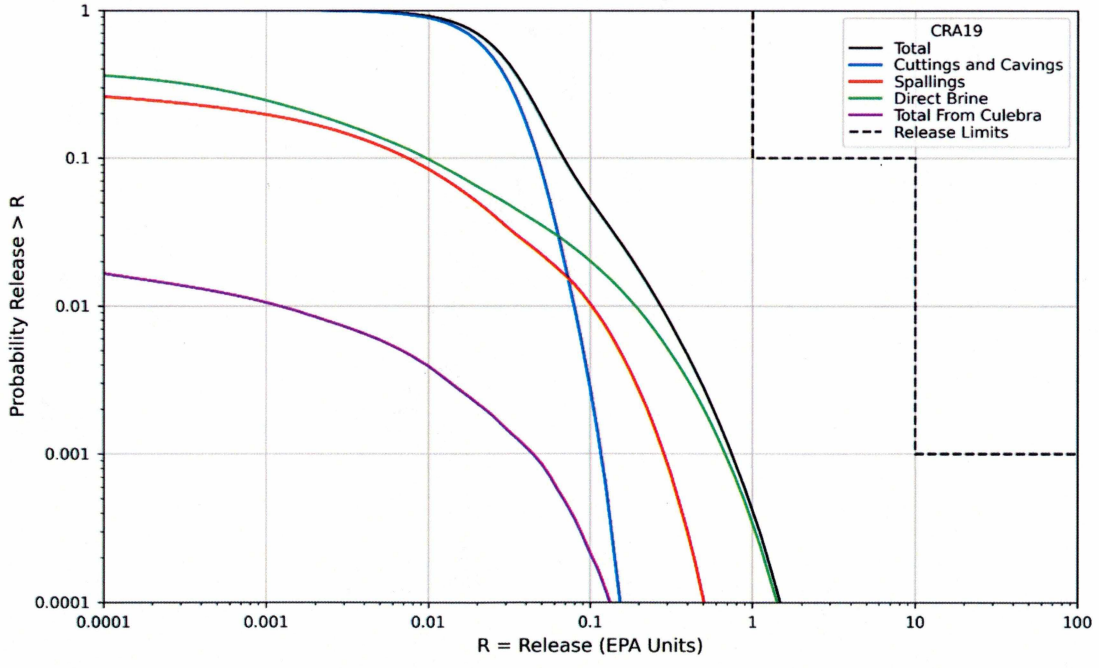

Figure 4-44. 3-Replicate Means for Release Components for the CRA-2019

Information Only

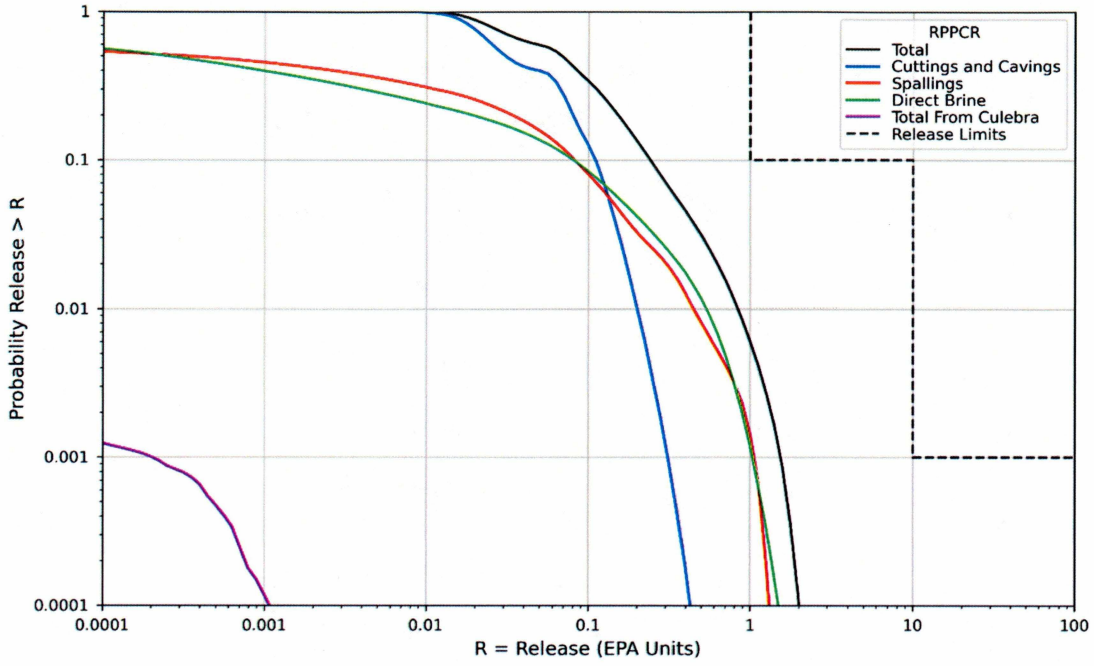

Figure 4-45. Three-Replicate Means for Release Components for the RPPCR

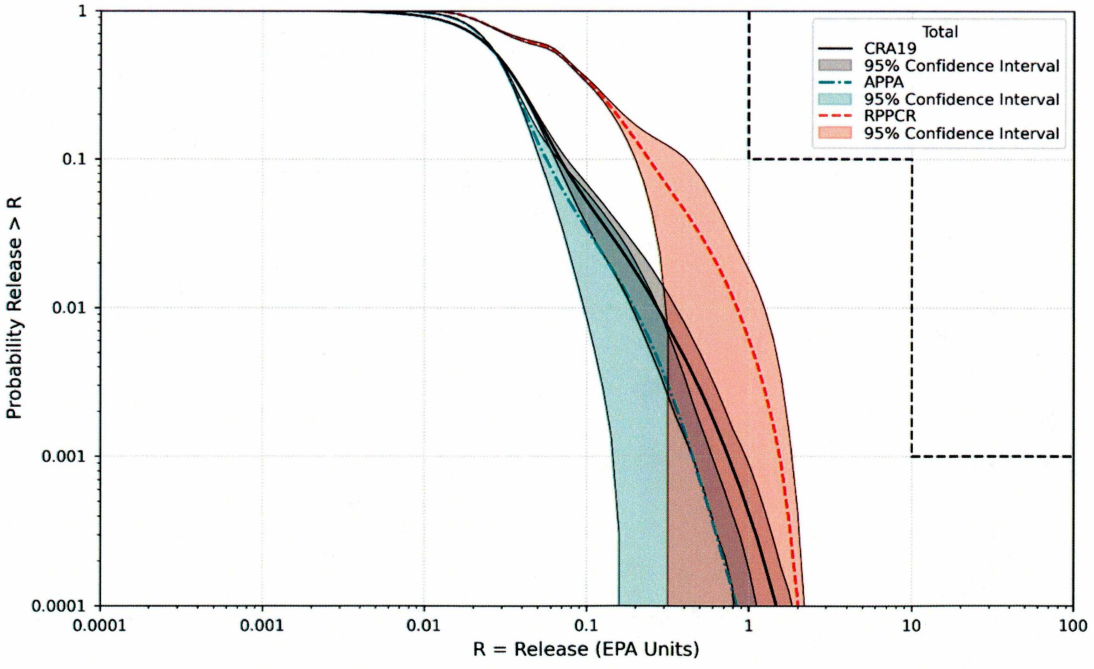

Figure 4-46. Confidence Limits on the Three-Replicate Mean for Total Releases

Information Only

Table 4-16. Statistics on the Three-Replicate Mean for Total Releases

Probability	Analysis	Mean Total Release	Lower 95% CL	Upper 95% CL	Release Limit
0.1	CRA-2019	0.0685	0.0636	0.0753	1
	APPA	0.0564	0.0515	0.0665	
	RPPCR	0.2418	0.1990	0.4073	
0.001	CRA-2019	0.7505	0.4487	0.9595	10
	APPA	0.4540	0.1475	0.5970	
	RPPCR	1.5541	0.3360	1.8716	

4.8.6 Sensitivity Analysis for Total Releases

Stepwise linear multiple rank regression analyses are performed to determine the relative importance of the sampled parameters in the uncertainty in releases using the code STEPWISE. Sensitivity analysis results for the RPPCR analysis are compared to the results of the CRA-2019 analysis. The sensitivity analysis identifies parameters which contribute most to the uncertainty in a model result (Brunell and Zeitler 2023).

In the sensitivity analysis results, the cumulative R^2 value represents the proportion of total uncertainty explained by the fitted rank regression using the listed variables, starting with the greatest contributor to the variance. The number of variables used in the regression model is determined by the stepwise regression procedure (Brunell and Zeitler 2023). Regression analyses are conducted for each replicate separately, so results for the CRA-2019 and the RPPCR analyses are therefore compared on a per-replicate basis.

To aid in interpretation and discussion of the results, highlighting indicates parameters with a change in R^2 greater than 0.05 between the current step and the previous step. While this threshold of 0.05 is somewhat arbitrary, the highlighted parameters are clearly influential and tend to have a more consistent ranking. Additionally, the displayed results are truncated after seven steps. For a full discussion of STEPWISE, see Appendix A of Brunell and Zeitler (2023).

Table 4-17 to Table 4-19 compare the sensitivity of mean total releases (mean of each CCDF) to uncertain parameters for each replicate of the CRA-2019 and RPPCR analyses.

In the CRA-2019 analysis, SOLMOD3:SOLVAR was the dominant parameter with regard to controlling variability in total releases for two replicates and BH_SAND:PRMX_LOG for one replicate, but that is not the case for RPPCR. S_HALITE:POROSITY is the dominant parameter in each replicate of RPPCR, controlling 27-36 % of the variability (0-3 % for CRA-2019).

The influence of SOLMOD3:SOLVAR has decreased (from 16-23 % to 2-3 %) likely due to multiple factors including a change in the parameter distribution (Zeitler 2023a), decreased number of vectors with Pu in the +III state (Kim 2023), and the decreased contribution to total releases of

Information Only

DBRs compared to spallings (Section 4.8.5). The parameter distribution has shifted down, resulting in decreased radionuclide concentrations (Figure 4-19).

The control of variability has decreased for BH_SAND:PRMX_LOG (from 6-17 % to 0-2 %) likely due to the change in the parameter distribution. This parameter showed decreased control of variability in spallings (Table 9 of Brunell and Zeitler, 2023), DBR volumes (Table 12 of Brunell and Zeitler, 2023), and releases to and from the Culebra (Section 4.8.4).

S_HALITE:POROSITY emerges as important for describing the variability in total releases due to its significant influence on pressure in the waste panel (Tables 17 through 20 of King, 2023) and its moderate influence on brine saturation in the waste panel (Tables 21 through 24 of King, 2023), and consequently, on spallings and direct brine release volumes. King (2023) explains that increased halite porosity increases brine availability in the host rock, which correlates with increased repository pressure, a direct contributor to spallings and DBRs. The updated porosity surface used in the RPPCR is the primary driver for increased brine saturation in the waste due to decreased waste pore volume for the new surface.

One of the other most dominant variables for controlling variability in total releases is BOREHOLE:TAUFAIL, which has maintained approximately the same control from CRA-2019 to RPPCR (from 11-15 % to 6-16 %). It is now the second most dominant variable for total releases in all three replicates. This variable is the dominant variable for cuttings and cavings releases and this release pathway has maintained approximately the same contribution to total releases.

CASTILER:PRESSURE (initial brine pore pressure in the Castile) remains one of the top contributing parameters with 4-8 % (6-9 % for CRA-2019) control across the three replicates. The GLOBAL:PBRINE parameter has only minor importance in variability in total releases, controlling 0-5 % (0-7 % for CRA-2019), but only appearing in the analysis results for Replicate 2.

Information Only

Table 4-17. Stepwise Ranked Regression Analysis for Mean Total Releases for Replicate 1 of the CRA-2019 and RPPCR Analyses

	CRA-2019 Replicate 1			RPPCR Replicate 1		
Step[a]	Variable[b, e]	R^2 [c]	SRRC[d]	Variable	R^2	SRRC
1	SOLMOD3:SOLVAR	0.23	0.51	S_HALITE:POROSITY	0.35	0.57
2	BOREHOLE:TAUFAIL	0.35	-0.35	BOREHOLE:TAUFAIL	0.41	-0.26
3	CASTILER:PRESSURE	0.44	0.31	CASTILER:PRESSURE	0.47	0.25
4	BH_SAND:PRMX_LOG	0.50	-0.27	SOLMOD3:SOLVAR	0.50	0.17
5	STEEL:CORRMCO2	0.53	-0.19	STEEL:CORRMCO2	0.53	-0.19
6	WAS_AREA:PROBDEG	0.56	0.17	WAS_AREA:PROBDEG	0.56	0.16
7	S_HALITE:POROSITY	0.59	0.15	DRZ_1:PRMX_LOG	0.58	0.16
8				SPALLMOD:PARTDIAM	0.60	-0.14
9				S_MB139:PRMX_LOG	0.62	0.14

[a] Steps in stepwise regression analysis

[b] Variables listed in order of selection

[c] Cumulative R^2 value with entry of each variable into regression model

[d] Standardized Rank Regression Coefficient

[e] Highlighting indicates parameters with a change in R2 greater than 0.05 from the previous step.

Table 4-18. Stepwise Ranked Regression Analysis for Mean Total Releases for Replicate 2 of the CRA-2019 and RPPCR Analyses

	CRA-2019 Replicate 2			RPPCR Replicate 2		
Step[a]	Variable[b, e]	R^2 [c]	SRRC[d]	Variable	R^2	SRRC
1	SOLMOD3:SOLVAR	0.23	0.48	S_HALITE:POROSITY	0.36	0.61
2	BOREHOLE:TAUFAIL	0.38	-0.40	BOREHOLE:TAUFAIL	0.43	-0.28
3	CASTILER:PRESSURE	0.47	0.28	CASTILER:PRESSURE	0.51	0.28
4	GLOBAL:PBRINE	0.54	0.28	GLOBAL:PBRINE	0.56	0.22
5	BH_SAND:PRMX_LOG	0.62	-0.27	DRZ_1:PRMX_LOG	0.58	0.17
6	S_HALITE:POROSITY	0.65	0.19	WAS_AREA:BIOGENFC	0.60	0.14
7	SHFTU:SAT_RGAS	0.67	-0.12	SOLMOD3:SOLVAR	0.62	0.14
8	STEEL:CORRMCO2	0.68	-0.12	SPALLMOD:PARTDIAM	0.64	-0.14
9				BH_SAND:PRMX_LOG	0.66	-0.12

[a] Steps in stepwise regression analysis

[b] Variables listed in order of selection

[c] Cumulative R^2 value with entry of each variable into regression model

[d] Standardized Rank Regression Coefficient

[e] Highlighting indicates parameters with a change in R2 greater than 0.05 from the previous step.

Information Only

Table 4-19. Stepwise Ranked Regression Analysis for Mean Total Releases for Replicate 3 of the CRA-2019 and RPPCR Analyses

	CRA-2019 Replicate 3			RPPCR Replicate 3		
Step[a]	Variable[b, e]	R^2 [c]	SRRC[d]	Variable	R^2	SRRC
1	BH_SAND:PRMX_LOG	0.17	-0.39	S_HALITE:POROSITY	0.27	0.49
2	SOLMOD3:SOLVAR	0.34	0.39	BOREHOLE:TAUFAIL	0.43	-0.39
3	BOREHOLE:TAUFAIL	0.45	-0.34	SPALLMOD:PARTDIAM	0.51	-0.28
4	GLOBAL:PBRINE	0.53	0.28	CASTILER:PRESSURE	0.55	0.20
5	CASTILER:PRESSURE	0.59	0.24	SOLMOD3:SOLVAR	0.58	0.17
6	DRZ_1:PRMX_LOG	0.62	-0.19	(Composite):MKD_U	0.61	-0.18
7	SPALLMOD:PARTDIAM	0.64	-0.17	WAS_AREA:SAT_WICK	0.64	0.17
8	CASTILER:COMP_RCK	0.67	0.13	DRZ_PCS:PRMX_LOG	0.66	-0.14
9	S_HALITE:PRESSURE	0.69	-0.14			
10	CULEBRA:MINP_FAC	0.70	0.13			
11	S_MB139:RELP_MOD	0.72	-0.15			
12	WAS_AREA:SAT_RBRN	0.74	-0.13			

[a] Steps in stepwise regression analysis

[b] Variables listed in order of selection

[c] Cumulative R^2 value with entry of each variable into regression model

[d] Standardized Rank Regression Coefficient

[e] Highlighting indicates parameters with a change in R2 greater than 0.05 from the previous step.

4.9 Comparison to EPA analysis

During the review of the 2019 Compliance Recertification Application (CRA-2019), the EPA conducted a series of PA calculations investigating alternative models and parameters, culminating in an analysis combining multiple alternatives. This combined analysis was named CRA19_COMB (U.S. EPA 2022a). The alternatives considered in the CRA19_COMB analysis include:

- A different borehole plugging pattern methodology.
- Revised actinide baseline solubility parameters.
- Revised colloidal enhancement parameters.
- Revised actinide oxidation state parameters.

The borehole plugging pattern probabilities used in the CRA-2019, CRA19_COMB, and RPPCR are shown in Table 4-20. The CRA19_COMB analysis used wells in the New Mexico portion of the Delaware Basin to derive the plugging pattern probabilities (U.S. EPA 2022a). As discussed in Section 2.12, the CRA-2019 used the wells in the designated potash area and the RPPCR uses wells in the nine-township area to derive wellbore plugging pattern probabilities.

The colloid enhancement parameters that differ between the CRA-2019, CRA19_COMB, and RPPCR are shown in Table 4-21. For the RPPCR, Lucchini and Swanson (2023) accepted the EPA

Information Only

recommended values for the Am and Th concentrations associated with intrinsic colloids (AM/TH:CONCINT). Lucchini and Swanson (2023) further recommended updates to the microbial colloid enhancement parameters for use in the RPPCR.

Baseline solubilities used in the CRA-2019, CRA19_COMB, and RPPCR are presented in Table 4-22. Baseline solubilities for radionuclides in the +III oxidation state are greater in the RPPCR than the CRA19_COMB. Baseline solubilities for radionuclides in the +IV oxidation state are less in the RPPCR than the CRA19_COMB. Baseline solubilities for radionuclides in the +V oxidation state are slightly greater or slightly less between the RPPCR and CRA19_COMB depending on the brine type and brine volume. As discussed in Section 2.2, updates to the oxidation state model and solubility uncertainty distributions are made in the RPPCR, which also impact radionuclide solubilities beyond the changes to the baseline solubilities shown here.

Mean CCDFs of total releases from the EPA CRA19_COMB analysis are documented in the EPA review of the 2019 Compliance Recertification Application Performance Assessment (U.S. EPA 2022a). Figure 4-47 compares mean total releases over all three replicates from the RPPCR analysis to mean total releases from the EPA's CRA19_COMB analysis. At high probabilities, the RPPCR sees larger total releases compared to the CRA19_COMB analysis. At low probabilities, the RPPCR sees lower total releases compared to the CRA19_COMB analysis.

Table 4-23 gives the mean total releases at the two compliance points with the 95% confidence interval for both analyses. As with the CCDFs, this table shows greater releases at the upper compliance point and less releases at the lower compliance point for the RPPCR compared to the CRA19_COMB. For both analyses, at both compliance points, the mean and 95% confidence interval fall below the release limits.

Table 4-20. Borehole Plugging Pattern Parameters

Material	Property	CRA19 Value (-)	CRA19_COMB Value (-)	RPPCR Value (-)
GLOBAL	ONEPLG	0.403	0.095	0.366
GLOBAL	TWOPLG	0.331	0.483	0.430
GLOBAL	THREEPLG	0.266	0.422	0.204

Information Only

Table 4-21. Colloid Enhancement Parameters

Material	Property	CRA19 Value	CRA19_COMB Value	RPPCR Value	Units
AM	CAPMIC	2.30E-09	6.28E-06	9.00E-07	mol/L
AM	CONCINT	9.50E-09	6.70E-07	6.70E-07	mol/L
AM	PROPMIC	3.00E-02	3.60E+00	3.52E+00	(-)
NP	CAPMIC	3.80E-08	1.27E-04	2.33E-06	mol/L
NP	PROPMIC	2.10E-01	1.20E+01	1.20E+01	(-)
PU	CAPMIC	3.80E-08	2.18E-05	1.22E-09	mol/L
PU	PROPMIC	2.10E-01	2.18E+00	3.00E-01	(-)
TH	CAPMIC	3.80E-08	2.12E-02	6.95E-04	mol/L
TH	CONCINT	4.30E-08	4.80E-07	4.80E-07	mol/L
TH	PROPMIC	2.10E-01	3.10E+00	3.10E+00	(-)
U	CAPMIC	3.80E-08	8.14E+00	2.22E-06	mol/L
U	PROPMIC	2.10E-01	2.10E-03	2.10E-03	(-)

Information Only

Table 4-22. Baseline Solubility Parameters

Material	Property	CRA19 Value (mol/L)	CRA19_COMB Value (mol/L)	RPPCR Value (mol/L)
SOLMOD3	SOLCOH	1.78E-07	1.43E-06	3.51E-06
SOLMOD3	SOLCOH2	1.63E-07	7.26E-07	1.93E-06
SOLMOD3	SOLCOH3	1.58E-07	5.16E-07	1.39E-06
SOLMOD3	SOLCOH4	1.54E-07	4.16E-07	1.13E-06
SOLMOD3	SOLCOH5	1.52E-07	3.56E-07	9.59E-07
SOLMOD3	SOLSOH	1.63E-07	2.14E-06	3.40E-06
SOLMOD3	SOLSOH2	1.58E-07	1.09E-06	1.86E-06
SOLMOD3	SOLSOH3	1.56E-07	7.74E-07	1.33E-06
SOLMOD3	SOLSOH4	1.55E-07	6.19E-07	1.07E-06
SOLMOD3	SOLSOH5	1.54E-07	5.28E-07	9.09E-07
SOLMOD4	SOLCOH	5.44E-08	5.84E-08	5.73E-08
SOLMOD4	SOLCOH2	5.44E-08	5.84E-08	5.74E-08
SOLMOD4	SOLCOH3	5.44E-08	5.85E-08	5.75E-08
SOLMOD4	SOLCOH4	5.44E-08	5.85E-08	5.75E-08
SOLMOD4	SOLCOH5	5.44E-08	5.85E-08	5.75E-08
SOLMOD4	SOLSOH	5.45E-08	5.50E-08	5.34E-08
SOLMOD4	SOLSOH2	5.45E-08	5.51E-08	5.34E-08
SOLMOD4	SOLSOH3	5.45E-08	5.51E-08	5.34E-08
SOLMOD4	SOLSOH4	5.45E-08	5.52E-08	5.34E-08
SOLMOD4	SOLSOH5	5.45E-08	5.52E-08	5.34E-08
SOLMOD5	SOLCOH	1.20E-06	1.82E-06	1.80E-06
SOLMOD5	SOLCOH2	7.27E-07	1.42E-06	1.50E-06
SOLMOD5	SOLCOH3	5.52E-07	1.28E-06	1.41E-06
SOLMOD5	SOLCOH4	4.61E-07	1.21E-06	1.36E-06
SOLMOD5	SOLCOH5	4.05E-07	1.17E-06	1.33E-06
SOLMOD5	SOLSOH	4.02E-07	4.38E-07	4.95E-07
SOLMOD5	SOLSOH2	2.83E-07	3.22E-07	4.21E-07
SOLMOD5	SOLSOH3	2.42E-07	2.82E-07	3.96E-07
SOLMOD5	SOLSOH4	2.21E-07	2.63E-07	3.84E-07
SOLMOD5	SOLSOH5	2.09E-07	2.51E-07	3.76E-07

Information Only

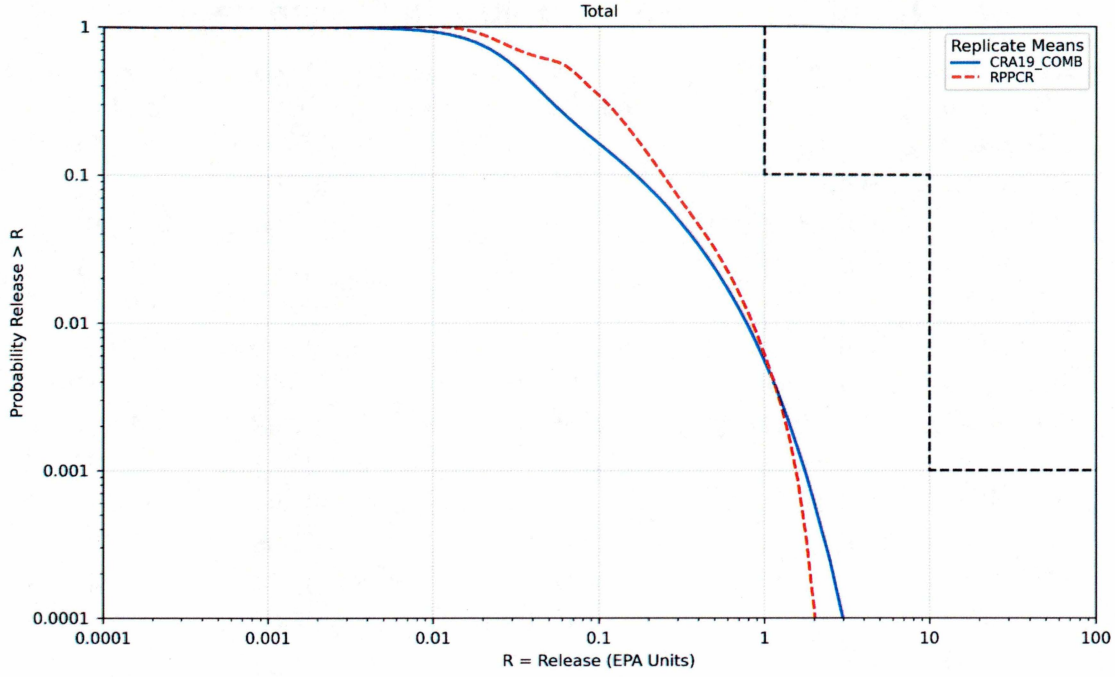

Figure 4-47. Total Mean Releases from the RPPCR and CRA19_COMB

Table 4-23. Statistics on the Overall Mean for Total Releases

Probability	Analysis	Mean Total Release	Lower 95% CI	Upper 95% CI	Release Limit
0.1	CRA19_COMB	0.1669	0.1552	0.1769	1
	RPPCR	0.2418	0.1990	0.4073	
0.001	CRA19_COMB	1.7661	1.2707	2.1676	10
	RPPCR	1.5541	0.3360	1.8716	

Information Only

5.0 ADDITIONAL ANALYSES

Two issues were raised during the execution of the RPPCR that merit further analysis. The first issue is around the homogeneous waste loading assumption used in the RPPCR. The second is understanding the effect on releases of the two replacement panels DOE is seeking permission to use without the effects of the seven additional panels that are anticipated to be needed to store the LWA limit of waste. These two issues were investigated in separate reports described below.

5.1 Homogeneous Waste Loading

To comply with 40 CFR Part 194.24(d), the WIPP PA assumes random emplacement of waste in the disposal system. Random emplacement is realized by using a homogeneous waste form in Salado flow and transport simulations. Past studies have shown that WIPP compliance is not affected by the assumption of random distribution of waste containers in the repository (Casey et al. 2003; Hansen et al. 2003).

The dilute and dispose surplus plutonium waste streams SR-KAC-HET and SR-KAC-PuOx are large-volume, relatively high activity waste streams in the WIPP repository. The EPA has raised concerns that if this waste was placed in a few panels, a significant fraction of the modeled radiolytic brine consumption and gas generation could occur in those panels, which may significantly affect DBRs and spallings releases from those panels. The EPA has asked the DOE to evaluate whether the PA calculations adequately address the effects on releases of placement of this waste stream in a limited number of panels (U.S. EPA 2022b, Section 10.0). King et al. (2023) evaluated a high loading of plutonium into a single panel in the WIPP and showed that the WIPP performance metrics of cumulative releases were not significantly different for a repository with the homogeneous waste form. With this conclusion, the RPPCR continues to assume a homogeneous waste form in the simulated repository.

5.2 Replacement Panel Performance

The DOE is not asking currently for approval for additional Panels 13 through 19. To meet the EPA expectation that the PA models the expected final design of the repository (U.S. EPA 2021), the RPPCR models the full 19-panel repository. Hansen et al. (2023b) evaluated the performance of a repository comprising the existing 10 waste panels and the replacement Panels 11 and 12, and estimated releases from this 12-panel repository. The analysis concluded that the 12-panel repository would comply with containment requirements by scaling the results the 19-panel repository model.

Information Only

This page intentionally left blank.

Information Only

6.0 SUMMARY

The Replacement Panels Planned Change Request (RPPCR) Performance Assessment (PA) was conducted to support the DOE's Planned Change Request (PCR) seeking approval for two replacement panels, labeled Panels 11 and 12. Current emplacement volumes indicate that seven additional panels, labeled Panels 13 through 19, are also needed to store the WIPP volumetric waste limit specified in the LWA. While the DOE is not currently seeking approval for the use of the seven additional panels pending a finalized design and additional site characterization data, the RPPCR models the anticipated final design of the WIPP repository, with two replacement panels and seven additional panels, in order to meet EPA expectations.

Additional changes from the CRA-2019 PA beyond those related to the replacement and additional panels have been incorporated into the RPPCR, including updates to the following items: drilling frequency, borehole plugging pattern probabilities, creep closure model, permeability distribution for boreholes after plug degradation, inventory, oxidation state model, baseline solubilities, solubility uncertainty distributions, and colloid enhancement parameters.

Results from the RPPCR analysis are compared to those obtained in the APPA and the CRA-2019 analyses in order to assess repository performance relative to previous performance assessments. Results from the CRA-2019 and the APPA show that the replacement and additional panels have little impact on cuttings, cavings, spallings and direct brine releases. Radionuclides entering the Culebra over the four western-most additional panels (Panels 15, 16, 17, and 18) generally travel in a different direction than releases over the existing panels and the other additional and the replacement panels. This change in flow direction results in higher releases through the Culebra for these four panels than releases over the existing panels. Releases through the Culebra from the replacement panels show similar behavior to those from the existing panels.

Mean total releases in the RPPCR continue to be dominated by cuttings and cavings at high probabilities. Spallings releases show an increased contribution to total releases at lower probabilities, becoming nearly equal with direct brine releases. Mean total releases have increased in the RPPCR compared to the APPA and the CRA-2019. The changes in releases mainly result from the changes to the model for salt creep closure onto the waste, the inventory, and the increased drilling frequency. Radionuclide activity entering the Culebra has been significantly reduced by the updated long-term borehole permeability distribution. As a result, releases from the Culebra are significantly reduced despite the potential for faster travel times of radionuclides from the western-most additional panels. The increased repository volume has a negligible impact on total releases.

Mean total releases from the RPPCR are also compared to total releases from the EPA's CRA19_COMB analysis. The RPPCR sees higher releases at the upper compliance point probability and lower releases at the lower compliance point probability compared to the CRA19_COMB results.

Mean total releases from the RPPCR are below the regulatory limits. As a result, the Replacement Panels Planned Change Request PA demonstrates that the WIPP repository with two replacement and seven additional panels remains in compliance with the containment requirement of 40 CFR Part 191. A separate analysis concludes that a repository with the two replacement panels, but not

Information Only

any of the seven additional panels, would also remain in compliance with the containment requirement.

Information Only

7.0 REFERENCES

Bethune, J. 2023. Culebra Flow and Transport Analysis Report for the Replacement Panels Planned Change Request (RPPCR). ERMS 579725. Carlsbad, NM: Sandia National Laboratories.

Bethune, J., and S. Brunell. 2022. Determination of Culebra Release Points Number and Locations in a Repository with New Panels. ERMS 576493. Carlsbad, NM: Sandia National Laboratories.

Bowman, D.O., R. Kushnereit, M. Pedrazas, P. Johnson, N. Deeds, and J. Pinkard. 2023. Analysis Report for AP-203: Analysis Report Documenting the Data, Generation, and Calibration of T-Fields for CRA-2024. ERMS 579507. Carlsbad, NM: Sandia National Laboratories.

Brunell, S. 2019. Analysis Package for Normalized Releases in the 2019 Compliance Recertification Application Performance Assessment (CRA-2019 PA). ERMS 571373. Carlsbad, NM: Sandia National Laboratories.

Brunell, S. 2022. Design Document and User's Manual for CCDFGF Version 8.01. ERMS 577625. Carlsbad, NM: Sandia National Laboratories.

Brunell, S. 2023. Update to Parameters Defining Drilling Rate and Plugging Pattern Probabilities in PA Calculations. ERMS 579154. Carlsbad, NM: Sandia National Laboratories.

Brunell, S., C. Hansen, D.C. Kicker, S. Kim, S. King, and J. Long. 2021. Summary Report for the 2020 Additional Panels Performance Assessment (APPA). ERMS 574494. Carlsbad, NM: Sandia National Laboratories.

Brunell, S., and T.R. Zeitler. 2023. Analysis Report for Normalized Releases in the Replacement Panels Planned Change Request Performance Assessment. ERMS 579727. Carlsbad, NM: Sandia National Laboratories.

Brush, L.H. 1991. Current Estimates of Gas Production Rates, Gas Production Potentials, and Expected Chemical Conditions Relevant to Radionuclide Chemistry for the Long-Term WIPP Performance Assessment. ERMS 307353. Carlsbad, NM: Sandia National Laboratories.

Brush, L.H., and J.W. Garner. 2005. Additional Justification of the Insignificant Effect of Np on the Long-Term Performance of the WIPP. Memorandum to D.S. Kessel, February 1, 2005. Carlsbad, NM: Sandia National Laboratories. ERMS 538533.

Casey, S., R. Patterson, M.B. Gross, K. Lickliter, and J. Stein. 2003. Regulatory Considerations of Waste Emplacement within the WIPP Repository: Random versus Non-Random Distributions. Tucson, AZ: Waste Management 2003 Conference.

Day, B.A. 2015. Review of the Technical Basis for REFCON: ASDRUM, DRROOM, and VROOM Performance Assessment Analysis Parameters with Comparison to the Currently Emplaced Steel Surface Area per Unit Volume in the WIPP Repository. ERMS 564670. Carlsbad, NM: Sandia National Laboratories.

Day, K. 2023. Memo to Steve Wagner. Subject: "Borehole Plugging Practices White Paper". ERMS 578970. Carlsbad, NM: Los Alamos Technical Associates.

Information Only

Docherty, P. 2023a. Analysis Report for Modeling the Castile Pressurized Brine Reservoir. ERMS 578976. Carlsbad, NM: Sandia National Laboratories.

Docherty, P. 2023b. Impact Analysis for the Software Problem Report SPR 22-001 for PRELHS Version 2.45. ERMS 578912. Carlsbad, NM: Sandia National Laboratories.

Docherty, P., and S. King. 2023. Direct Brine Release Analysis Report for the Replacement Panels Planned Change Request (RPPCR). ERMS 579724. Carlsbad, NM: Sandia National Laboratories.

Domski, P.S. 2023a. Th(IV), Np(V), and Am(III) Baseline Solubilities for the Replacement Panels Planned Change Request (RPPCR) Performance Assessment ERMS 579512. Carlsbad, NM: Sandia National Laboratories.

Domski, P.S. 2023b. Uncertainty Analysis of Actinide Solubilities for the Replacement Panels Planned Change Request (RPPCR) Performance Assessment. ERMS 579529. Carlsbad, NM: Sandia National Laboratories.

Domski, P.S. 2023c. An Update to the WIPP EQ3/6 Database DATA0.FM1 with the Creation of DATA0.FM6. ERMS 579370. Carlsbad, NM: Sandia National Laboratories.

Falta, R., M. Hu, E.M. Kwicklis, C.I. Steefel, S.C. Williams-Stroud, and J.A. Thies. 2021. Additional Panels Performance Assessment (APPA) Changed Conceptual Models Peer Review Report. Carlsbad, NM: U.S. Department of Energy, Carlsbad Field Office.

Gjerapic, G., J.L. Bean, E.N. Matteo, and M.B. Gross. 2023. Analyses to Bound the Permeability of Degraded Fill Materials in Intrusion Boreholes for WIPP Performance Assessment. ERMS 579102. Carlsbad, NM: Salado Isolation Mining Contractors, LLC.

Gross, M.B., and G. Gjerapic. 2022. Analysis to Bound Brine Reservoir Volumes for WIPP Performance Assessment. Carlsbad, NM: Nuclear Waste Partnership, LLC.

Hansen, C. 2020. Analysis Plan for the Additional Panels Performance Assessment. AP-185, ERMS 573557. Carlsbad, NM: Sandia National Laboratories.

Hansen, C. 2021. Review of Conceptual Models for the Additional Panels Performance Assessment. ERMS 575130. Carlsbad, NM: Sandia National Laboratories.

Hansen, C. 2023. Upper Bound for Degraded Borehole Permeabilities. ERMS 579160. Carlsbad, NM: Sandia National Laboratories.

Hansen, C., S. King, J. Bethune, and S. Brunell. 2023a. Analysis Plan for the Performance Assessment for Replacement Panels Planned Change Request. AP-204, Rev. 1, ERMS 579449. Carlsbad, NM: Sandia National Laboratories.

Hansen, C.W., S. Brunell, and S. King. 2023b. Estimation of Releases From a 12-Panel Repository ERMS 580656. Carlsbad, NM: Sandia National Laboratories.

Hansen, C.W., L.H. Brush, M.B. Gross, F.D. Hansen, B.Y. Park, J.S. Stein, and T.W. Thompson. 2003. Effects of Supercompacted Waste and Heterogeneous Waste Emplacement on Repository Performance. ERMS 532475. Carlsbad, NM: Sandia National Laboratories.

Information Only

Hart, D.B., R.L. Beauheim, and S.A. McKenna. 2009. Analysis Report for Task 7 of AP-114: Calibration of Culebra Transmissivity Fields. ERMS 552391. Carlsbad, NM: Sandia National Laboratories.

Hart, D.B., R.M. Holt, and S.A. McKenna. 2008. Analysis Report for Task 5 of AP-114: Generation of Revised Base Transmissivity Fields. ERMS 552391. Carlsbad, NM: Sandia National Laboratories.

Helton, J.C., J.E. Bean, J.W. Berglund, F.J. Davis, K. Economy, J.W. Garner, J.D. Johnson, R.J. MacKinnon, J. Miller, D.G. O'Brien, J.L. Ramsey, J.D. Schreiber, A. Shinta, L.N. Smith, D.M. Stoelzel, C. Stockman, and P. Vaughn. 1998. Uncertainty and Sensitivity Analysis Results Obtained in the 1996 Performance Assessment for the Waste Isolation Pilot Plant. SAND98-0365. Albuquerque, NM: Sandia National Laboratories.

International Commission on Radiological Protection (ICRP) 2008. "Nuclear Decay Data for Dosimetric Calculations," ICRP Publication 107. Annals of the ICRP, Vol. 38, No. 3.

Kicker, D.C. 2019. Analysis Package for Inventory EPA Units in the 2019 Compliance Recertification Application Performance Assessment (CRA-2019 PA). ERMS 571372. Carlsbad, NM: Sandia National Laboratories.

Kicker, D.C. 2023a. Analysis Report for Cuttings, Cavings, and Spallings in the Replacement Panels Planned Change Request (RPPCR). ERMS 579723. Carlsbad, NM: Sandia National Laboratories.

Kicker, D.C. 2023b. Analysis Report for Inventory EPA Units in the Replacement Panels Planned Change Request Performance Assessment (RPPCR PA). ERMS 579731. Carlsbad, NM: Sandia National Laboratories.

Kicker, D.C. 2023c. Radionuclide Inventory Screening Analysis for the Replacement Panels Planned Change Request Performance Assessment (RPPCR PA). ERMS 578878. Carlsbad, NM: Sandia National Laboratories.

Kim, S. 2023. Analysis Report for Actinide Mobilization and Salado Transport in the Replacement Panels Planned Change Request (RPPCR). ERMS 579726. Carlsbad, NM: Sandia National Laboratories.

Kim, S., and L.M. Feng. 2023. Input Parameter Report for the Replacement Panels Planned Change Request Performance Assessment (RPPCR PA). ERMS 579730. Carlsbad, NM: Sandia National Laboratories.

King, S. 2021a. Analysis Package for Direct Brine Release in the Additional Panels Performance Assessment (APPA). ERMS 574498. Carlsbad, NM: Sandia National Laboratories.

King, S. 2021b. APPA 2D Salado Flow Grid Development. SAND2021-8603PE. Carlsbad, NM: Sandia National Laboratories.

King, S. 2021c. Methodology for Calculating Initial Waste Area Pressure in the Salado Flow Calculation. ERMS 576464. Carlsbad, NM: Sandia National Laboratories.

King, S. 2021d. Recalculating of Iron Surface Area for Iron Corrosion in the WIPP PA Calculation. ERMS 576428. Carlsbad, NM: Sandia National Laboratories.

Information Only

King, S. 2023. Salado Flow Analysis Report for the Replacement Panels Planned Change Request (RPPCR). ERMS 579722. Carlsbad, NM: Sandia National Laboratories.

King, S., P.C. Docherty, and C.W. Hansen. 2023. Impact Analysis of High Plutonium Loading in a Single WIPP Waste Panel. ERMS 580466. Carlsbad, NM: Sandia National Laboratories.

Kirchner, T., A. Gilkey, and J. Long. 2014. Summary Report on the Migration of the WIPP PA Codes from VMS to Solaris. AP-162, Rev. 1. ERMS 561757. Carlsbad, NM: Sandia National Laboratories.

Kirchner, T., A. Gilkey, and J. Long. 2015. Addendum to the Summary Report on the Migration of the WIPP PA Codes from VMS to Solaris. AP-162. ERMS 564675. Carlsbad, NM: Sandia National Laboratories.

Kirkes, G.R. 2021. Features, Events, and Processes Assessment for the Additional Panels Performance Assessment. ERMS 574493. Carlsbad, NM: Sandia National Laboratories.

Kirkes, G.R. 2023. Features, Events, and Processes Analysis for the Replacement Panels Planned Change Request Performance Assessment. ERMS 579720. Carlsbad, NM: Sandia National Laboratories.

Long, J. 2019. Computational Code Execution and File Management for the 2019 Compliance Recertification Application Performance Assessment (CRA-2019 PA). ERMS 571375. Carlsbad, NM: Sandia National Laboratories.

Long, J. 2020. Analysis Plan for Migration of Files from the Oracle/Solaris Cluster to the HPC/Linux Cluster and Qualification of Codes from the Solaris Cluster on the Linux Cluster. AP-184. ERMS 572888. Carlsbad, NM: Sandia National Laboratories.

Long, J. 2023. Computational Code Execution and File Management for the Replacement Panels Planned Change Request (RPPCR). ERMS 579728. Carlsbad, NM: Sandia National Laboratories.

Long, J., and S. King. 2022. Summary Report on the Migration of the WIPP PA Codes from Solaris to Linux. ERMS 577606. Carlsbad, NM: Sandia National Laboratories.

Lord, D.L., D.K. Rudeen, J.F. Schatz, A. Gilkey, and C.W. Hansen. 2006. DRSPALL: Spallings Model for the Waste Isolation Pilot Plant 2004 Recertification. SAND2004-0730. Albuquerque, NM: Sandia National Laboratories.

Lucchini, J., and J. Swanson. 2023. LANL ACRSP Parameter Recommendations for the CRA-2024 Performance Assessment. LCO-ACP-34. ERMS 578969. Carlsbad, NM: Los Alamos National Laboratory Carlsbad Operations.

Marcinowski, F. 2004. Letter to R.P. Detwiler (Subject: Approving the DOE's Request to Dispose of Compressed (Supercompacted) Waste from the Advanced Mixed Waste Treatment Program in the WIPP). 26 March 2004. ERMS 534327. Washington, D.C.: U.S. Environmental Protection Agency, Office of Air and Radiation.

Nemer, M., J. Stein, and W. Zelinski. 2005. Analysis Report for BRAGFLO Preliminary Modeling Results with New Gas Generation Rates Based Upon Recent Experimental Results. ERMS 539437. Carlsbad, NM: Sandia National Laboratories.

Information Only

New Mexico Environment Department (NMED). 2023. WIPP Hazardous Waste Facility Permit. November, 2023. Santa Fe, NM: New Mexico Environment Department Hazardous Waste Bureau.

Sanchez, L.C., J. Liscum-Powell, J.S. Rath, and H.R. Trellue. 1997. EPAUNI: Estimating Probability Distribution of EPA Unit Loading in the WIPP Repository for Performance Assessment Calculations. Document Version 1.01. ERMS 243843. Albuquerque, NM: Sandia National Laboratories.

Santillan, J. 2023. "PBRINE Telecon, Issue 4 (Pu oxidation state), and Issue 19 (Boreholes)," Email to Anderson Ward. February 24, 2023. ERMS 579254.

Shumaker, N. 2021. Relationship Between DBR Volume and Placement of Wellbore Intrusion in Upper Panels. ERMS 576148. Carlsbad, NM: Sandia National Laboratories.

Sjomeling, D. 2019. "2:30 Meeting Information," an email to Paul Shoemaker with the attachment "West Mains and Panels peer review info Final 091219.pdf." ERMS 572682. Carlsbad, NM: Nuclear Waste Partnership, LLC.

Sandia National Laboratories (SNL). 2022. Software Problem Report for PRELHS Version 2.45. ERMS 577795. Carlsbad, NM: Sandia National Laboratories.

U.S. Congress. 1992. WIPP Land Withdrawal Act, Public Law 102-579, 106 Stat. 4777, 1992; as amended by Public Law 104-201, 110 Stat. 2422, 1996.

U.S. Congress. 1996. Public Law 102-579. Waste Isolation Pilot Plant Land Withdrawal Act of 1992, as amended by Public Law 104-201, 1996.

U.S. Department of Energy (DOE). 1996. Title 40 CFR Part 191 Compliance Certification Application for the Waste Isolation Pilot Plant (October). 21 Vols. DOE/CAO-1996-2184. Carlsbad, NM: U.S. Department of Energy Carlsbad Area Office.

U.S. Department of Energy (DOE). 2019. Title 40 CFR Part 191 Compliance Recertification Application for the Waste Isolation Pilot Plant. DOE/WIPP-19-3609. Carlsbad, NM: U.S. DOE Carlsbad Field Office.

U.S. Department of Energy (DOE). 2021. Department of Energy Response 10 to U.S. Environmental Protection Agency's Completeness Comments, Letter dated September 11, 2020 and November 13, 2020, from Tom Peake to Mike Brown. Carlsbad, NM: U.S. Department of Energy, Carlsbad Field Office.

U.S. Department of Energy (DOE). 2022a. Annual Transuranic Waste Inventory Report – 2022. DOE/TRU-22-3425 Rev 0, December 2022. Carlsbad, NM: U.S. Department of Energy, Carlsbad Field Office.

U.S. Department of Energy (DOE). 2022b. Delaware Basin Monitoring Annual Report. DOE/WIPP-22-2308. Rev. 0. Carlsbad, NM: U.S. Department of Energy, Carlsbad Field Office.

U.S. Department of Energy (DOE). 2023. Planned Change Notice. Subject: Addition of Four Shielded Containers. Letter dated April 25, 2023, from Mark Bollinger to Lee Ann B. Veal. CBFO:ERCD:MG:JV:23-0090. Carlsbad, NM: U.S. Department of Energy, Carlsbad Field Office.

Information Only

U.S. Environmental Protection Agency (EPA). 1993. 40 CFR Part 191: Environmental Radiation Protection Standards for the Management and Disposal of Spent Nuclear Fuel, High-Level and Transuranic Radioactive Wastes; Final Rule. Federal Register, Vol. 58. 66398-416.

U.S. EPA. 1996. 40 CFR Part 194: Criteria for the Certification and Recertification of the Waste Isolation Pilot Plant's Compliance with the 40 CFR Part 191 Disposal Regulations: 61 Federal Register, 5223-5245 (February 9, 1996)

U.S. Environmental Protection Agency (EPA). 2004. Discussion of Major Issues Associated with EPA's Compressed Waste Review. Washington, D.C.: U.S. Environmental Protection Agency, Office of Air and Radiation.

U.S. Environmental Protection Agency (EPA). 2021. Letter from L. Veal, Director, Radiation Protection Division to R. Knerr, Manager, Carlsbad Field Office. ERMS 575119. April 20, 2021. Washington, DC.

U.S. Environmental Protection Agency (EPA). 2022a. Overview of EPA Review of U.S. Department of Energy 2019 WIPP Compliance Recertification Application Performance Assessment. EPA-HQ-OAR-2019-0534-0049. Washington, DC: U.S. Environmental Protection Agency, Office of Radiation and Indoor Air.

U.S. Environmental Protection Agency (EPA). 2022b. Technical Support Document for Sections 194.23 Evaluation of the Compliance Recertification Application (CRA-2019) Actinide Source Term, Gas Generation, Backfill Efficacy, Water Balance, and Culebra Dolomite Distribution Coefficient Values. EPA-HQ-OAR-2019-0534-0052. Washington, D.C.: U.S. Environmental Protection Agency, Office of Radiation and Indoor Air.

U.S. Environmental Protection Agency (EPA). 2022c. Technical Support Document for Sections 194.33. Review of Borehole Drilling Rate and Plugging Pattern Frequency Calculations in the CRA-2019 Performance Assessment. EPA-HQ-OAR-2019-0534. Washington, D.C.: U.S. Environmental Protection Agency, Office of Radiation and Indoor Air.

U.S. Environmental Protection Agency (EPA). 2023. Letter From: Lee Ann B. Veal, Department of Environmental Protection Agency To: Mark Bollinger, Department of Energy. Dated September 15, 2023. Subject: Re: Addition of Four New Shielded Containers. Washington, D.C.: U.S. Environmental Protection Agency, Office of Radiation and Indoor Air.

Van Soest, G.D. 2022. Performance Assessment Inventory Report – 2022 for the Replacement Panels Planned Change Request. INV-PA-22, Rev. 0. Carlsbad, NM: Los Alamos National Laboratory.

Vignes, C., J.E. Bean, and B. Reedlunn. 2023. Improved Modeling of Waste Isolation Pilot Plant Disposal Room Porosity. SAND2023-04826. Carlsbad, NM: Sandia National Laboratories.

Zeitler, T.R. 2019. Analysis Package for the Sensitivity of Releases to Input Parameters in the 2019 Compliance Recertification Application Performance Assessment (CRA-2019 PA). ERMS 571374. Carlsbad, NM: Sandia National Laboratories.

Zeitler, T.R. 2023a. Analysis Report for Parameter Sampling in the Replacement Panels Planned Change Request (RPPCR). ERMS 579721. Carlsbad, NM: Sandia National Laboratories.

Information Only

Zeitler, T.R. 2023b. Consideration of TDEM Data for PBRINE Parameter Including Replacement Panels. ERMS 580108. Carlsbad, NM: Sandia National Laboratories.

Information Only